Conceptual Design Optimization for Handling Qualities Applied to Tiltrotor Aircraft in Conversion Mode

Haoyu Feng

Delft University of Technology

TU Delft

The XV-15 tiltrotor aircraft in vertical flight at the NASA Dryden Flight Research Center, Oct. 1980, NASA Photo.

Conceptual Design Optimization for Handling Qualities Applied to Tiltrotor Aircraft in Conversion Mode

by

Haoyu Feng

in partial fulfillment of the requirements for the degree of

Master of Science
in Aerospace Engineering

at the Delft University of Technology,
to be defended publicly on Friday October 15, 2021 at 10:00 AM.

Supervisor:	Dr. M.D. Pavel,	TU Delft
Thesis committee:	Dr. M.D. Pavel,	TU Delft
	Dr. G. la Rocca,	TU Delft
	Dr. M.A. Mitici,	TU Delft

TU Delft Delft University of Technology

ACKNOWLEDGEMENTS

I chose this topic on tiltrotor handling qualities and design because of my particular interest on flight dynamics modelling, tiltrotor aircraft design, and Urban Air Mobility. I am very thankful that Dr. Pavel provided me with the opportunity to study this topic under her supervision. I used to know nothing about rotorcraft, it is Dr. Pavel who opened this fascinating world to me. I would like to thank Dr. Pavel for her support, interesting advice on beautiful spots in the Netherlands, and thoughtful tips on job searching during the past year. Here, I would also like to thank my parents and my girlfriend Na for giving their support and care to me all the way. Finally, my gratitude goes to my friends Riccardo, Liangjian, Sheng, Hao, Zhan. I could not be more happy to have spent this time with you all.

Haoyu Feng
Delft, October 2021

SUMMARY

A tiltrotor has the features of both a fixed-wing aircraft and a helicopter, thereby blending the vertical flight capabilities of helicopters with the speed, altitude, and range of fixed-wing aircraft. Compared to conventional helicopters, tiltrotors are more competent in the application of military transportation, medical and rescue service, and offshore platform transportation. With the prosperity of the Urban Air Mobility industry, tiltrotor aircraft has the potential to be widely used in the future. However, as an important aspect of piloted aircraft, the handling qualities of tiltrotor aircraft have not been studied extensively. Few studies have investigated the tiltrotor handling qualities in conversion mode. This thesis aims to add knowledge to the bare-airframe handling qualities of tiltrotor aircraft in conversion mode and contribute to the tiltrotor design for handling qualities. To achieve this goal, this study was divided into four stages. In Stage 1, a TU Delft in-house 3 degrees of freedom tiltrotor model was improved and necessary functions such as trim and linearization were implemented. Stage 2 was to use the improved tiltrotor model to locate the handling qualities deficiencies. In Stage 3, the design parameters were selected, the design space was generated and explored. In Stage 4, optimization was performed to find the optimal sets of design parameters under different constraints.

A flight dynamic model is the basis of this study. Thus, in Stage 1, a TU Delft in-house 3 degrees of freedom tiltrotor model based on the published data of the XV-15 tiltrotor aircraft was improved to obtain better accuracy. In Stage 2, the handling qualities criteria were selected, including control anticipation parameter (CAP), bandwidth, pitch dropback, and quickness. These criteria were selected from rotorcraft handling quality specification ADS-33E and fixed-wing handling quality specification MIL-HDBK-1797A. Control anticipation parameter is a measure of predictability of the pitch response. Bandwidth is an indication of the highest frequency at which the pilot-aircraft loop can be closed without introducing instability. Pitch dropback is a criterion used in conjunction with the CAP or bandwidth criteria. It compares the ratio of the peak to steady-state pitch rate with the ratio of pitch attitude dropback to the steady-state pitch rate. Quickness is a measure of the aircraft's ability to achieve rapid attitude changes. Other than the four handling qualities criteria, two maneuverability parameters, namely the peak normal load factor during the pull-up and the acceleration time, were also evaluated. In this thesis, the design parameters are disk loading, rotor solidity, blade loading, tip speed, and tail volume coefficient. Based on the improved model from Stage 1, handling qualities of multiple points in the flight envelope were evaluated to identify the handling qualities deficiencies. Results demonstrated that the quickness and the pitch dropback were the primary handling problems in conversion mode. In most cases, CAP and bandwidth were satisfactory but they would degrade when flying very close to the boundaries of the flight envelope.

In Stage 3, an analysis tool was developed to automate the process of configuration generation, trim and linearization, weight evaluation, and handling quality analysis. The 100 knots flight at 30 degrees nacelle angle was selected as the design case. With the help of this analysis tool, thousands of designs were generated to form the design space. The prediction profilers, which contain the sensitivity curves of each handling quality parameter with respect to each design parameter, were then created. Two different rotor blade loading conditions were studied, one with a fixed blade loading and the other with blade loading as a design parameter. Under both conditions, it was found that none of the selected design parameters showed observable influence on the quickness parameters. Thus, the quickness parameters were dropped out. Under the first condition with a fixed blade loading, the rotor tip speed had the largest impact on handling qualities parameters. Next to it, the tail volume coefficient was considered the parameter that had the second-largest impact on handling qualities parameters. By decreasing the tip speed and increasing the tail volume coefficient, the dropback parameter can be improved significantly. However, decreasing the tip speed and increasing the tail volume coefficient always led to additional weight. Under the second condition, the inclusion of blade loading as a design parameter provided more space for tip speed to decrease. Also, the blade loading itself had a strong influence on the dropback parameter and bandwidth frequency.

Based on the knowledge gained from the design space, an optimization study was conducted. Cases with different constraints were investigated. The results showed that the dropback can be improved but not to the desired region with blade loading fixed. After removing the constant blade loading constraint and making it a design parameter, the dropback can be improved to the desired region. However, the flight envelope was largely compressed due to a higher design blade loading. Finally, a design with a satisfactory dropback was

found by applying reasonable constraints on weight and acceleration time. This design can also satisfy all other handling qualities criteria in the meantime. But it requires weight investment and more power to fly, implying a shorter range.

In conclusion, this thesis presented a conceptual design and optimization framework to improve the handling qualities of the XV-15 tiltrotor aircraft. Handling qualities deficiencies of the XV-15 in conversion mode were investigated. The results in this thesis exhibited the influence of each design parameter on the handling qualities. The six optimization cases demonstrated that the handling qualities can be improved by adjusting the design parameters, but the increases in aircraft empty weight and power required are inevitable. The work done in this thesis contributes to the understanding of these design parameters' role in tiltrotor handling qualities, thus provides future tiltrotor designs with valuable knowledge. Although this thesis focused on the conversion mode, the developed framework can be applied to any flight mode.

CONTENTS

List of Figures

List of Tables

List of Symbols

Abbreviations

AI	[-]	Autorotative index
CAP	[-]	Control anticipation parameter
CG	[-]	Center of gravity
DB	[-]	Pitch attitude dropback
DL	[-]	Disk loading
IAS	[-]	Indicated airspeed
POS	[-]	Probability of success
$SIGMA$	[-]	Rotor solidity
TVC	[-]	Tail volume coefficient
UAM	[-]	Urban Air Mobility
VT	[-]	Tip speed

Greek symbols

α	[rad]	Angle of attack
α_c	[rad]	Angle of attack of the control plane
α_f	[rad]	Angle of attack of the fuselage
δ_0	[-]	Blade airfoil drag coefficient
δ_1	[1/rad]	Blade airfoil drag coefficient
δ_2	[1/rad^2]	Blade airfoil drag coefficient
δ_e	[rad]	Elevator deflection
η	[rad]	Nacelle tilt angle
γ	[-]	Blade lock number, $\gamma = \rho a_0 c R^4 / I_b$
γ	[rad]	Flight path angle
λ_c	[-]	non-dimensional inflow velocity of the control plane, $\lambda_c = V sin\alpha_c / (\Omega R)$
λ_i	[-]	non-dimensional induced velocity, $\lambda_i = v_i / (\Omega R)$
μ	[-]	Advance ratio, $\mu = V cos\alpha_c / (\Omega R)$
Ω	[rad/s]	Rotor rotational speed
ω_n	[rad/s]	Natural frequency
ω_{BW}	[rad/s]	Bandwidth frequency
ω_{sp}	[rad/s]	Short period natural frequency

ρ	[kg/m^3]	Air density
σ	[-]	Rotor solidity
θ	[rad]	Pitch attitude angle
θ_0	[rad]	Rotor collective pitch
θ_c	[rad]	Rotor longitudinal cyclic pitch
θ_f	[rad]	Fuselage pitch attitude angle
ζ_{ph}	[-]	Phugoid damping ratio
ζ_{sp}	[-]	Short-period damping ratio

Latin symbols

A	[m^2]	Rotor area
a_0	[-]	Blade airfoil lift coefficient
a_0	[rad]	Coning angle
a_1	[rad]	Longitudinal tilt angle of rotor tip path plane w.r.t. control plane
b	[m]	Wing span
c	[m]	Blade chord
C_H	[N]	Rotor H-force coefficient
C_T	[N]	Rotor thrust coefficient
d	[-]	Dropback distance
g	[m/s^2]	Gravitational acceleration
H	[N]	Rotor H-force, $H = C_H \rho \pi R^2 (\Omega R)^2$
I_b	[kg$\cdot$m^2]	Blade flapping inertia
I_y	[kg$\cdot$m^2]	Moment of inertia around the pitch axis
K_β	[N/rad]	Rotor hub spring stiffness
M	[-]	Pitching moment
m	[kg]	Aircraft mass
M_q	[-]	The derivative of pitching moment w.r.t. pitch rate
M_w	[-]	The derivative of pitching moment w.r.t. body Z-velocity
$M_{\delta e}$	[-]	The derivative of pitching moment w.r.t. elevator deflection
$M_{\dot{w}}$	[-]	The derivative of pitching moment w.r.t. body vertical acceleration
N	[-]	Number of blades
n_z	[g's]	Normal acceleration
n_{zpk}	[g]	Peak normal load factor
P	[W or hp]	Power
q	[rad/s]	Pitch rate

Q_γ	[m]	Pitch agility quickness
Q_θ	[m]	Pitch attitude quickness
q_{pk}	[rad/s]	Peak pitch rate
q_{ss}	[rad/s]	Steady-state pitch rate
R	[m]	Rotor radius
T	[N]	Rotor thrust, $T = C_T \rho \pi R^2 (\Omega R)^2$
t	[s]	Time
$T_{\theta 2}$	[s]	Incidence lag
u	[m/s]	X velocity component in body reference frame
V	[m/s]	Airspeed
v_i	[m/s]	Rotor induced velocity
V_T	[rad/s]	Tip speed
w	[m/s]	Z velocity component in body reference frame
X	[N]	Force in the X axis of body reference frame
X_u	[-]	The derivative of X-force w.r.t. body X-velocity
$X_{\delta e}$	[-]	The derivative of X force w.r.t. elevator deflection
X_{COL}	[inch]	Collective lever travel
X_{LN}	[inch]	Longitudinal stick travel
Z	[N]	Force in the Z axis of body reference frame
Z_u	[-]	The derivative of Z-force w.r.t. body X-velocity
Z_w	[-]	The derivative of Z-force w.r.t. body Z-velocity
$Z_{\delta e}$	[-]	The derivative of Z force w.r.t. elevator deflection

I

INTRODUCTION

1. ORIENTATION

This thesis project aims to add knowledge to the handling qualities of tiltrotor aircraft in conversion mode and to investigate the influences of various tiltrotor design parameters on the handling qualities in conversion mode. To gain sufficient background knowledge for the project to proceed, the literature study hence needs to cover the following topics:

- Characteristics of tiltrotor aircraft. Their differences from conventional helicopters and airplanes.
- Existing rotorcraft and fixed-wing aircraft handling qualities criteria.
- Previous studies on tiltrotor handling qualities.
- Design methodologies and optimization techniques that are applicable to this project.

This literature study is then laid out to cover these topics consecutively. Section 2 introduces the history of tiltrotor aircraft and its characteristics. Section 3 discussed the handling qualities standards and previous studies on tiltrotor handling qualities. Section 4 presents the design and optimization methodologies used in literature.

2. TILTROTOR AIRCRAFT

2.1. A BRIEF HISTORY OF THE TILTROTOR AIRCRAFT

A tiltrotor has the features of both a fixed-wing aircraft and a helicopter, thereby blending the vertical flight capabilities of helicopters with the speed, altitude, and range of fixed-wing transport aircraft. This concept has been conceived by aeronautic pioneers since the 1920s. In the 1920s, Henry Berliner designed a fixed-wing biplane with a large diameter propeller mounted on a vertical shaft near the tip of each wing. For forward flight, the shafts would be tilted forward but could not be converted fully to the horizontal. [1] Later in September 1930, a flying machine with tiltable rotors was patented by George Lehberger [2]. His design included the basic concept of the tiltrotor aircraft, which was the use of a relatively low disk loading propeller that can be tilted from the vertical to the horizontal. But at that time, many technology advancements were required to make these concepts come true. Until the end of the 1950s, the feasibility of this concept was first proved by the Bell XV-3. The data and experience gained from the XV-3 were later applied to the development of the XV-15. [1] Extensive experiments and flight tests have been carried out with the XV-15 to help engineers develop design tools and guidelines for tiltrotors, which paved the way for the V-22 [1]. Besides the military applications, tiltrotors also have huge potentials on civil missions such as Urban Air Mobility (UAM), medical and rescue service, offshore platform transportation, etc. [3] Currently at AgustaWestland, the AW609 is at its final certification phase and will probably enter into service in 2021, which will make it the first civil tiltrotor aircraft. The XV-3, XV-15, and AW609 are shown in Figure I.1

(a) Bell XV-3 in airplane mode (b) Bell XV-15 in hover (c) AW609 in airplane mode

Figure I.1: XV-3, XV-15, and AW609 [1]

2.2. CHARACTERISTICS OF THE TILTROTOR AIRCRAFT

The feature that distinguishes a tiltrotor from a helicopter or a fixed-wing aircraft is its tiltable nacelles. Different nacelle angles correspond to three flight modes. For instance, the nacelles of the XV-15 tiltrotor aircraft can tilt from 0 to 95°. With 0° being the horizontal position, its three flight modes are:

- Helicopter mode: 80-95°
- Airplane mode: 0°
- Conversion mode: all other angles

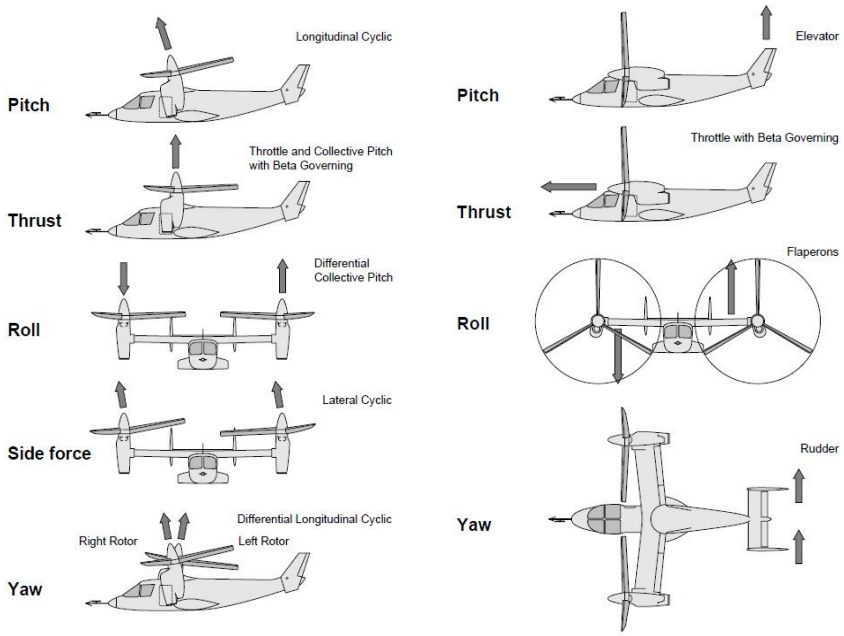

(a) Helicopter mode (b) Airplane mode

Figure I.2: XV-15 controls [4]

When flying in helicopter mode, the nacelles are at the vertical position. This configuration is used for VTOL(Vertical take-off and landing), hover, and low-speed flight. By tilting the nacelles forward, the tiltrotor

[1] Image source for the XV-3: "Bell XV-3", Wikipedia, last modified on 1 January 2021, https://en.wikipedia.org/wiki/Bell_XV-3#/media/File:Bell_XV-3_in_level_flight.jpg
Image source for the XV-15: "XV-15 tilt rotor takeoff - first NASA Dryden flight", NASA - Dryden Flight Research Center Photo Collection, last Modified on 6 February 2002, https://www.dfrc.nasa.gov/Gallery/Photo/XV-15/HTML/ECN-13850.html
Image source for the AW609: "(Originally Bell-Augusta) Augusta Westland AW-609 in airplane mode (Paris Air Show 2007)", Dmitry Mottl, 18 June 2007, https://commons.wikimedia.org/wiki/File:BA609_02.jpg

enters the conversion mode and achieves the airplane mode when the nacelles reach the 0° position. Tiltrotors all have a "conversion corridor", which is the flight envelope that limits the operational nacelle angle vs. flight speed.

Tiltrotor aircraft use different controls in different modes. The controls of the XV-15 tiltrotor aircraft are illustrated in Figure I.2. In helicopter mode, the pitch control is achieved by longitudinal cyclic and elevator deflection. The roll control is achieved by differential collective. The yaw control uses differential longitudinal cyclic. By applying the lateral cyclic, the XV-15 can perform sideward flight. The control surfaces such as the elevators, the rudders, and the ailerons are active in all modes but ineffective at low speed. As the nacelles tilt forward and the tiltrotor enters the conversion mode, the rotor controls are automatically phased out and the control surfaces start to generate moments as the the dynamic pressure builds up. In airplane mode, the XV-15 uses conventional airplane control surfaces. However, other control strategies are also possible. For example, AW609 uses the differential collective for the yaw control instead of the rudder in airplane mode.

3. HANDLING QUALITIES

3.1. FLYING QUALITIES AND HANDLING QUALITIES

Before introducing the concept of "Handling Qualities", it is convenient to first introduce the concept of "Flying Qualities", as these two are closely related and hardly distinguishable. Phillips [5] defines "Flying Qualities" as *"the stability and control characteristics that have an important bearing on the safety of flight and on the pilots' impressions of the ease of flying an airplane in steady flight and in maneuvers."* From this definition, flying qualities not only concern the performance of the aircraft, but also the pilots' impressions of controlling the aircraft. Cooper and Harper [6] defines "Handling Qualities" as *"those qualities or characteristics of an aircraft that govern the ease and precision with which a pilot is able to perform the tasks required in support of an aircraft role"*. In the same report, Cooper and Harper emphasized that handling qualities include more than just stability and control characteristics. Other factors such as the cockpit interface (e.g., displays, controls), the aircraft environment (e.g., weather conditions, visibility, turbulence), and stress also influence the handling qualities. In most tests, the evaluation of handling qualities will take into account all these factors. The definitions of "Flying Qualities" and "Handling Qualities" both contain the performance of the aircraft, as well as the pilot's ease to fly the aircraft. Colloquially, handling qualities are used to refer to the flying qualities of aircraft [7]. Cooper and Harper also noted that the generally accepted meaning of "Flying Qualities" is similar to the above definition of "Handling Qualities". Therefore, no attempt will be made to further distinguish these two concepts in this report. The concept "Handling Qualities" will be used throughout the report except when referring to flying qualities specifications.

3.2. HANDLING QUALITIES STANDARDS

The handling qualities have been a subject of considerable concern during the development of aircraft. It was noted that 25%-50% of the flight testing time might be spent on improving the handling qualities in the development program [8]. In fixed-wing aircraft design, relatively simple static analyses can provide a good prediction of a vehicle's stability, control, and handling qualities through the use of parameters like tail volume coefficients and location of the center of gravity. However, such methods cannot be readily applied to rotorcraft design, since most bare-airframe rotorcraft are inherently unstable and require a stability augmentation system to make them handleable. [7] Therefore, during the development of a rotorcraft, handling qualities were often treated as an outcome of the overall design and left unresolved until the flight tests were performed. [8]

To adequately inform the aircraft design process for good handling qualities to prevent any accidents due to handling problems, the handling qualities discipline has never stopped growing since the first real specification for flying qualities written by Gilruth [9] and published by NACA in 1943. This growth has now reached a point where the performance standards, the criteria and test techniques, the understanding of aeromechanics and control, and the design tools, are available to designers to *"ensure that handling deficiencies never again have to define the boundary of the operational flight envelope."* [8] However, there still exists a shortfall in handling qualities standards for unconventional aircraft configurations, for example, the tiltrotor aircraft. Accidents due to handling qualities problems are still occurring today. During a flight test on 30 October 2015, the second of the prototypes of AW609 entered a "Dutch roll" instability and disintegrated in midair, killing two test pilots on board. Later investigators found that this was due to the pilot-induced oscillations which is a severe handling qualities problem. [10] This accident infers that work is still needed to develop the handling qualities standards, as well as the methods and tools for the prediction of handling

qualities problems.

The handling qualities standards for fixed-wing aircraft and helicopters have already been well-defined: the fixed-wing standard MIL-HDBK 1797A [11] and the rotorcraft standard, ADS-33E-PRF [12]. In the respective helicopter/fixed-wing flight mode, tiltrotor designers may refer to these standards. But specific standards for tiltrotor aircraft in the conversion mode is still lacking. The MIL-83300, published in 1970, is the only standard for V/STOL aircraft. It addressed the flight regime up to the conversion speed (the speed at which the aircraft enters the airplane mode). It was adopted by the US. Navy to guide the development of V-22. However, because the MIL-83300 paid very little attention to the handling qualities requirements for transition and operating the entire mission at intermediate thrust vector settings, the V-22 program could hardly rely on it and had to develop a list of handling qualities requirements on its own. [13] Also, Meyer and Padfield [4] pointed out that in the BA609 program, the majority of the certification basis for performance and handling qualities had to be either adapted from regulations in Federal Aviation Regulations (FAR) for fixed-wing aircraft and rotorcraft or newly-created.

In MIL-HDBK 1797A, handling qualities are divided by aircraft classes, flight phases, and levels of performance as shown in Table I.1, I.2, I.3.

Table I.1: Aircraft classes

Class	Description
I	Small, light-weight, medium maneuverability airplanes
II	Medium-weight, low to medium maneuverability airplanes
III	Large, heavy-weight, low maneuverability airplanes
IV	High-maneuverability airplanes

Table I.2: Flight phase categories

Category	Description
A	Nonterminal flight phases that require rapid maneuvering, precise tracking, or precise flight path control.
B	Nonterminal flight phases that are accomplished with gradual maneuvers (climb, cruise, descent)
C	Terminal flight phases such as takeoff or landing

Table I.3: Flying qualities levels

Level	Description
1	Flying qualities clearly adequate for the mission flight phase
2	Flying qualities adequate to accomplish the mission flight phase, with some increase in pilot workload or degradation of mission effectiveness
3	Flying qualities such that the aircraft can be controlled safely, but pilot workload is excessive or mission effectiveness is inadequate

The structure of ADS-33E is shown in Figure I.3 from Ref. [13]. ADS-33E adopts the Mission-Task-Element (MTE) approach. The operational missions are defined by the user according to the aircraft's role. Each mission can be seen as a combination of a series of MTEs. ADS-33E provides a menu of MTEs that are suitable for each helicopter category, together with the required level of agility for each MTE. In the core of all handling qualities standards are the dynamic response criteria which cover aircraft responses to controls, disturbances, and trim characteristics [14]. Besides the dynamic response criteria, ADS-33E also includes other factors that affect the handling qualities, e.g., the usable cue environment (UCE) and operational environment.

MISSION TASK ELEMENTS APPROACH

Mission-Task-Element (MTE) is an element of a mission that can be treated as a handling qualities task. Regardless of the aircraft class or size, the key handling qualities issues center on the mission tasks. [15]. This

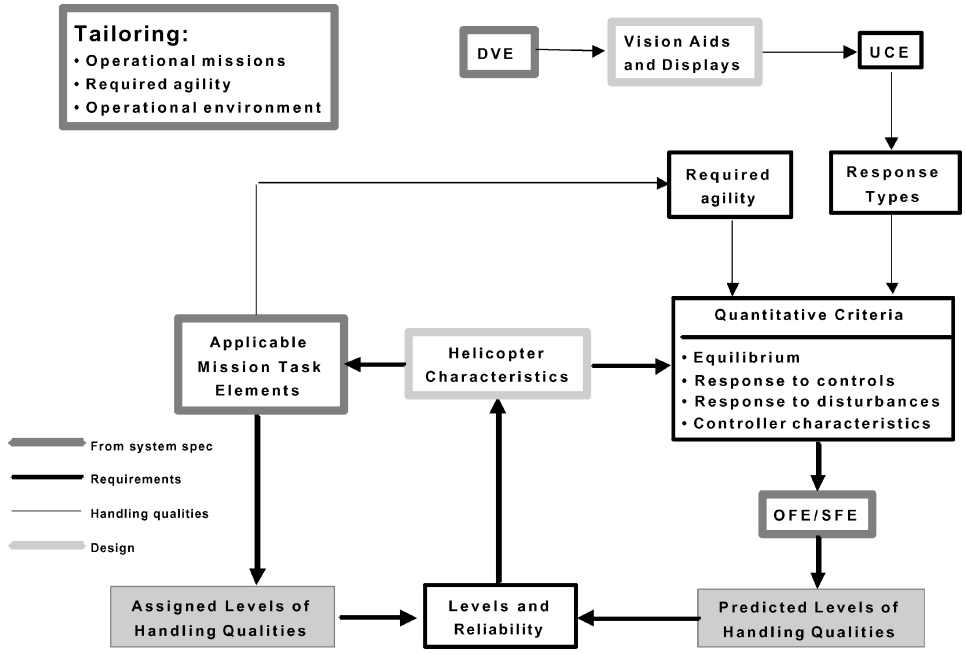

Figure I.3: ADS-33 structure [13]

forms the basis of using the MTEs in handling qualities standards. As indicated in Figure I.3, on the one hand, with the required agility derived from the applicable MTEs, designers use quantitative criteria to obtain the predicted levels of handling qualities. On the other hand, the applicable MTEs are translated to flight test maneuvers (FTMs), which can be evaluated by test pilots in flight simulators to obtain the assigned levels of handling qualities through the use of Cooper–Harper rating [6]. Ideally, the predicted levels and the assigned levels of handling qualities should be equal. In the case of inconsistency, investigations need to be carried out to find out what factors contribute to the difference.

DYNAMIC MANEUVER ENVELOPE/RESPONSE TYPES

The dynamic response of aircraft can be divided into areas in a frequency-amplitude chart as shown in the center of Figure I.4 from Ref. [15]. The maneuver envelope line defines the achievable maneuvers, the amplitude of which decreases as frequency increases. According to Ref. [14], four areas, two relating to stability and the other two relating to agility (agility is the rate of change of maneuverability. Maneuverability can be defined as the aircraft's ability to change the flight path by applying acceleration. Hence, agility can be thought of as the quickness of entering or exciting different maneuver states, making it more appropriate to use agility rather than maneuverability in Figure I.4 to describe control power and quickness.), can be distinguished within this envelope. Examples of the criteria for stability and agility are shown in the outer four charts in Figure I.4.

- **Bandwidth** Defined by Padfield [14]: *"Response bandwidth defines the upper end of the frequency range where the pilot can close the loop on a particular motion without having to apply significant lead to avoid closed-loop instability."* The complementary parameter on the bandwidth charts is the phase delay defined to avoid the pilot-induced oscillation (PIO).
- **Mid-long term stability** The stability boundaries for mid to long term motion are defined by the frequency-damping charts. For both rotorcraft and fixed-wing aircraft, a minimum damping ratio of 0.35 is required for all axes to meet level 1 requirements.
- **Control power** Large-amplitude attitude changes are characterized by control power. For instance, in ADS-33E for the hover and low-speed condition, control power for different axes are defined as the achievable angular rate or the achievable attitude angle according to different response types. The Higher the agility required by a maneuver, the larger the control power is required.
- **Quickness** Moderate-amplitude attitude changes are defined by the quickness parameter. In ADS-33E, it is defined as the peak attitude change rate to attitude change achieved during a sharp attitude-change

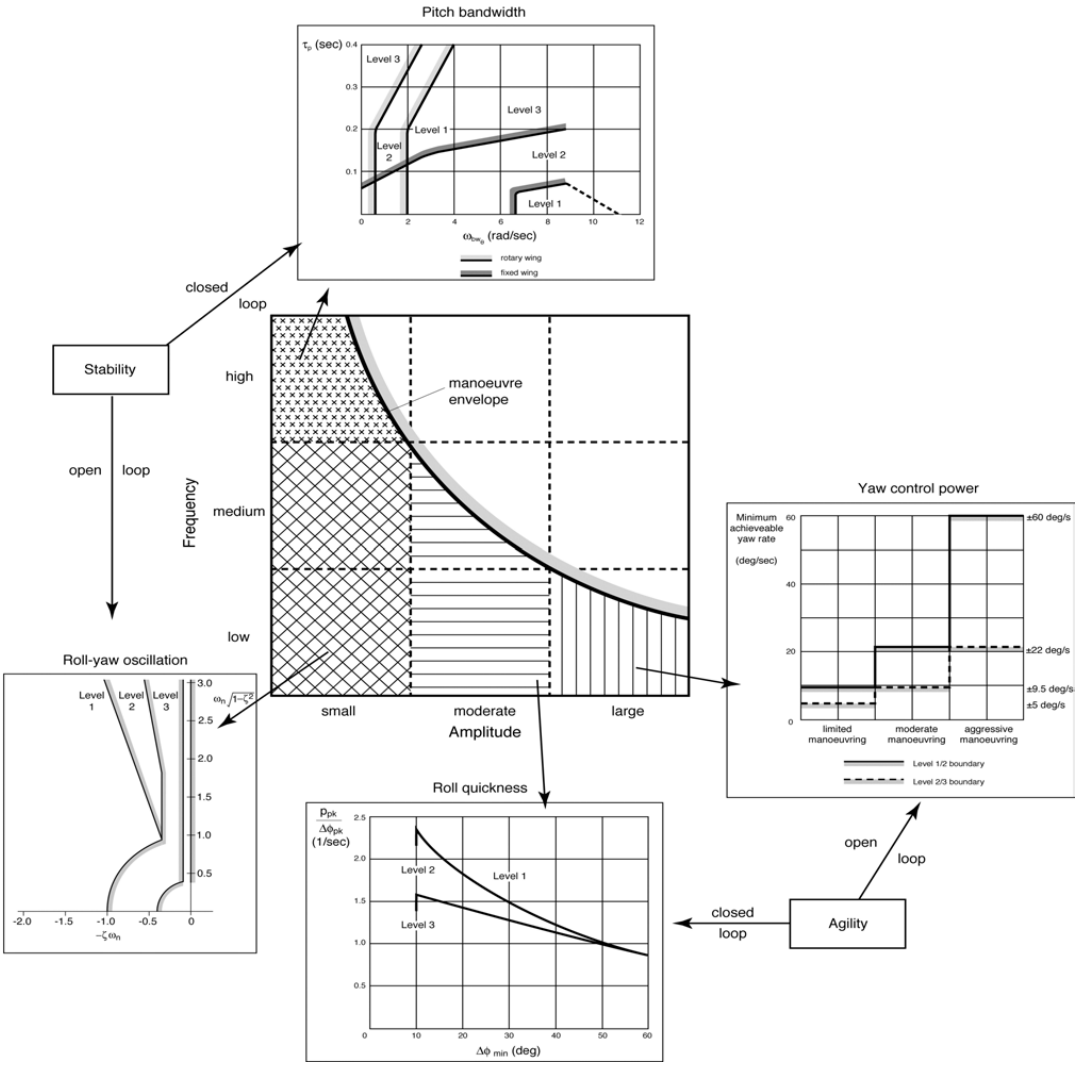

Figure I.4: Dynamic response criteria [15]

maneuver. Quickness reflects how quickly can the pilot command an attitude change. It is described as a 'closed-loop' agility parameter due to the fact that it originates from the analysis of closed-loop maneuvers. [14]

3.3. STUDIES ON TILTROTOR HANDLING QUALITIES

For the purpose of gaining knowledge on the handling qualities characteristics and challenges of tiltrotors, a search on the existing literature with respect to these topics resulted in finding that few studies have covered the handling qualities of tiltrotor aircraft. Among these studies, the handling qualities in the helicopter mode and airplane mode constitute the majority of the contents. The handling qualities in the conversion mode have been given very little attention. Most studies treated the conversion mode as a "transient process", instead of a mode at which the aircraft will operate the entire mission. For example, the search and rescue mission may require the tiltrotor to follow the terrain and loiter in the rescue zone in the speed range between 80 and 120 knots, for which the conversion mode is most suitable. For a tiltrotor flying in this speed range, the airplane mode will stall and the conversion mode is more efficient than the helicopter mode. [16] In the following two sections, the literature on the lateral and directional handling qualities, and the longitudinal handling qualities will be reviewed. Key results and conclusions from them will be presented.

LATERAL AND DIRECTIONAL HANDLING QUALITIES

In Ref. [4], Meyer and Padfield presented the first results of the handling qualities work package of the RHILP project (Rotorcraft Handling, Interactions and Loads Prediction. A critical technology program sponsored

by the European Commission), where a step-by-step approach to the development of civil tiltrotor handling qualities was outlined. It was suggested that ideally, a specific tiltrotor handling qualities manual should combine the criteria of the helicopter mode, the conversion mode, and the airplane mode into one single criteria or at least in one single format. For this purpose, Meyer and Padfield conducted a compatibility analysis to search for the commonality and distinctions between the fixed-wing aircraft and rotorcraft handling qualities criteria. They identified the major gaps as the absence of data on the aircraft characteristics and handling qualities criteria in the conversion mode. In an attempt to fill such gaps, pilot-in-the-loop simulations were performed to evaluate the handling qualities of an XV-15 model, particularly in the roll axis. A roll-step test maneuver was designed to expose the deficiencies in the critical responses including the roll attitude quickness, the roll attitude bandwidth and phase delay. Simulation results and pilot comments showed that the tracking tasks boundary in the ADS-33E is more appropriate to be used as the roll attitude quickness boundary for the XV-15. Also, the roll bandwidth and phase delay characteristics of the XV-15 in the conversion mode (60°nacelle angle) appeared to correlate well with the ADS-33E boundaries for helicopters in forward flight.

Rollet *et al.* [17] performed a study on the lateral and directional handling qualities of tiltrotor aircraft. Piloted simulation results exposed several handling qualities problems in all flight modes with (Stability Augmentation System) SAS off. In low-speed helicopter mode, significant PIO tendency in pitch, roll, and heave was discovered. Due to the large inertia and poor aerodynamic damping in yaw, the yaw response was judged sluggish during large amplitude rotations but small-amplitude heading change was rather easy to achieve. In forward flight helicopter mode, the handling qualities were rated level 2. Adverse dihedral effect and an evident decrease in pitch damping in steep climb conditions were also reported by pilots. This study did not cover the handling qualities of flight in the conversion mode, only conversion and reconversion maneuvers were considered. Apart from the need for pilots to compensate for the large trim changes in pitch, conversions and reconversions were judged easy to achieve. In airplane mode, three problems were discovered. The first was the oversensitivity in pitch, which was fixed by increasing the control force with airspeed. The second problem was the insufficient stiffness and damping in pitch at high altitude. Besides using the SAS to fix this problem, Rollet *et al.* also suggested that enlarging the stabilizer could be another solution. The third problem was the poor damping in yaw. This phenomenon became worse when the altitude increased and eventually led to divergent dutch-roll mode beyond 3000m. Again, switching on the SAS helped the aircraft restore level 2 handling qualities.

LONGITUDINAL HANDLING QUALITIES

Padfield and Meyer [15] and Cameron and Padfield [18] studied the pitch-axis handling qualities of tiltrotor aircraft. They discussed the inconsistency between the pilot ratings from piloted simulation tests and the predicted handling quality levels based on the frequency and damping of the short-period dynamics, pitch bandwidth, and the control anticipation parameter. The difference was caused by the adverse effects of the attitude dropback, which were solved by referring to Gibson's dropback parameter. Ref. [18] exceeds the scope of Ref. [15] in that a new handling quality parameter that can be used together with the CAP to capture the influence of the dropback in one single criterion was derived. The key process and results of these two articles are presented as follows to help gain insights into the pitch-axis handling problems.

Figure I.5a from Ref. [15] shows the pitch attitude quickness of the XV-15 model in all modes with SCAS off plotted together with the boundaries from both ADS-33E tracking tasks and MIL-STD-1797A. It was concluded that the aircraft should possess adequate performance in the pitch axis to fly moderately aggressive tasks in all modes. The performance margin also increases with flight speed. The short period mode was also studied. The root loci of the short period mode for different IAS (Indicated airspeed) and configurations were given in Figure I.5b from Ref. [15]. As the IAS increases and the aircraft converts from helicopter to airplane mode, the damping ratio reduces and the short period frequency increases. In the airplane mode, 200knots, 6000m density altitude, the damping ratio reduces below the 0.35 level 1 boundary. Another parameter, the incidence lag ($T_{\theta 2}$) which also influences the pitch handling qualities, was discussed as well. The incidence lag is the lag between the flight path and pitch attitude response after an elevator step input. The transfer function of the flight path to pitch attitude response is shown in Equation I.1.

$$\frac{\gamma}{\theta} = \frac{1}{T_{\theta 2} s + 1} \tag{I.1}$$

The lag $T_{\theta 2}$ can be approximated using Equation I.2. The denominator Z_w is the heave damping, which is the

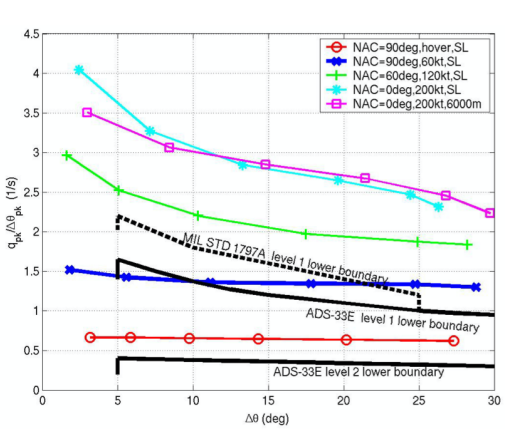

(a) XV-15 pitch attitude quickness (SCAS off). (NAC=nacelle angle, SL=sea level

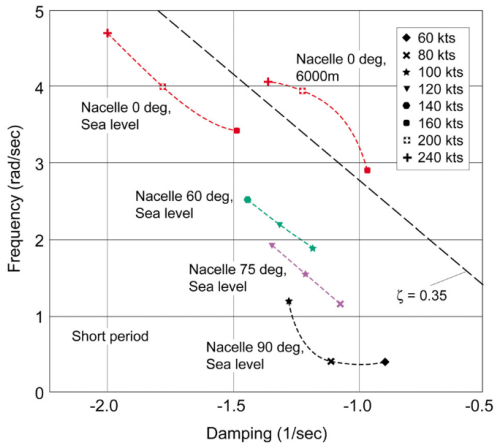

(b) XV-15 short-period mode root loci (SCAS off)

Figure I.5: XV-15 pitch attitude quickness and short-period mode root loci [15]

derivative of the body vertical force w.r.t. a step change in the body vertical velocity.

$$T_{\theta 2} = -\frac{1}{Z_w} \tag{I.2}$$

This lag results in an overshoot in the pitch response before the stiffness (M_w, the derivative of pitching moment w.r.t a step change in the body vertical velocity) due to the incidence change starts to pull the nose towards the opposite direction. Padfield and Meyer [15] described that this overshoot, if large, can make it difficult for pilots to predict the control movement required to achieve a given attitude change. Gibson [19] presented the generic pitch time response as shown in Figure I.6, in which other parameters including the dropback, the steady-state pitch rate, the peak pitch rate, etc. were defined, which will be discussed later.

Incidence lag was treated more in detail by Cameron and Padfield in Ref. [18]. According to the flight simulation results, the incidence lag decreases with airspeed for XV-15 in airplane mode. Though too large a pitch rate overshoot should be avoided, pilots may prefer some overshoots because this provides a faster response to a control input. [18] Furthermore, the dropback should never become negative as this will lead to a sluggish and unpredictable response. Later in Ref. [18], the control anticipation parameter (CAP) was included to capture the complex pitch response. The control anticipation parameter is a measure of predictability of the pitch responses of fixed-wing aircraft. Before the introduction of CAP, the evaluation of short-period dynamics were based on the "thumbprint" plot, in which the short-period undamped natural frequency is plotted against the short-period damping ratio. The thumbprint plot fails to account for the zeros in the numerator of the short period transfer function, specifically the $1/T_{\theta 2}$, as shown in equation I.3. [20]

$$\frac{q(s)}{\delta_e(s)} = \frac{M_{\delta_e}(s + \frac{1}{T_{\theta 2}})}{s^2 + 2\zeta_{sp}\omega_{sp}s + \omega_{sp}^2} \tag{I.3}$$

Bihrle [21] introduced the CAP to tackle this. CAP is defined as the ratio of initial pitch acceleration ($\dot{q}(0)$) to steady-state normal acceleration ($\dot{n}(\infty)$).

$$CAP = \frac{\dot{q}(0)}{\dot{n}_z(\infty)} \tag{I.4}$$

Cotting [20] made an intelligible explanation of the meaning of the CAP:

> The human vestibular system is very sensitive to pitch acceleration and is the first feedback to the pilot that the aircraft is changing motion. The desired aircraft pitch change results in an angle of attack (α), and ultimately a change in g-loading on the aircraft as the flight path changes. This g-loading (n_z) of the aircraft is sensed by the pilot and is used to command aircraft flight path. Closing this loop by the human requires that the dynamic relationship between pitch attitude acceleration and aircraft loading be within human sensing capabilities. [20]

Gibson [19] pointed out that CAP was widely misunderstood to be a measure of the quality of attitude response. As explained by Cotting, the g-loading due to a change in angle of attack sensed by the pilot is used to

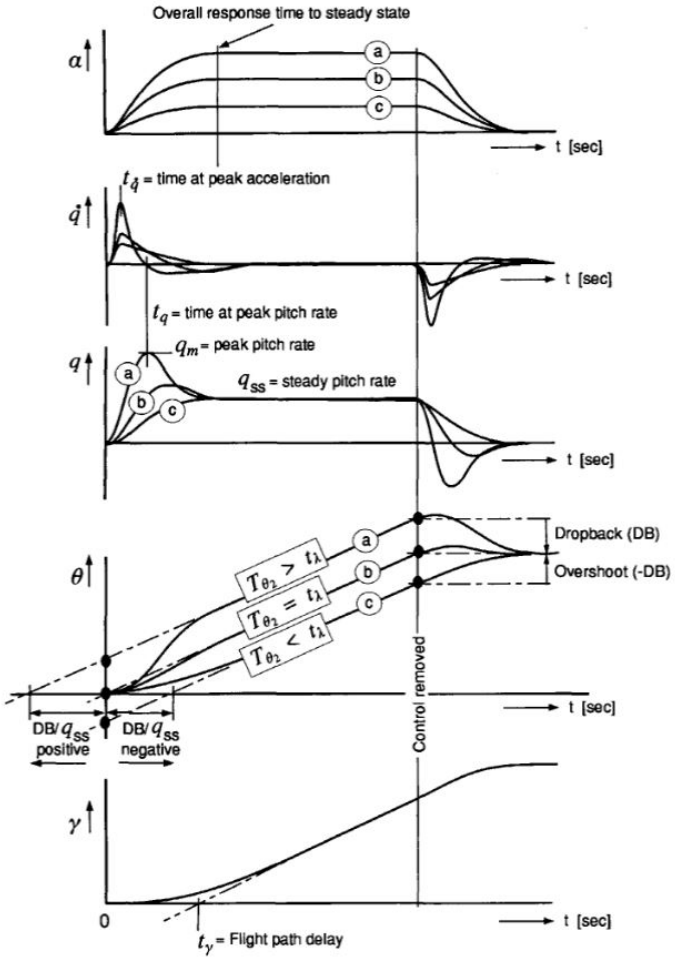

Figure I.6: Generic pitch short period time response [19]

predict the flight path change. In fact, CAP is a measure of predictability in flight path control, where the incidence lag is an important parameter. The following derivations demonstrate how the incidence lag is related to the CAP [22].

Recalling Equation I.3, the pitch attitude to elevator input transfer function can be expressed as:

$$\frac{\theta(s)}{\delta_e(s)} = \frac{M_{\delta_e}(s+\frac{1}{T_{\theta 2}})}{s(s^2+2\zeta_{sp}\omega_{sp}s+\omega_{sp}^2)} \tag{I.5}$$

Thus, the pitch acceleration to elevator input transfer function is:

$$\frac{\ddot{\theta}(s)}{\delta_e(s)} = \frac{s^2\theta(s)}{\delta_e(s)} \tag{I.6}$$

Using the initial value theorem of Laplace transform, the initial pitch acceleration to a unit step elevator input can be calculated as:

$$\ddot{\theta}(0) = s\ddot{\theta}(s)\Big|_{s\to\infty} = \frac{\theta(s)}{\delta_e(s)} = \frac{s^2(M_{\delta_e}(s+\frac{1}{T_{\theta 2}}))}{s^2+2\zeta_{sp}\omega_{sp}s+\omega_{sp}^2}\frac{1}{s}\Big|_{s\to\infty} \approx M_{\delta_e} \tag{I.7}$$

The steady state normal acceleration can be written as:

$$n_z(\infty) = \frac{V}{g}q(\infty) \tag{I.8}$$

In which the steady state pitch rate to a unit step elevator input can then be calculated using the final value theorem:

$$q(\infty) = s\frac{s\theta(s)}{\delta_e(s)}\frac{1}{s}\Big|_{s\to 0} = \frac{M_{\delta_e}(s+\frac{1}{T_{\theta 2}})}{s^2+2\zeta_{sp}\omega_{sp}s+\omega_{sp}^2}\frac{1}{s}\Big|_{s\to 0} \approx \frac{M_{\delta_e}\frac{1}{T_{\theta 2}}}{\omega_{sp}^2} \tag{I.9}$$

Hence,

$$CAP = \frac{\ddot{\theta}(0)}{n_z(\infty)} \approx \frac{g}{V}\frac{M_{\delta_e}}{\frac{M_{\delta_e}\frac{1}{T_{\theta 2}}}{\omega_{sp}^2}} = \frac{g\omega_{sp}^2 T_{\theta 2}}{V} \tag{I.10}$$

In Ref. [18], Cameron and Padfield obtained level 1 handling qualities for precision tracking tasks using bandwidth and CAP criteria. The heave-hop MTE was selected to evaluate the pitch and flight path handling qualities in the small amplitude-high frequency region. A series of piloted simulation tests demonstrated that the handling qualities of XV-15 only met level 2 in such tasks. Cameron and Padfield quoted the method proposed by Mitchell *et al.* [23] who noticed that responses with large attitude rate overshoots fail to meet the CAP or bandwidth criteria. It was suggested that the handling quality levels can be predicted correctly by jointly using the dropback parameter and the CAP/bandwidth criteria. Figure I.7a illustrates how to obtain the parameters needed by the dropback criterion. The dropback criterion compares the ratio of the peak to steady-state pitch rate with the ratio of pitch attitude dropback to the steady-state pitch rate. As shown in Figure I.7b, if the resulting point lies above the boundary line, the handling quality level based on CAP/bandwidth should be degraded by one level. If the point lies below the boundary line, the handling qualities remain the same.

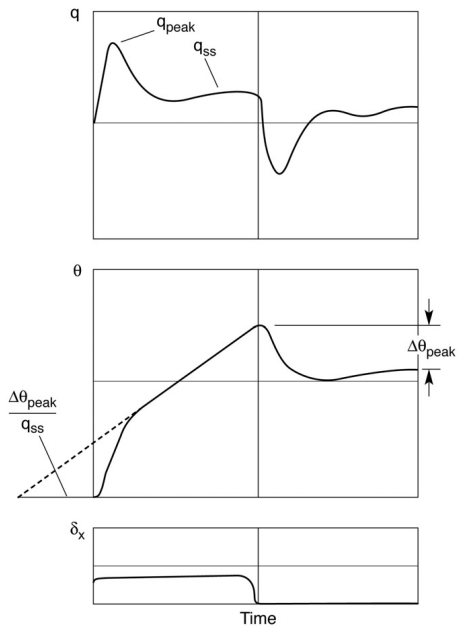

(a) Pitch response to pulse longitudinal input - dropback definition

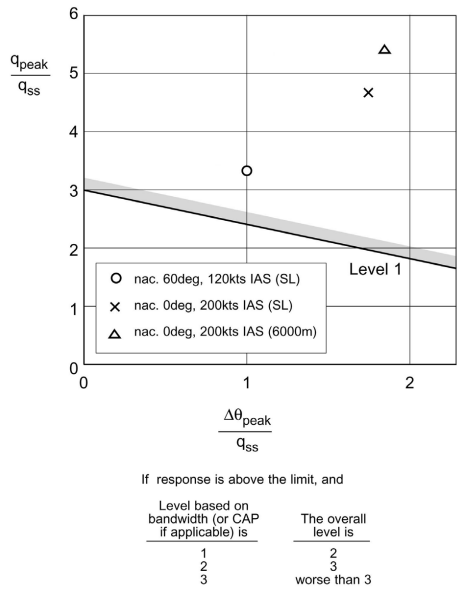

(b) Pitch dropback - overshoot criteria

Figure I.7: Pitch dropback - overshoot definition and criteria [15]

Padfield and Meyer [15] concluded that for pitch maneuvers, ADS-33E is appropriate for tiltrotor aircraft in low-speed helicopter mode while fixed-wing criteria are needed in conversion and airplane modes. In Figure I.8 from Ref. [15], the XV-15 responses to a 1-inch step longitudinal control input were plotted for all 3 modes, which clearly shows that the pitch rate response, pitch attitude response, and flight path response of the XV-15 in conversion mode resemble that in airplane mode. For the XV-15 in helicopter mode, the pitch attitude settles to a steady value, while in conversion and airplane mode the pitch rate settles to a steady value. In conversion and airplane mode, the pitch attitude and flight path angle will settle to an almost constant slope while in helicopter mode, the flight path angle will start to drop shortly after the input. However, the pitch rate overshoot and dropback in conversion mode behave similarly to that in helicopter mode because they do not show a significant overshoot and dropback as observable in the airplane mode. This is because

in airplane mode, the large in-plane prop-rotors make positive contributions (destabilizing) to the pitching moment derivative M_w, causing the damping ratio of the short period mode to reduce. Moreover, the heave damping Z_w is also relatively low, leading to a slow build-up in lift. [18] These factors together result in the large pitch rate overshoot and pitch dropback.

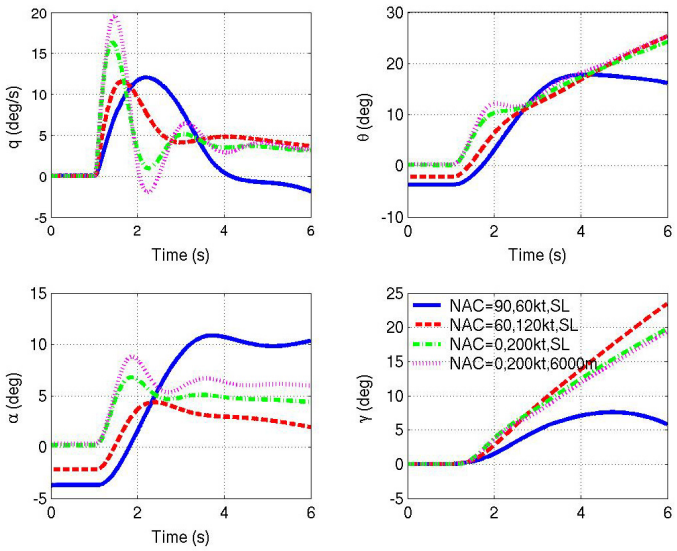

Figure I.8: XV-15 response to a 1 inch step longitudinal control input SCAS off [15] (NAC=nacelle angle, SL=sea level)

These studies disclose the complexity of the handling qualities problems on the tiltrotor aircraft. The mixed-use of helicopter and airplane responses criteria are required. Since the goal of this section is to prepare the knowledge to help understand the tiltrotor handling qualities characteristics in the conversion mode, several key conclusions from these studies that are considered useful for this thesis project are summarized below:

- The bare-airframe handling qualities levels of the XV-15 are usually level 2 or level 3.
- For XV-15-sized tiltrotor aircraft which are designed to perform the search and rescue mission, the tracking tasks boundary in the ADS-33E is more appropriate for most of the tasks.
- For pitch maneuvers, ADS-33E is appropriate for tiltrotor aircraft in low-speed helicopter mode while fixed-wing criteria are needed in conversion and airplane modes.
- The roll bandwidth and phase delay characteristics of the XV-15 in the conversion mode (60°nacelle angle) appeared to correlate well with the ADS-33E boundaries for helicopters in forward flight.
- The damping in yaw is insufficient in both helicopter and airplane modes. The damping in pitch may become insufficient at high altitude. These suggest the option to increase the area of the empennage.
- When using the CAP and bandwidth criteria, the pitch rate overshoots and the pitch attitude dropback should also be taken into account.

Furthermore, the problem of couplings between axes also troubles the handling qualities of the tiltrotor aircraft at high speeds in conversion mode. For example, the proverse roll-yaw coupling will occur due to the differential collective control. Careful design of the gearing between airplane and helicopter controls as a function of nacelle angle can alleviate this problem. Also, a heave-surge coupling due to the application of collective pitch will upset speed control during flight-path adjustment. This can be treated with a better gearing design between elevator and helicopter controls.

4. DESIGN FOR HANDLING QUALITIES

As discussed in the previous section, in the early days of aircraft, especially rotorcraft development, handling qualities were treated as an outcome of the overall design and were left until flight test to evaluate and fix. This

can result in project delay and a large amount of cost if severe deficiencies are found after the completion of the overall design and manufacturing. Padfield [8] suggested that handling qualities were not given their proper place in the early design trade-space. With mature standards, comprehensive design tools, and high computation power at hand, handling qualities should feature at the highest level in the system architecture and be addressed substantially in preliminary design. Though nowadays the massive application of fly-by-wire system enables us to tune the stability and control augmentation system (SCAS) to modify the output handling qualities of the aircraft, the inherent bare-airframe handling qualities should never lose its importance for two reasons. 1) The bare-airframe handling qualities influence the safety of flight in case of failure of the stability augmentation systems. As specified in ADS-33E, the complete or partial loss of any function of the flight control system shall not cause dangerous or intolerable flying qualities. 2) Better bare-airframe handling qualities can make it easier for designers to tune the handling qualities later and give the aircraft more margins in future improvements. Padfield emphasized in Ref. [14] that the requirements in the modern handling quality standards drive for more sophisticated flight control augmentation system and careful design of the interface between pilots and autopilot functions, but it is always worth considering to improve natural stability with aerodynamic 'fixes' which reduce the requirements on the control augmentation system when upgrading the handling qualities of an existing design.

With the intention to improve the bare-airframe handling qualities of tiltrotor aircraft with aerodynamic "fixes", this section will introduce the methodologies applied by other authors [7] [24] [25] who have taken efforts to investigate and improve rotorcraft maneuverability and stability. Though their goals differ from the current project, maneuverability and stability are essentially subsets of handling qualities. Thus, reviewing their work is beneficial in terms of learning how to approach the design problems. Besides the methodologies themselves, some figures showing important results from the literature are also presented here. This thesis can learn from these figures on how to perform the analysis and how to present the results. In addition, these results can provide information about the selection of design parameters and the influence of these design parameters on aircraft performance.

4.1. DESIGN METHODOLOGIES

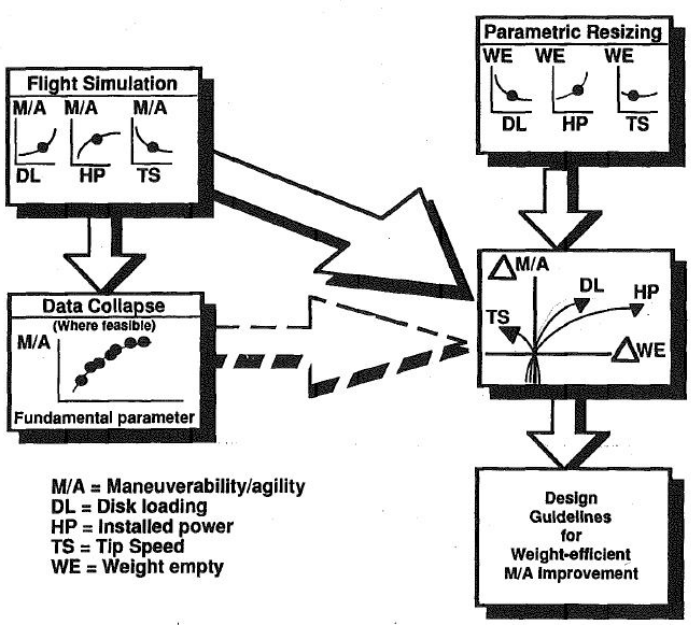

Figure I.9: Design approach used by Ref. [24]

Oslon and Scott presented a methodology in Ref. [24] for the investigation of the influence of the design parameters on the maneuverability of a single main rotor helicopter. The design process is illustrated in Figure I.9. Eight maneuvers, which can reflect the rate of climb, acceleration and deceleration capability, etc. were selected for the study. To ensure the identical maneuvers being commanded repeatedly, a maneuver controller was adopted to adjust the control inputs based on the errors between the actual maneuver flown and the reference state. The measure of maneuverability for each maneuver was defined differently according

to the characteristics of the maneuver. For example, the measure of maneuverability of acceleration is the elapsed time to accelerate to a certain speed and that of pull-up maneuver is the maximum achieved load factor. Six design variables, namely the disk loading, blade loading, installed power, tip speed, flapping hinge offset, and blade lock number, were selected. Disk loading characterizes the hover performance and shows how loaded is the rotor. Usually, low disk loading indicates high thrust efficiency. Rotor solidity is the ratio of total blade area to disk area. It impacts the stall margin or the maneuverability potential of the rotor. Blade loading shows how loaded is the blade and indicates how close to stall is the blade operating. Rotor tip speed characterizes the noise and the performance of the rotor. Blade flapping hinge offset is the offset of blade hinge to rotor center. This offset strongly affects the dynamic response of the blade. Blade lock number is the ratio of the aerodynamic force to the inertia force acting on a blade. It influences the dynamic response of the rotor and the autorotative landing capability of the aircraft. By varying each design parameter independently, the sensitivity of each maneuver to design parameters were established. In some cases, the effects of some design variables on one maneuverability measurement could be captured by a more fundamental parameter which served as a common denominator for these different design variables. Where feasible, that fundamental parameter was utilized to plot the trends. It was called "collapse" of the trends in their article. Figure I.10a shows the example where the fundamental parameter for the bob-up maneuver was the thrust-to-weight ratio and the effects of four design variables were summarized by it. Those design parameters which had significant influences on the maneuvers are illustrated in Figure I.10b, where the direction of the arrow indicates whether that parameter needs to increase or decrease to improve that maneuver.

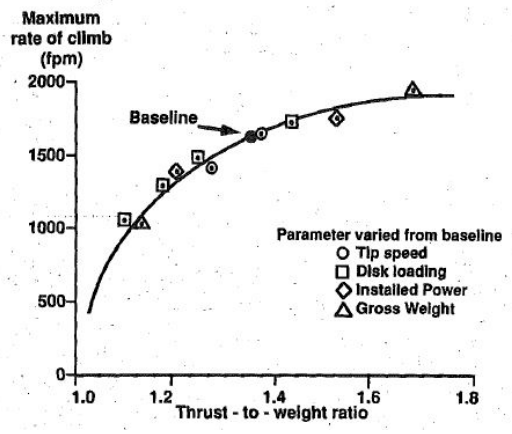

(a) Collapse of hover bob-up performance using thrust-to-weight ratio

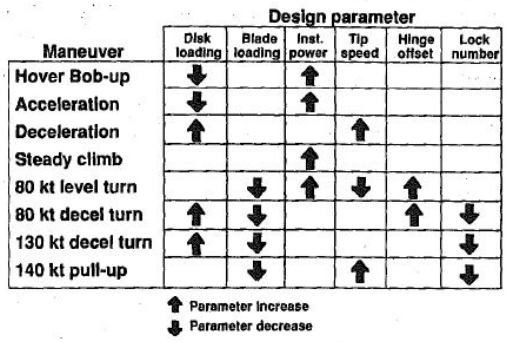

(b) Design parameters with major influence on maneuvers

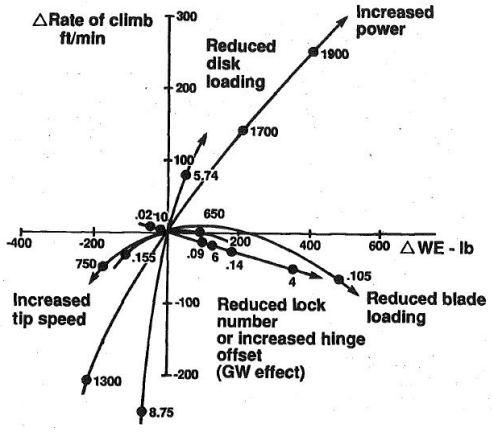

(c) Sensitivity of rate of climb to weight for individual design parameters

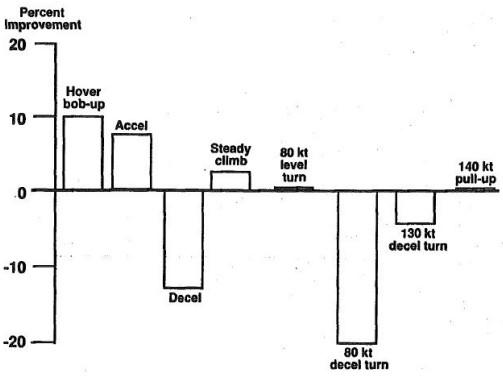

(d) 100 pounds weight investment to reduce disk loading

Figure I.10: Type of plots in Ref. [24]

In addition, Oslon and Scott investigated the weight change. The baseline helicopter was resized after each change of the design parameters to maintain its capability to perform the same mission. Figure I.10c illustrates the impact of various design changes on the rate of climb and the associated weight change. The curve that has the highest slope (i.e., reducing the disk loading) means that this design change is the most

efficient one in improving the rate of climb in terms of bringing the least amount of weight penalty. Finally, Oslon and Scott discussed the design for overall maneuverability. It was argued that most design changes have influences on more than one maneuver, but the influence may be in the opposite direction. The impact of 100 pounds weight investment to reduce the disk loading is shown in Figure I.10d, in which the climb and acceleration performance were improved but the deceleration performance was decreased.

Patterson *et al.* [25] developed a design methodology for rotorcraft maneuverability during the conceptual design phase, as shown in Figure I.11. They utilized several powerful design tools but the design process is, in essence, similar to that applied by Oslon and Scott [24]. The major difference is that the methodology developed by Patterson *et al.* focuses on the conceptual design phase where no baseline model is available. Therefore, they first had the design goal and configuration defined, which was, in their example, designing a coaxial helicopter with a pusher propeller for high maneuverability and agility. The acceleration, deceleration, longitudinal and lateral quickness, and power loading were selected as design metrics. Before starting the design process, a screening design was run to identify the parameters that had major influences on the design metrics. Next, these selected design parameters were varied within the prescribed range utilizing the design of experiments [2] to generate the design space, represented by the response surface [3]. After the completion of the response surface, a prediction profiler was used to visualize the response surface equations which were in the form of second-order polynomials. As illustrated in Figure I.12, the prediction profiler shows the sensitivity of each design metric (on the vertical axis) to each design parameter (on the horizontal axis) at the design point. Designers can adjust each design parameter to observe the changes in the trends instantaneously.

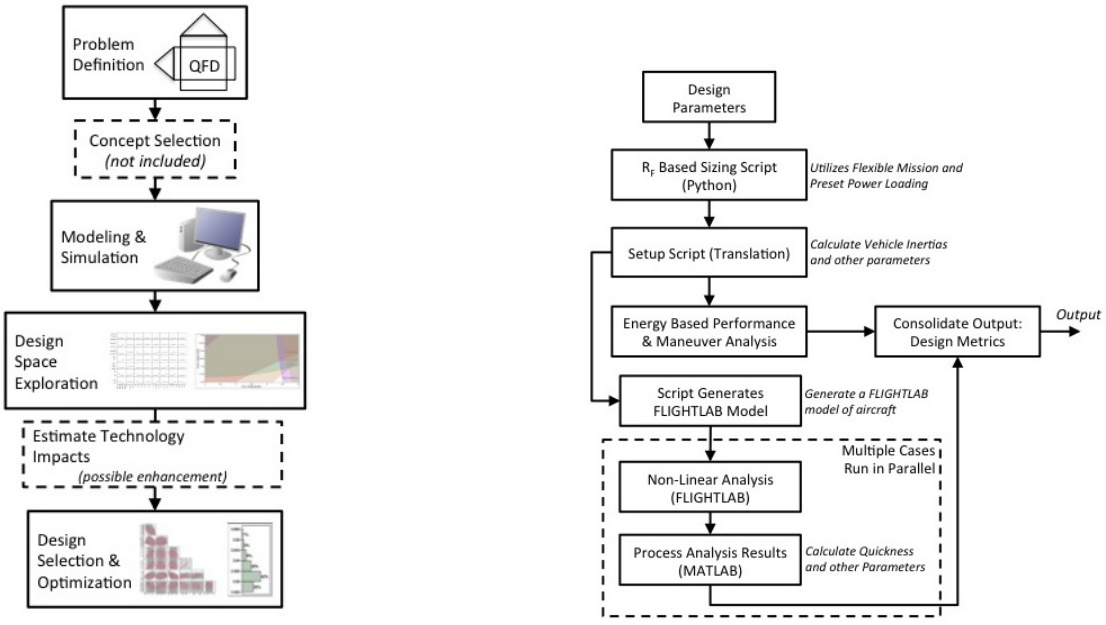

(a) General methodology

(b) Model and simulation (M&S) environment

Figure I.11: Methodology and M&S environment used in Ref. [25]

Another tool used by Patterson *et al.* [25] is the design space contour plot as shown in Figure I.13. In this plot, the design metrics, the power loading, and the disk loading make up the axes. The design metrics are plotted as shaded constraints, which can be varied by adjusting the design parameters. The white space

[2] The design of experiments (DoE) is the design of any task that aims to describe and explain the variation of information under conditions that are hypothesized to reflect the variation. An experiment aims at predicting the outcome by introducing a change of the preconditions, which is represented by one or more independent variables, also referred to as "input variables" or "predictor variables." The change in one or more independent variables is generally hypothesized to result in a change in one or more dependent variables, also referred to as "output variables" or "response variables." ("Design of experiments", Wikipedia, last modified 21 December 2020, https://en.wikipedia.org/wiki/Design_of_experiments)

[3] In statistics, response surface methodology (RSM) explores the relationships between several explanatory variables and one or more response variables. The method was introduced by George E. P. Box and K. B. Wilson in 1951. The main idea of RSM is to use a sequence of designed experiments to obtain an optimal response. ("Response surface methodology", Wikipedia, last modified 19 December 2020, https://en.wikipedia.org/wiki/Response_surface_methodology)

remaining represents the feasible design space. This tool helps the designers understand how the design parameters affect the design metrics which in turn alter the design space.

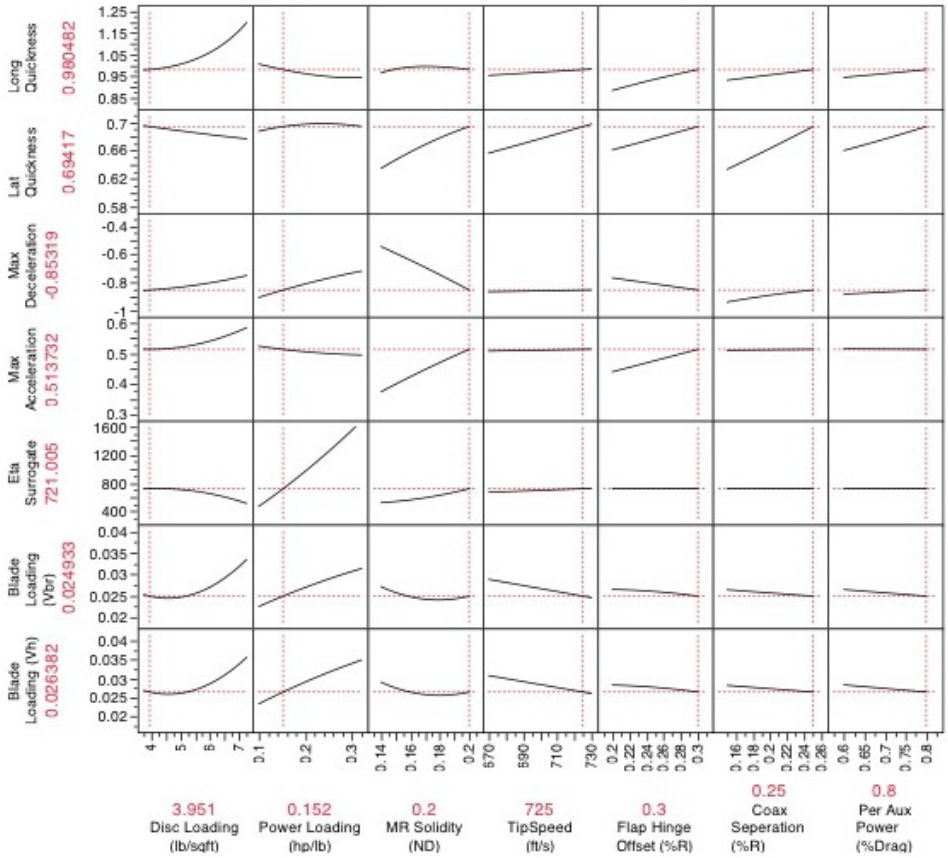

Figure I.12: Prediction profiler [25]

In Ref. [7], Lawrence *et al.* presented a tool, SIMPLI-FLYD, which can perform modelling and analysis for the assessment of the handling qualities of the rotorcraft conceptual designs. The architecture of this tool is illustrated in Figure This tool integrates the flight dynamic modelling, control system modelling, and control gains optimization. The output includes control and stability derivatives, HQ parameter values, and HQ design margins for each axis at the specified flight condition. Since this thesis project will focus on the bare-airframe handling qualities, the control augmentation system included in SIMPLI-FLYD is not of interest. In the results section, Lawrence *et al.* demonstrated the capability of this tool by conducting a sensitivity analysis on the effects of design parameters on the control and stability derivatives. Two cases were analyzed, one is the pitch axis of an XV-15 like tiltrotor in airplane mode at 200 knots, the other one is the yaw axis of a UH-60A like helicopter in hover. The results shown in Figure I.15 is the tiltrotor case. The vertical axis contains the names for the stability and control derivatives being examined. The bottom axis is for the names of the input parameters. The third axis is for the value of the sensitivities which is calculated using equation I.11.

$$\frac{\partial(\frac{\partial X_i}{\partial x_k})}{\partial P_j} = \left| \frac{\frac{\partial X_i}{\partial x_k}_{(-P_j)} - \frac{\partial X_i}{\partial x_k}_{(+P_j)}}{2P_j} \tau \right|, P_j = W_j \Delta_j \tag{I.11}$$

The enlightening part of their study is that the sensitivity derivatives $\frac{\partial X_i}{\partial x_k}$ were scaled using the scaling parameter τ to allow fairly comparisons among different derivatives. The perturbation variables P_j have been weighted to ensure a plausible amount of perturbations been applied to different input parameters such that the effect of them on the overall aircraft can be compared equally. An example used by Lawrence *et al.* to explain this was that perturbing rotor radius and chord by the same dimensional amount would be inappropriate.

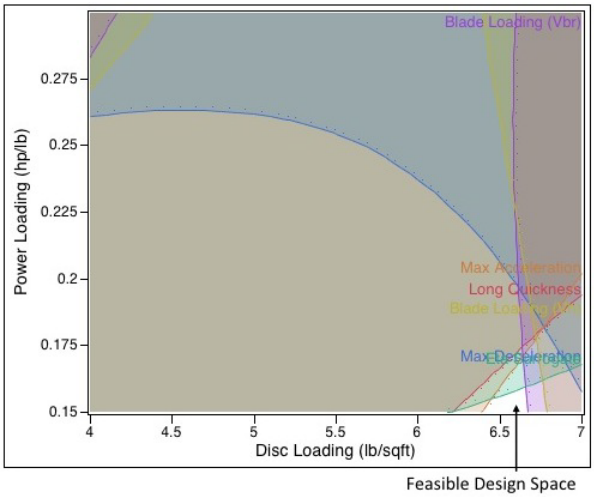

Figure I.13: Design space contour plot [25]

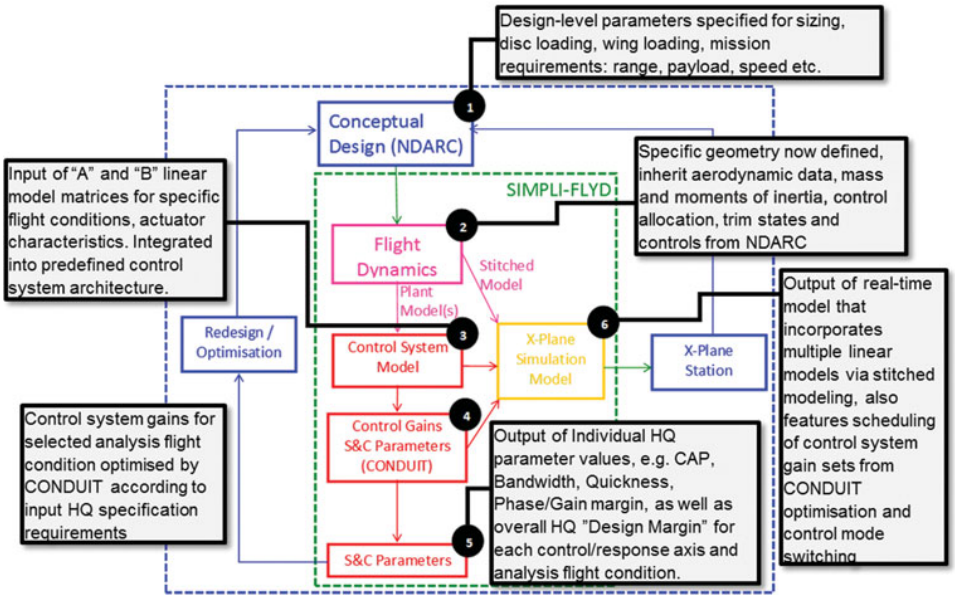

Figure I.14: SIMPLI-FLYD architecture [7]

In summary, the core of all these methodologies is the sensitivity analysis, which reveals the sensitivity of each design metric to each design parameter. These three studies take different approaches to perform sensitivity analysis. Probably due to the lack of computation power and analysis tools at that time, Oslon and Scott [24] could only analyze the sensitivity of one or two performance metric(s) to the change in design parameters each time. Only the major trends could be obtained when comparing the sensitivity results of multiple design metrics together. With the availability of more advanced computers and tools, Patterson *et al.* [25] and Lawrence *et al.* [7] were able to integrate the results together to show the complete picture of the sensitivity results. In the design case presented by Patterson *et al.*, 20000 random designs were automatically generated to create the response surfaces. The prediction profiler, based on these response surfaces, adopted by them is so powerful that it allows the designer to freely modify each design input and reflects the influence of the shift in design point on every design metric simultaneously. This is very helpful in the early design phase when designers do not have a clear picture of how each design parameter affects the design metrics. Moreover, the design space contour plot enables the visualization of the feasibility of each design, which assists the designers to set reasonable design goals. In the tool proposed by Lawrence *et al.*, sensitivity results were scaled to allow fair comparisons among different sensitivity results. This helps in terms of locating the

most influenced design parameters which differ in dimensions. For this thesis project, because no previous study has investigated the same design problem, gaining understandings of the effects of design parameters and design metrics on the design space is crucial for the successful formulation of the optimization problem later.

4.2. OPTIMIZATION METHOD

In addition to the attempt to gain knowledge of the influence of the design parameters on the handling qualities, the author also plans to incorporate the final optimization process, during which the design parameters are tuned to obtain the desired handling qualities, into this thesis project.

Continuing the sensitivity analysis presented in the last section, Patterson *et al.* [25] also introduced an optimization method based on the Joint Probabilistic Decision Making technique [26].

1. Generate a joint cumulative probability distribution, as given in Equation I.12 and I.13. $F(x_1, x_2, ..., x_m)$ denotes the probability of the events $X_1 = x_1, X_m = x_m, ..., X_m = x_m$ happening simultaneously. x_i denote the target values which are the desired values of the design metrics, while a_i stand for the sample values of the design metrics.

2. Calculate the probability of success (POS) (Equation I.14) which reflects the feasibility of a design. The minimal and maximal values of a design metric are up to the designer to set. Too big a POS indicates the design goal is too low while too small a POS indicates the design goal is too stringent, meaning that a small design change could lead to an infeasible design. Therefore, the range of each design metric should be determined carefully to ensure a feasible and competitive design.

3. Use gradient-based methods to obtain a set of design parameters that bring about the optimized design goals.

$$F(x_1, x_2, ..., x_m) = \frac{1}{m} \sum_{i=1}^{m} I(a_{i1} \leq x_1, a_{i2} \leq x_2, ..., a_{im} \leq x_m) \tag{I.12}$$

$$\frac{1}{m} \sum_{i=1}^{m} I(a_{i1} \leq x_1, a_{i2} \leq x_2, ..., a_{im} \leq x_m) = \begin{cases} 1, for(a_{i1} = x_1, a_{i2} = x_2, ..., a_{im} = x_m) \\ 0, otherwise \end{cases} \tag{I.13}$$

$$POS = \frac{1}{m} \sum_{i=1}^{m} I(x_{imin} \leq a_i \leq x_{imax}) \tag{I.14}$$

This joint-probabilistic method is very suitable for situations where designers possess incomplete knowledge about the system and the design goals. It is often the case that multi-criteria optimization methods require deterministic information about the criteria, however, this kind of information may be inadequate for those fields which few studies have touched upon. The handling qualities of tiltrotors is one of those fields. The previous literature review has shown that currently, no specific handling qualities standard exists for tiltrotor aircraft, and only a limited number of researches have been done to study the handling qualities in the helicopter mode and the airplane mode. The handling qualities in the conversion mode have barely been carefully treated. Moreover, for flight in the conversion mode, the sensitivity of handling qualities metrics to design parameters has never been studied. As a result, during the optimization phase, the author of this thesis project does not have the knowledge of how much can each of the selected handling quality metrics being improved. For instance, if the baseline model demonstrates level 2 handling quality in pitch bandwidth under certain flight conditions, what would be the goal of the improvement? It is possible that no feasible design solution can be found if level 1 is the goal, or other metrics degrade heavily in the meantime. Therefore, the joint probability distribution can be very helpful in terms of helping the designer to understand the influence of the values of the design metrics on the design space so that reasonable and balanced design goals can be determined.

5. RESEARCH QUESTION

The literature study has disclosed the knowledge gaps in tiltrotor handling qualities in conversion mode. No systematic approach has been taken to investigate the influences of design parameters on the bare-airframe handling qualities in conversion mode. The objective of this thesis is to add knowledge to these gaps and to

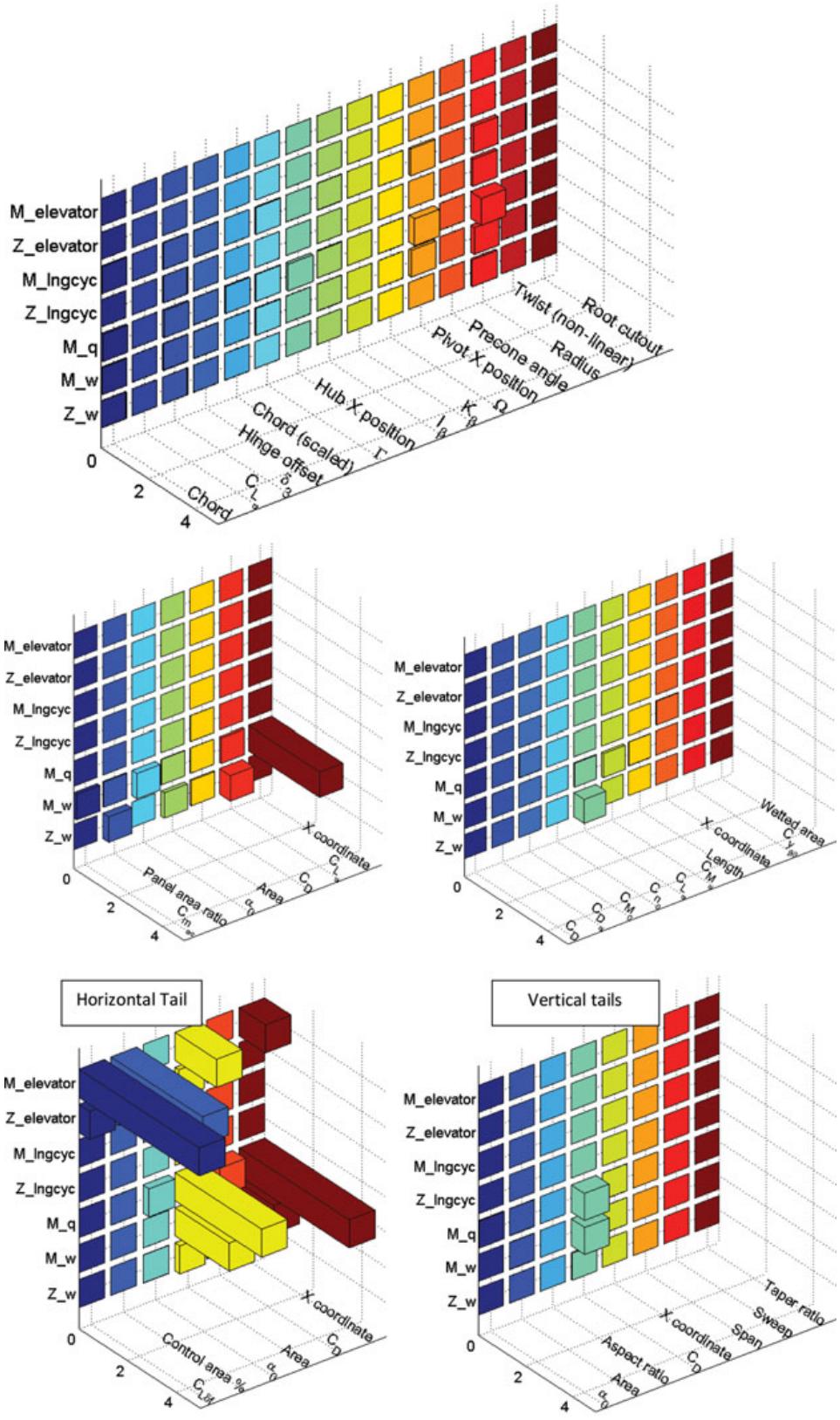

Figure I.15: Sensitivity of component pitch stability and control derivatives to input parameters [7]

form design guidelines for better bare-airframe handling qualities in conversion mode. The main research question is then formulated:

How to improve the bare-airframe handling qualities of the XV-15 tiltrotor aircraft in conversion mode?

The basis of this thesis is a good flight dynamic model of the XV-15 tiltrotor aircraft. In the Control and Simulation group of the Faculty of Aerospace Engineering at TU Delft, a 3 degrees of freedom (DoF) flight dynamic model of the XV-15 tiltrotor aircraft was developed prior to this thesis. This model has been chosen as the baseline model in this thesis. But some improvements and extensions need to be done before this model is ready to be used for this study. Therefore, to answer the main research question, this thesis is divided into three stages.

1. Stage 1: Improve the TU Delft in-house 3-DoF XV-15 tiltrotor model and implement necessary functions.
2. Stage 2: Use the improved tiltrotor model to locate the handling qualities deficiencies.
3. Stage 3: Select design parameters, generate and explore the design space.
4. Stage 4: Perform the optimization to find the optimal set of design parameters.

Stage 1 prepares the flight dynamic model for this study. The main research question is then broken down into three sub-questions corresponding to Stage 2, 3, and 4. These sub-questions are ordered in such a way that each of them provides the necessary knowledge for answering the next question.

1. *What are the existing problems of the handling qualities of the XV-15 tiltrotor aircraft in conversion mode?*
2. *What are the design parameters to be selected and how do they influence the handling qualities?*
3. *How to find the optimal values of design parameters?*

6. LAYOUT OF THE REPORT

Chapter 2 describes 3-DoF XV-15 tiltrotor model and the improvements done to it. It also includes the mathematical description on the trim and linearization process. Chapter 3 introduces the selected handling qualities parameters. The definition of these parameters are explained. The handling qualities over the flight envelope are investigated. In Chapter 4, the design parameters are selected and the weight evaluation methods are described in detail. The analysis tool developed in this study is introduced and the results of the design space exploration are presented. Six optimization cases are performed to investigate the trade-offs in design and the influences of constraints. In Chapter 5, reasonable conclusions are made to answer the research questions. Finally, the recommendations for future work are outlined.

II

Flight Dynamics Model

1. Introduction to the 3-DoF XV-15 tiltrotor model

The original TU Delft in-house model of the XV-15 tiltrotor aircraft is a 3-DoF model describing the longitudinal dynamics. It has been selected as the baseline model of this study. Figure II.1 sketches the important angles, aerodynamic forces and moments, and body reference frame of this model. The rotor is modelled as an articulated type using the Blade element momentum theory (BEM), with H-force and hub spring included. The flapping equation is solved using the quasi-static solution, which assumes that all transients decay rapidly and the blade flaps in simple harmonic motion, limited to the first harmonic and a steady term (conning angle). The wing downwash angle and flap/flaperon in the figure are not modelled in the baseline model but have been added into the improved model.

The computation scheme of the model is illustrated in Figure II.2. The blade element momentum theory uses nondimensional aerodynamic velocities. The convergence of the thrust coefficient based on the BEM method and the Glauert theory gives the longitudinal disk tilt angle, inflow ratio, and thrust coefficient. Next, the coning angle and later disk tilt can be obtained. With these parameters, the thrust, the H-force, and the hub spring reaction moment are then calculated. The aerodynamic forces and moments generated by the wing, the horizontal tail, and the fuselage are calculated in their local reference frames. Finally, all forces and moments are transformed to the body reference frame (attached to the CG) and summed to compute the state derivatives.

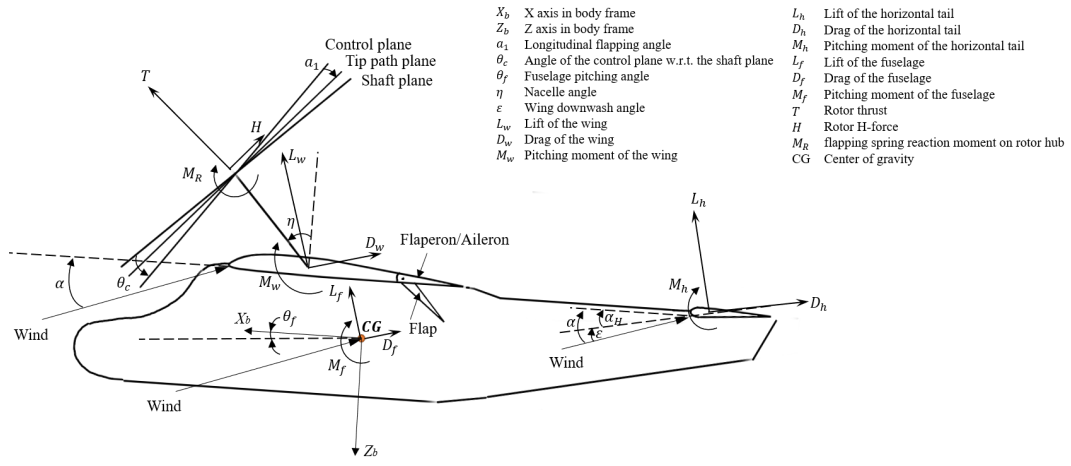

Figure II.1: Forces and moments acting on the XV-15 tiltrotor model (vertical tails not shown)

The inputs to the model are states, state derivatives, and controls. The outputs are state derivatives. State variables include the body velocity in the x and z direction, pitch rate, and pitch angle:

$$[u, w, q, \theta_f]^T$$

Aircraft parameters:	Aircraft mass and moments of inertia; parameters and look-up tables of rotor, wing, horizontal tail, and fuselage.
Control settings:	η, flap/flaperon setting
Control variables:	X_{COL}, X_{LN}
State variables:	u, w, q, θ_f

$\theta_0 = f(X_{COL}, \eta)$ Gearing

$\theta_c = f(X_{LN}, \eta)$ Gearing

$V = \sqrt{u^2 + w^2}$

$\alpha_f = arctan\frac{w}{u}$

$\alpha_c = \eta + \theta_c - \alpha_f$

$\mu = \frac{Vcos\alpha_c}{\Omega R}$

$\lambda_c = \frac{Vsin\alpha_c}{\Omega R}$

Choose λ_i until $f(\lambda_i) = 0$
$a_1 = f(\mu, \lambda_c, \lambda_i, \theta_0, \theta_c, q, \Omega, \gamma, K_\beta)$
$C_{T\_BEM} = f(a_1, N, \mu, \lambda_c, \lambda_i, \theta_0, \theta_c, \gamma, K_\beta, R)$
$C_{T\_Glauert} = f(V, a_1, \alpha_c, \lambda_i, \Omega, \mathrm{R})$
$f(\lambda_i) = C_{T\_BEM} - C_{T\_Glauert}$

The following parameters are now known: λ_i, a_1, C_T

$a_0 = f(\mu, \lambda_c, \lambda_i, \theta_0, \theta_c, \Omega, \gamma, K_\beta)$

$b_1 = f(\mu, \lambda_c, \lambda_i, \theta_0, \theta_c, \Omega, q, \gamma, K_\beta)$

Blade loading limit: $\frac{C_{T\_max}}{\sigma} = f(\mu)$

$C_T = \min(C_T, C_{T\_max})$

$C_H = f(a_0, a_1, b_1, N, \mu, \lambda_c, \lambda_i, \theta_0, \theta_c, q, \Omega, \gamma, K_\beta, R, c, \delta_0, \delta_1, \delta_2)$

$T = 2 \cdot C_T \rho \pi R^2 (\Omega R)^2$

$H = 2 \cdot C_H \rho \pi R^2 (\Omega R)^2$

Forces and moments summation:

$X_{sum}, Z_{sum}, M_{sum}$ = Aerodynamic forces and moments of all components are transformed from their local reference frames to the body reference frame.

State derivatives:

$\dot{u} = -gsin\theta_f - qw + \frac{X_{sum}}{m}$

$\dot{w} = -gcos\theta_f + qu + \frac{Z_{sum}}{m}$

$\dot{q} = \frac{M_{sum}}{I_y}$

$\dot{\theta} = q$

Figure II.2: Computation scheme of the improved model

State derivative variables:

$$[\dot{u}, \dot{w}, \dot{q}, \dot{\theta_f}]^T$$

Control variables include the travel of collective lever and the travel of longitudinal stick:

$$[X_{COL}, X_{LN}]^T$$

The flap/flaperon and nacelle angle are control settings rather than control variables because they are selected prior to the start of the simulation and are not changeable during the simulation. Since the dynamic process of transition and flap deflection is not part of the study, this limitation will not influence the study. The computation scheme is shown in Figure II.2.

During the simulation, the process of updating state variables is as follows:

1. Using the initial condition to calculate the accelerations:

$$[\dot{u}_{t+1}, \dot{w}_{t+1}, \dot{q}_{t+1}, \dot{\theta}_{ft+1}]^T = MODEL\Big([u_t, w_t, q_t, \theta_{ft}]^T, [\dot{u}_t, \dot{w}_t, \dot{q}_t, \dot{\theta_{ft}}]^T, [X_{COL(t)}, X_{LN(t)}]^T\Big) \tag{II.1}$$

2. Update the state variables, where Δt is the simulation step length:

$$\begin{aligned} u_{t+1} &= u_t + \dot{u}_{t+1}\Delta t \\ w_{t+1} &= w_t + \dot{w}_{t+1}\Delta t \\ q_{t+1} &= q_t + \dot{q}_{t+1}\Delta t \\ \theta_{ft+1} &= \theta_{ft} + \dot{\theta}_{ft+1}\Delta t \end{aligned} \tag{II.2}$$

3. Using the result of this step to perform the next-step calculation:

$$[\dot{u}_{t+2}, \dot{w}_{t+2}, \dot{q}_{t+2}, \dot{\theta}_{ft+2}]^T = MODEL\Big([u_{t+1}, w_{t+1}, q_{t+1}, \theta_{ft+1}]^T, [\dot{u}_{t+1}, \dot{w}_{t+1}, \dot{q}_{t+1}, \dot{\theta}_{ft+1}]^T, [X_{COL(t+1)}, X_{LN(t+1)}]^T\Big) \tag{II.3}$$

In the original model, several simplifications were made which limit the accuracy of the model.

1. Fuselage aerodynamics was approximated by a flat plate with only drag being taken into account.
2. The gimballed rotor of the XV-15 was modelled as an articulated rotor.
3. The perpendicular velocity seen by the rotor blade element was assumed to be much smaller than the tangential velocity. Therefore, it was omitted during the blade element calculation. This simplification will lead to inaccurate results in high-speed flights at large tilt angles.
4. Wing/rotor downwash on the horizontal stabilizer was not included.
5. Rotor downwash on the main wing and the empennage was not included.
6. Wing aerodynamics varying with the mast angle was not included.
7. CG shift due to nacelle tilt was not included.
8. Flap/flaperon was not included.
9. The gearing of the collective stick control was not modelled because the rotor RPM governor was not modelled. In the real XV-15, the collective lever control on the collective pitch is phased out as a function of the nacelle tilt angle. In airplane mode, the collective lever only controls the power setting of the engine. The collective pitch is fully controlled through the governor to maintain the pilot-selected RPM. [27]

2. IMPROVEMENTS TO THE MODEL

To improve the accuracy of the baseline model, some of the above-mentioned simplifications were removed. Look-up tables from [28] were implemented to model the following:

1. Fuselage aerodynamics.
2. Effect of the tilt angle on the wing aerodynamics.
3. Flap/flaperons aerodynamics.
4. Wing downwash on the horizontal tail.

Apart from the look-up tables, the updated model derived in this thesis also have the following improved:

1. CG shift due to nacelle tilt was included.
2. Aircraft moment of inertia change due to nacelle tilt was included.
3. Maximum blade loading C_T/σ and power available were added as constraints.

The wing downwash on the horizontal tail is very important for longitudinal handling quality analysis. Because the deflected flow after the wing has a large influence on the angle of attack of the horizontal tail. The rotor downwash on the wing and the horizontal tail is less important. According to the study of Ref. [29], the rotor downwash on the wing can be ignored at a forward speed of 60 knots. Results in Ref. [30] show that the rotor wake on the horizontal tail is very small after a tilt angle of 30 degrees. Its influence on the horizontal tail is the strongest at low speed (40-60 knots) but diminishes as the speed increases.

Another modification is the travel limit of the collective lever. The rotor rpm governor system is used in all modes. It maintains the pilot-selected rpm by adjusting the blade pitch. In helicopter mode, the collective pitch inputs from the governor are superimposed on the collective pitch inputs from the collective lever and the differential collective pitch inputs from the lateral stick. As the aircraft converts from helicopter mode to airplane mode, the collective pitch inputs from the collective lever are phased out. [27] In airplane mode, the collective pitch is controlled through the rpm governor alone. [31] The baseline model used 10 inches as the limit for all modes, which is the actual travel limit of the XV-15 collective lever. But that should come together with the RPM governor. Without the implementation of the RPM governor, a more representable value should be used. In Ref. [28], the collective pitch is calculated via Equation II.4.

$$\theta_{0R} = \frac{\partial \theta_0}{\partial X_{COL}}(X_{COL}) + \theta_{0LL} + \theta_{0R/G} + \theta_{0diff} \tag{II.4}$$

The subscript R indicates the right rotor.
θ_{0R} is the collective pitch.
X_{COL} is the position of the collective lever.
θ_{0LL} is the low limit of blade pitch at 0.75 blade radius.
$\theta_{0R/G}$ is the governor blade pitch. -5 deg $< \theta_{0R/G} <$ 33.5 deg
θ_{0diff} is the blade pitch due to differential collective.

This thesis only studies 3 degrees of freedom, thus the differential collective can be ignored. Table II.1 lists the collective pitch gearing and θ_{0LL}.

In the improved model, a constant gearing ratio $\partial\theta_0/\partial X_{COL} = 1.6$ is used. The collective pitch in airplane model is controlled through the governor alone, so the only two terms left in Equation II.4 is θ_{0LL} and $\theta_{0R/G}$. In the absence of the governor, assuming $\theta_{0R/G}$ in airplane model is still controlled by the collective lever through a gearing ratio of 1.6. Finally, the limit of X_{COL} can be obtained by dividing the maximum value of $\theta_{0R/G}$ by 1.6, as shown in Equation

$$X_{COL(max)} = \frac{\theta_{0R/G(max)}}{1.6} = \frac{33.5}{1.6} = 20.94\text{inches} \tag{II.5}$$

Table II.1: Collective pitch gearing and low limit of blade pitch at 0.75 blade radius. Table 8a-IV in Ref. [28]

Table 8a-IV, XV-15 Collective Pitch Gearing, $\left(\frac{\partial \theta_o}{\partial X_{COL}}; \theta_{oLL} \text{ at } 0.75 \text{ R}\right)$

Mast Angle, β_m, deg	$\frac{\partial \theta_o}{\partial X_{COL}}$, deg/in	θ_{oLL} at 0.75 R, deg
0	1.6	-2.3
10	1.5	-1.0
20	1.35	1.0
30	1.13	4.0
40	0.92	7.0
50	0.71	10.2
60	0.52	13.5
70	0.34	16.7
80	0.15	19.5
90	0	21.3

3. TRIM AND LINEARIZATION

3.1. TRIM

To trim an aircraft means to find the control settings so that the aircraft can maintain the prescribed attitude and speed. Trimming is the essential stage before performing stability or handling quality analysis. Since for most cases, these analyses start from an aircraft flying in a steady state. In our case, steady level flight. After finding the trim point, the model can then be linearized around this point for further analysis.

A nonlinear set of dynamics is given by

$$\dot{\mathbf{x}} = \mathbf{f}(\mathbf{x}, \mathbf{u}) \tag{II.6}$$

where $\dot{\mathbf{x}}$ is the state vector, $\mathbf{u}$ is the vector of inputs, and $\mathbf{f}$ is a nonlinear vector function that describes the dynamics. A trim point is analogous to an equilibrium point - a point for which if the system starts there it will remain there for all future time. An equilibrium point is characterized by setting the state derivative to zero:

$$\dot{\mathbf{x}} = \mathbf{f}(\mathbf{x}, \mathbf{u}) = 0 \tag{II.7}$$

The result is an algebraic set of equations that must be solved for both $\mathbf{x_0}$ and $\mathbf{u_0}$, where the subscript 0 denotes the equilibrium.

In the 3-DoF model, the control variables used to trim the aircraft are fuselage pitch angle (θ_f), collective control (X_{COL}), and longitudinal control (X_{LN}). Not to be confused with the blade pitch control angles, the collective control and longitudinal control here are "stick position". The trim process is defined as follows:

1. Select the trim condition. For steady level flight, choose flight speed (V), mast angle (η), and flap setting.

2. Give an initial guess to the control variables θ_f, X_{COL}, X_{LN}. Then each time the control variables get updated, the input state variables need to be updated accordingly.

$$u = V cos(\theta_f) \qquad w = V sin(\theta_f) \tag{II.8}$$

3. Minimize the following function, which is the sum of the square of all acceleration terms.

$$F(\theta_f, X_{COL}, X_{LN}) = \dot{u}^2 + \dot{w}^2 + \dot{q}^2 \tag{II.9}$$

3.2. LINEARIZATION

Linearization is the process of finding the linear model around the trim point. For small perturbations in a short time, it is valid to assume that the system properties remain constant. Thus, the linear time-invariant state-space model is utilized.

$$\begin{aligned}\dot{\mathbf{x}}(t) &= A\mathbf{x} + B\mathbf{u}(t)\\ \mathbf{y}(t) &= C\mathbf{x} + D\mathbf{u}(t)\end{aligned} \tag{II.10}$$

Define the actual state as $\mathbf{x}(t) = \mathbf{x_0} + \delta\mathbf{x}(t)$ and the actual control inputs as $\mathbf{u}(t) = \mathbf{u_0} + \delta\mathbf{u}(t)$. Then the linearized equations can be developed using the Taylor series expansion about $\mathbf{x_0}$ and $\mathbf{u_0}$

Recall equation II.6, each equation of which

$$\dot{x}_i = f_i(\mathbf{x}, \mathbf{u}) \tag{II.11}$$

can be expanded as

$$\begin{aligned}\frac{d}{dt}(x_{0i} + \delta x_i) &= f_i(\mathbf{x_0} + \delta\mathbf{x}, \mathbf{u_0} + \delta\mathbf{u})\\ &\approx f_i(\mathbf{x_0}, \mathbf{u_0}) + \left.\frac{\partial f_i}{\partial \mathbf{x}}\right|_0 \delta\mathbf{x} + \left.\frac{\partial f_i}{\partial \mathbf{u}}\right|_0 \delta\mathbf{u}\end{aligned} \tag{II.12}$$

where

$$\frac{\partial f_i}{\partial \mathbf{x}} = \begin{bmatrix}\frac{\partial f_i}{\partial x_1} & \cdots & \frac{\partial f_i}{\partial x_n}\end{bmatrix}$$

The higher order terms are ignored because the variations are small. Since $\frac{d}{dt}x_{ei} = f_i(\mathbf{x_0}, \mathbf{u_0})$, then we have

$$\frac{d}{dt}(\delta x_i) \approx \left.\frac{\partial f_i}{\partial x}\right|_0 \delta x + \left.\frac{\partial f_i}{\partial u}\right|_0 \delta u \tag{II.13}$$

Combining for all n state equations, gives that

$$\begin{aligned}\frac{d}{dt}\delta x &= \begin{bmatrix}\left.\frac{\partial f_1}{\partial \mathbf{x}}\right|_0\\ \left.\frac{\partial f_2}{\partial \mathbf{x}}\right|_0\\ \vdots\\ \left.\frac{\partial f_n}{\partial \mathbf{x}}\right|_0\end{bmatrix}\delta\mathbf{x} + \begin{bmatrix}\left.\frac{\partial f_1}{\partial \mathbf{u}}\right|_0\\ \left.\frac{\partial f_2}{\partial \mathbf{u}}\right|_0\\ \vdots\\ \left.\frac{\partial f_n}{\partial \mathbf{u}}\right|_0\end{bmatrix}\delta\mathbf{u}\\ &= A\delta\mathbf{x} + B\delta\mathbf{u}\end{aligned} \tag{II.14}$$

where

$$A = \begin{bmatrix}\frac{\partial f_1}{\partial x_1} & \frac{\partial f_1}{\partial x_2} & \cdots & \frac{\partial f_1}{\partial x_n}\\ \frac{\partial f_2}{\partial x_1} & \frac{\partial f_2}{\partial x_2} & \cdots & \frac{\partial f_2}{\partial x_n}\\ & & \vdots & \\ \frac{\partial f_n}{\partial x_1} & \frac{\partial f_n}{\partial x_2} & \cdots & \frac{\partial f_n}{\partial x_n}\end{bmatrix}_0 \qquad B = \begin{bmatrix}\frac{\partial f_1}{\partial u_1} & \frac{\partial f_1}{\partial u_2} & \cdots & \frac{\partial f_1}{\partial u_m}\\ \frac{\partial f_2}{\partial u_1} & \frac{\partial f_2}{\partial u_2} & \cdots & \frac{\partial f_2}{\partial u_m}\\ & & \vdots & \\ \frac{\partial f_n}{\partial u_1} & \frac{\partial f_n}{\partial u_2} & \cdots & \frac{\partial f_n}{\partial u_m}\end{bmatrix}_0 \tag{II.15}$$

Typically the "δ" can be dropped, thus the state equation can be written as

$$\dot{\mathbf{x}}(t) = A\mathbf{x} + B\mathbf{u}(t) \tag{II.16}$$

which is of the same form as equation II.10

Following this approach, the A and B matrix of our model is computed column by column, i.e., by varying each state variable at one time. The detailed method is illustrated below.

1. At the trimmed point, add a small perturbation $+\epsilon$ to the first state variable u_0

$$\dot{\mathbf{x}}_\mathbf{1} = \begin{bmatrix} \dot{u}_1 \\ \dot{w}_1 \\ \dot{q}_1 \\ \dot{\theta}_{f1} \end{bmatrix} = MODEL\Bigg(\begin{bmatrix} u_0 + \epsilon \\ w_0 \\ q_0 \\ \theta_{f0} \end{bmatrix} + \begin{bmatrix} X_{COL_0} \\ X_{LN_0} \end{bmatrix} \Bigg) \tag{II.17}$$

2. Add a small variation $-\epsilon$ to the first state variable u_0

$$\dot{\mathbf{x}}_\mathbf{2} = \begin{bmatrix} \dot{u}_2 \\ \dot{w}_2 \\ \dot{q}_2 \\ \dot{\theta}_{f2} \end{bmatrix} = MODEL\Bigg(\begin{bmatrix} u_0 - \epsilon \\ w_0 \\ q_0 \\ \theta_{f0} \end{bmatrix} + \begin{bmatrix} X_{COL_0} \\ X_{LN_0} \end{bmatrix} \Bigg) \tag{II.18}$$

3. Then the first column of the A matrix is

$$\begin{bmatrix} \frac{\partial f_1}{\partial u}\Big|_0 \\ \frac{\partial f_2}{\partial u}\Big|_0 \\ \vdots \\ \frac{\partial f_4}{\partial u}\Big|_0 \end{bmatrix} = \frac{\dot{\mathbf{x}}_\mathbf{1} - \dot{\mathbf{x}}_\mathbf{2}}{2\epsilon} \tag{II.19}$$

4. Repeat step 1-3 but add the variation ϵ to the other three state variables w, q, θ individually to compute the other three columns of the A matrix. Similarly, the B matrix can be obtained as well.

4. RESULTS OF THE IMPROVED MODEL

This section presents the trim and dynamic stability results of the improved model. Trim results of the baseline model are also used for comparison.

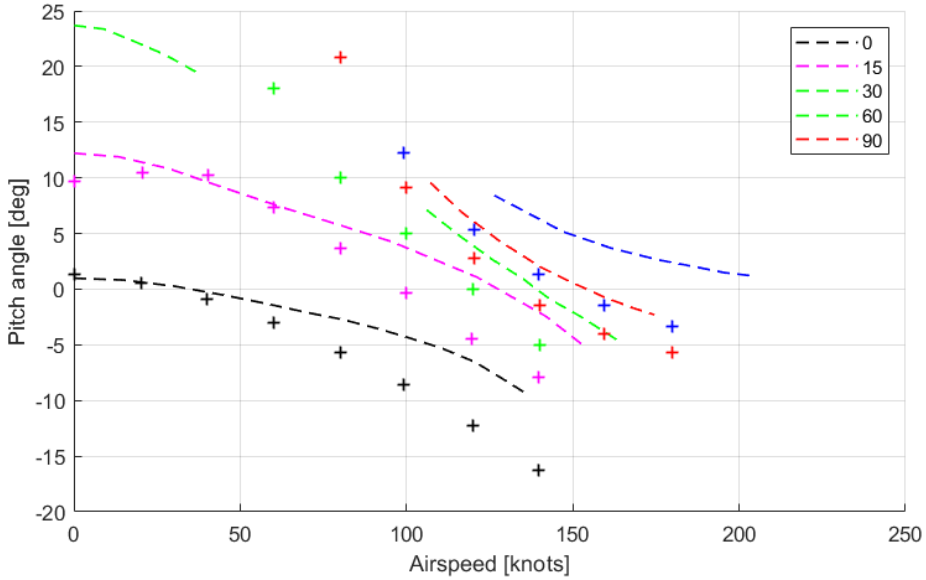

Figure II.3: Level flight pitch trim curve. Baseline model, After CG, Flap/flaperon=40/25

Figure II.3 shows the pitch trim curves in level flight of the original model (dashed line) plotted against the published data ("+" marker) from Ref. [32]. The results show a large discrepancy between these two.

The baseline model tends to over-predict the pitch angle, especially at high speed. Also, the curves of the 0 degrees, 15 degrees, and 30 degrees cases fail to follow the published trends well. There is an area between 40 and 100 knots where the 30 degrees configuration cannot be trimmed, which largely violates the published data.

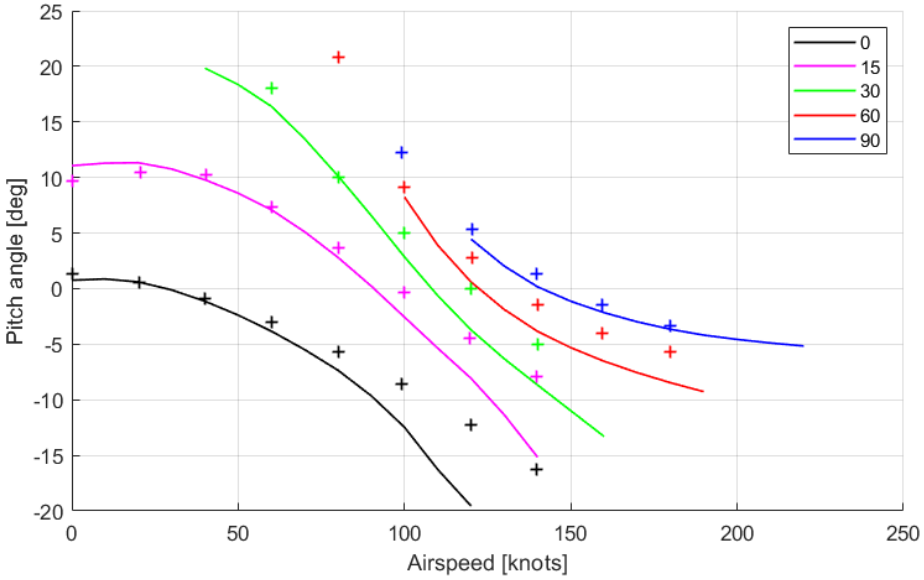

Figure II.4: Level flight pitch trim curve. Improved model, After CG, Flap/flaperon=40/25

Figure II.4 shows the pitch trim curves in level flight of the improved model (dashed line) plotted against the published data ("+" marker) from Ref. [32]. Compared to the baseline model, there is an evident improvement in the trim curves. For each nacelle angle, the improved model tends to under-predict the pitch angle as the airspeed becomes higher. The reason could be that only the tangential flow into the rotor is considered. If both tangential and perpendicular velocities are considered, the vector sum of the total inflow will cause a larger pitching up moment which grows with speed. In general, the solid lines correlate well with the published data. The improvement is largely due to the implementation of the wing downwash effects on the horizontal tail [30], the flap/flaperons aerodynamics, and fuselage pitching moment.

Table II.2: Eigenvalues comparisons. After CG, Flap/flaperon=40/25, Ref. [33]

Table 10.1 Comparison of FXV-15 eigenvalues (italics) with published data

	H-mode hover (SL)	H-mode 120 kts (SL)	C-mode (60) 120 kts (SL)	A-mode 170 kts (SL)	A-mode 260 kts (SL)
Pitch S-P	*−0.68, −0.143* −1.32, −0.105[b] –0.807, –0.20	*−1.41 ± 2.79i* −1.44 ± 3.3*i*[a] –1.18+2.24i (118kts)	*−1.29 ± 2.5i* −1.302 ± 2.86*i*[a] – 1.07+1.28i	*−1.53 ± 3.71i* −1.21 ± 1.82*i*[b] –1.29+1.42i	*−2.20 ± 4.59i* −2.23 ± 4.19*i*[a] –4.23, –0.861
Long. phugoid	*0.15 ± 0.42i* 0.268 ± 0.513*i*[b] 0.123+0.429i	*−0.054 ± 0.076i* −0.034 ± 0.12*i*[a] –0.223, 0.06 (118kts)	*−0.077 ± 0.173i* −0.073 ± 0.27*i*[a] –0.081+0.108i	*−0.15 ± 0.16i* –0.218+0.324i	*−0.17 ± 0.17i* −0.012 ± 0.015*i*[a] 0.173+0.492i

[a]Ref. 10.12 (Harendra).
[b]Ref. 10.51 (Tischler 1987).
[c]Ref. 10.52 (Tischler 2012).
[d]Refs. 10.49, 10.50 (Fergusen, Schroers).

The eigenvalues of the short-period and phugoid modes are shown in Table II.2 taken from Ref. [33].

There are three rows for each mode. The first row gives the results of the FXV-15 model; the second row gives the results from flight tests and validated mathematical models; the third row in red colour gives the results of our improved model. The FXV-15 model is a 6-DoF XV-15 model developed by the University of Liverpool in FLIGHTLAB (A comprehensive analysis and simulation tool for rotorcraft developed by Advanced Rotorcraft Technology, Inc.). Ref. [34] contains a complete description of this model. In helicopter mode, conversion mode, and low-speed airplane mode, the predictions made by the improved model compare well with the data in the table, but a few differences stand out. The short-period frequencies predicted by the improved model in all modes are lower than others. In high-speed helicopter mode (120 kts), the phugoid mode predicted by the improved model becomes unstable while other results indicate a stable phugoid. However, all results show that the phugoid pole will move closer to the imaginary axis as the airspeed increases. The phugoid poles of FXV-15 and Harendra's model [32] are extremely close to the imaginary axis at 120 kts. Thus, the unstable phugoid of the model is not completely unreasonable. In low-speed airplane mode (170 kts), the predicted short-period is close to Tischler's result [35], but the predicated phugoid frequency is almost two times that of the FXV-15's. The largest discrepancy occurs in the high-speed airplane mode (260 kts). The predicted short period damping is too large that it is no longer oscillatory and the phugoid frequency is higher than the published data. However, it can be seen from this table that the FXV-15's results are not very close to flight test data. The FXV-15 contains the inflow dynamics and 6 degrees of freedom, which make its results closer to flight test data compared to the 3-DoF model. Considering the complexity and assumptions of the improved 3-DoF model, achieving such results is reasonably good.

III

LONGITUDINAL DYNAMICS AND HANDLING QUALITIES

1. MISSION TASK

One primary role of XV-15 sized tiltrotor aircraft is Search and Rescue (SAR). During SAR missions, the aircraft may need to perform the terrain-following MTE. In such missions, the aircraft has to fly near the ground surface in order to detect the rescue site and to search the injured personnel. The pilot needs to constantly maneuver the aircraft to fly the terrain contours at medium speed. Such maneuvers include rapid control of flight path, airspeed, roll angle, and heading. These bring issues to the handling quality of the aircraft. The critical requirement is on the short-term pitch and flight path responses. Because the ability to establish and sustain a load factor as rapidly as possible depends on the aircraft pitch and flight path response characteristics to the longitudinal control input. Sufficient control power, attitude quickness, and maneuver stability are also important.

The SAR mission context suggests that most of the time the tiltrotor aircraft needs to fly in the conversion mode. Taking into account the acceptable computation power when running design calculations, two conditions are selected to be evaluated in this study, 80 knots with 30° nacelle angle and 120 knots with 60° nacelle angle.

2. APPROXIMATE LONGITUDINAL DYNAMICS

For the conventional angle-of-attack response type, two classical longitudinal modes are phugoid and short period. "The short period is a relatively rapid mode that governs the transient changes in angle of attack, pitch, flight path and normal load factor that occur following rapid control or gust inputs" [36]. The phugoid motion is commonly a low-frequency and lightly damped oscillation in flight speed and pitch angle. It has a nearly constant angle of attack due to a repeated exchange of airspeed and altitude. While the short period characteristics have a strong influence on accurate flight-path control, the phugoid is usually not a problem because its period is too long (typically 20-60 sec) that a pilot can correct it without even noticing it. Next, the longitudinal equations of motion are presented, following the derivations in Ref. [37][38].

The linearized longitudinal equations of motion of the aircraft are:

$$m\dot{u} = X_u u + X_w w + X_q q + X_{\delta_e}\delta_e - mgcos\theta_0\theta \tag{III.1}$$

$$m(\dot{w} - qU_0) = Z_u u + Z_w w + Z_{\dot{w}}\dot{w} + Z_q q + Z_{\delta_e}\delta_e - mgsin\theta_0\theta \tag{III.2}$$

$$I_y\dot{q} = M_u u + M_w w + M_{\dot{w}}\dot{w} + M_q q + M_{\delta_e}\delta_e \tag{III.3}$$

$$\dot{\theta} = q \tag{III.4}$$

where u, w, q, θ, and δ_e denote small deviations from the equilibrium state. θ_0 is the pitch angle around which we obtain the linearized equations. Same for the U_0, it is the airspeed around which we obtain the linearized equations. Non-dimensionalize $\hat{X}_u = X_u/m$, $\hat{M}_q = \frac{M_q}{I_y}$, $\hat{\Gamma} = \frac{\hat{M}_{\dot{w}}}{1-\hat{Z}_{\dot{w}}}$. Put these equations in the matrix form, as shown in Equation III.5.

$$\begin{bmatrix} \dot{u} \\ \dot{w} \\ \dot{q} \\ \dot{\theta} \end{bmatrix} = \begin{bmatrix} \hat{X}_u & \hat{X}_w & 0 & -g cos\theta_0 \\ \frac{\hat{Z}_u}{1-\hat{Z}_{\dot{w}}} & \frac{\hat{Z}_w}{1-\hat{Z}_{\dot{w}}} & \frac{\hat{Z}_q + U_0}{1-\hat{Z}_{\dot{w}}} & \frac{-g sin\theta_0}{1-\hat{Z}_{\dot{w}}} \\ \hat{M}_u + \hat{Z}_u\hat{\Gamma} & \hat{M}_w + \hat{Z}_w\hat{\Gamma} & \hat{M}_q + (\hat{Z}_q + U_0)\hat{\Gamma} & -g sin\theta_0\hat{\Gamma} \\ 0 & 0 & 1 & 0 \end{bmatrix} \begin{bmatrix} u \\ w \\ q \\ \theta \end{bmatrix} + \begin{bmatrix} \hat{X}_{\delta_e} \\ \hat{Z}_{\delta_e} \\ \hat{M}_{\delta_e} \\ 0 \end{bmatrix} \delta_e \tag{III.5}$$

2.1. SHORT PERIOD DYNAMICS

The forward speed remains almost constant during short-period oscillations [19]. Hence, the speed variable u and the force X can be omitted, resulting in the 2×2 system in Equation .

$$\begin{bmatrix} \dot{w} \\ \dot{q} \end{bmatrix} = \begin{bmatrix} \hat{Z}_w & U_0 \\ \hat{M}_w + \hat{Z}_w\hat{M}_{\dot{w}} & \hat{M}_q + U_0\hat{M}_{\dot{w}} \end{bmatrix} \begin{bmatrix} w \\ q \end{bmatrix} + \begin{bmatrix} \hat{Z}_{\delta_e} \\ \hat{M}_{\delta_e} \end{bmatrix} \delta_e \tag{III.6}$$

With

$$\hat{Z}_w w = \frac{Z_w w}{m} = \frac{Z}{m} = \dot{w} = sw$$

The term $\hat{M}_w + \hat{Z}_w\hat{M}_{\dot{w}}$ can be rewritten as $\hat{M}_w + s\hat{M}_{\dot{w}}$. Since $U_0\hat{M}_{\dot{w}}$ is much smaller than $\hat{M}_q$, it can be dropped out. Then Equation III.6 can be written as

$$\begin{bmatrix} \dot{w} \\ \dot{q} \end{bmatrix} = \begin{bmatrix} \hat{Z}_w & U_0 \\ \hat{M}_w + s\hat{M}_{\dot{w}} & \hat{M}_q \end{bmatrix} \begin{bmatrix} w \\ q \end{bmatrix} + \begin{bmatrix} \hat{Z}_{\delta_e} \\ \hat{M}_{\delta_e} \end{bmatrix} \delta_e \tag{III.7}$$

Solve this equation for the transfer function that relates q and δ_e, we get

$$\frac{q(s)}{\delta_e(s)} = \frac{(\hat{M}_{\delta_e} + \hat{Z}_{\delta_e}\hat{M}_{\dot{w}})\left(s + \frac{\hat{M}_w\hat{Z}_{\delta_e} - \hat{Z}_w\hat{M}_{\delta_e}}{\hat{M}_{\delta_e} + \hat{Z}_{\delta_e}\hat{M}_{\dot{w}}}\right)}{s^2 + (-\hat{M}_q - \hat{Z}_w - U_0\hat{M}_{\dot{w}})s + \hat{M}_q\hat{Z}_w - \hat{M}_w U_0} \tag{III.8}$$

We can also ignore the lift generated by the control surface deflection $\hat{Z}_{\delta_e}$. This is because 1. its contribution to overall lift is very small compared to the rotors and main wing; 2. its pitching moment effect is much larger than lift effect. [36] Therefore, this equation can be further simplified to

$$\frac{q(s)}{\delta_e(s)} = \frac{\hat{M}_{\delta_e}\left(s - \hat{Z}_w\right)}{s^2 + (-\hat{M}_q - \hat{Z}_w - U_0\hat{M}_{\dot{w}})s + \hat{M}_q\hat{Z}_w - \hat{M}_w U_0} \tag{III.9}$$

The short period transfer function in the general form is

$$\frac{q(s)}{\delta_e(s)} = \frac{\hat{M}_{\delta_e}(s + \frac{1}{T_{\theta_2}})}{s^2 + 2\zeta_{sp}\omega_{sp}s + {\omega_{sp}}^2} \tag{III.10}$$

Compare Equation III.10 and III.9, the expression for short period natural frequency and damping ratio can be obtained:

$$\begin{aligned} 2\zeta_{sp}\omega_{sp} &= -\hat{M}_q - \hat{Z}_w - U_0\hat{M}_{\dot{w}} \\ {\omega_{sp}}^2 &= \hat{M}_q\hat{Z}_w - \hat{M}_w U_0 \end{aligned} \tag{III.11}$$

2.2. PHUGOID DYNAMICS

During phugoid motion, changes to w and q are very small compared to u, so a constant pitch rate $\dot{q} = 0$ and a constant $\dot{w} = 0$ (corresponds to a constant angle of attack) can be assumed. Therefore, we can set $\dot{q} = 0$,

$\dot{w} = 0$, and $\theta_0 = 0$ in Equation III.5.

$$\begin{bmatrix} \dot{u} \\ 0 \\ 0 \\ \dot{\theta} \end{bmatrix} = \begin{bmatrix} \hat{X}_u & \hat{X}_w & 0 & -gcos\theta_0 \\ \dfrac{\hat{Z}_u}{1-\hat{Z}_{\dot{w}}} & \dfrac{\hat{Z}_w}{1-\hat{Z}_{\dot{w}}} & \dfrac{\hat{Z}_q + U_0}{1-\hat{Z}_{\dot{w}}} & \dfrac{-gsin\theta_0}{1-\hat{Z}_{\dot{w}}} \\ \hat{M}_u + \hat{Z}_u\hat{\Gamma} & \hat{M}_w + \hat{Z}_w\hat{\Gamma} & \hat{M}_q + (\hat{Z}_q + U_0)\hat{\Gamma} & -gsin\theta_0\hat{\Gamma} \\ 0 & 0 & 1 & 0 \end{bmatrix} \begin{bmatrix} u \\ w \\ q \\ \theta \end{bmatrix} + \begin{bmatrix} \hat{X}_{\delta_e} \\ \hat{Z}_{\delta_e} \\ \hat{M}_{\delta_e} \\ 0 \end{bmatrix} \delta_e \tag{III.12}$$

Then following the derivation in Ref. [37], we can obtain the coarse approximation for phugoid as shown in Equation III.13, in which the control variables δ_e is left out.

$$\begin{bmatrix} \dot{u} \\ \dot{\theta} \end{bmatrix} = \begin{bmatrix} \hat{X}_u & -g \\ \dfrac{-\hat{Z}_u}{U_0} & 0 \end{bmatrix} \begin{bmatrix} u \\ \theta \end{bmatrix} \tag{III.13}$$

The eigenvalue of the A matrix gives the approximation for phugoid natural frequency and damping ratio.

$$\begin{aligned} 2\zeta_{ph}\omega_{ph} &= -\hat{X}_u \\ {\omega_{ph}}^2 &= \frac{-g\hat{Z}_u}{U_0} \end{aligned} \tag{III.14}$$

The damping ratio can be further extracted out

$$\zeta_{ph} = \frac{-\hat{X}_u U_0}{2\sqrt{2}g} \tag{III.15}$$

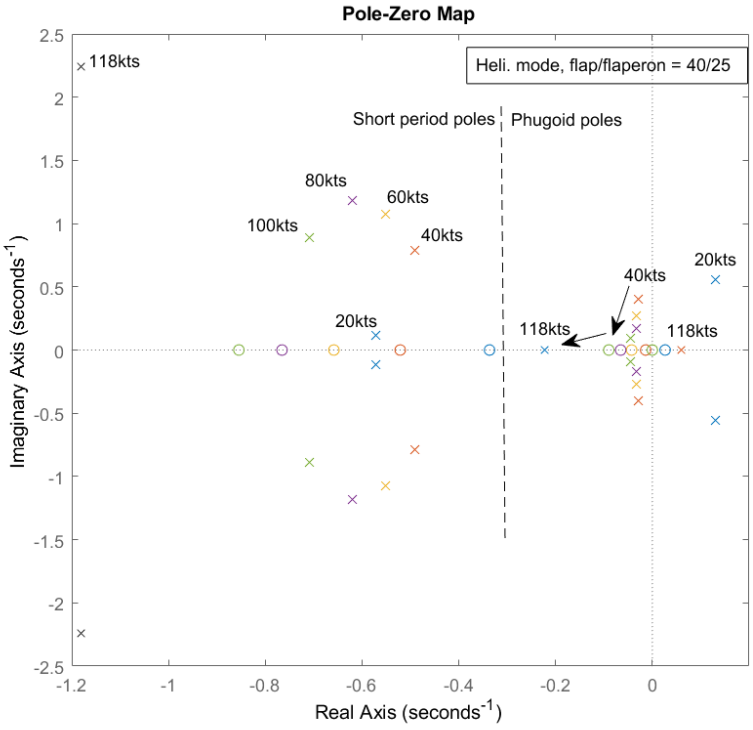

Figure III.1: Pole-zero map predicted by the improved model ("x": poles; "o": zeros)

In Table II.2, it was found that in helicopter mode, the phugoid became unstable at 120 knots. Figure III.1 shows the short period and phugoid poles and zeros in helicopter mode at various speeds predicted by the

improved model. As the airspeed grows, the phugoid poles continue approaching the real axis. In Equation III.15, $\hat{X}_u$ will become more negative and U_0 will be higher as airspeed increases. Thus, the resulting phugoid damping ratio will increase as well. At 120 knots, it finally exhibits a non-oscillatory behavior. One of the phugoid poles moves to the right-half plane, leading to an unstable aircraft.

From the discussion above, it can be seen that short period motion is dominated by the pitching moment derivatives M_q, M_w and Z force derivatives Z_w. Phugoid is dominated by force derivative X_u and Z_u. In this thesis, we mainly concern the short-period dynamics which govern the pitch tracking ability of the aircraft. The dominant factors in short period damping and frequency are M_q, M_w, and Z_w. The largest contribution to the derivatives of the pitching moment with respect to the pitch rate and heave speed comes from the horizontal tail. The heave damping term Z_w is influenced by the rotor and wing. Consequently, the selection of design parameters should take these into account.

3. SELECTED CRITERIA FOR EVALUATION

This section will introduce in detail the selected criteria in this study. In addition to handling quality parameters, two maneuverability parameters are also included. One is the peak normal load factor during the pull-up and the other is the acceleration time from 100 knots to 150 knots. Figure III.2 shows the handling quality parameters and whether they come from helicopter standards or fixed-wing standards. By selecting a mixed set of criteria from both helicopter and fixed-wing standards, the uniques of the tiltrotor aircraft can be reflected.

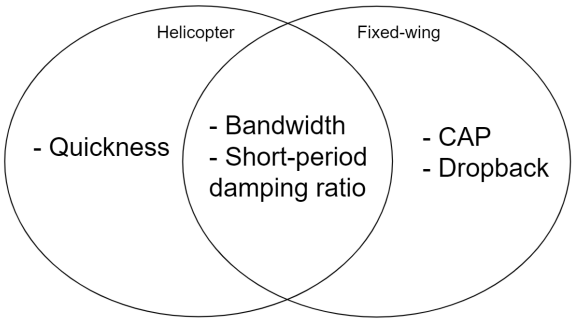

Figure III.2: Selected handling quality criteria

3.1. BANDWIDTH

Bandwidth is designed to indicate the highest frequency at which the pilot-aircraft loop can be closed without introducing instability (i.e. PIO). The main advantages of using the bandwidth criteria are that it applies to all response types and thus is ideal for highly augmented aircraft, and it can be readily extracted from the bode plot of the higher-order system. [39] Figure III.3 shows the definition of bandwidth taken from ADS-33E. It is defined as the frequency where the phase margin is 45 degrees or where the gain margin is 6dB.

The bandwidth boundaries are task-dependent, because the characteristic frequency of the command varies for different tasks. For most configurations, the phase margin bandwidth is lower than the gain margin bandwidth, which means they are phase margin limited. For configurations that are gain margin limited, they tend to be PIO prone. [39]

Because this model describes only the bare-airframe dynamics, i.e., no control augmentation system in the loop, there is no higher-order delay in the pitch transfer function. In the absence of the time delay parameter, the bode plot of the pitch attitude to longitudinal stick input transfer function has no intersection with the -180 degrees line. By definition, it means the phase delay equals 0 and thus the bandwidth is only limited by the phase margin, which is in accordance with the rule stated above. In ADS-33E, the pitch bandwidth must be higher than 2 rad/sec to achieve level 1 for target acquisition and tracking tasks.

3.2. CONTROL ANTICIPATION PARAMETER

Control anticipation parameter is a measure of predictability of the pitch response. Figure III.4 is the CAP criterion for Category A landing and approach specified in MIL-HDBK-1797A [11].

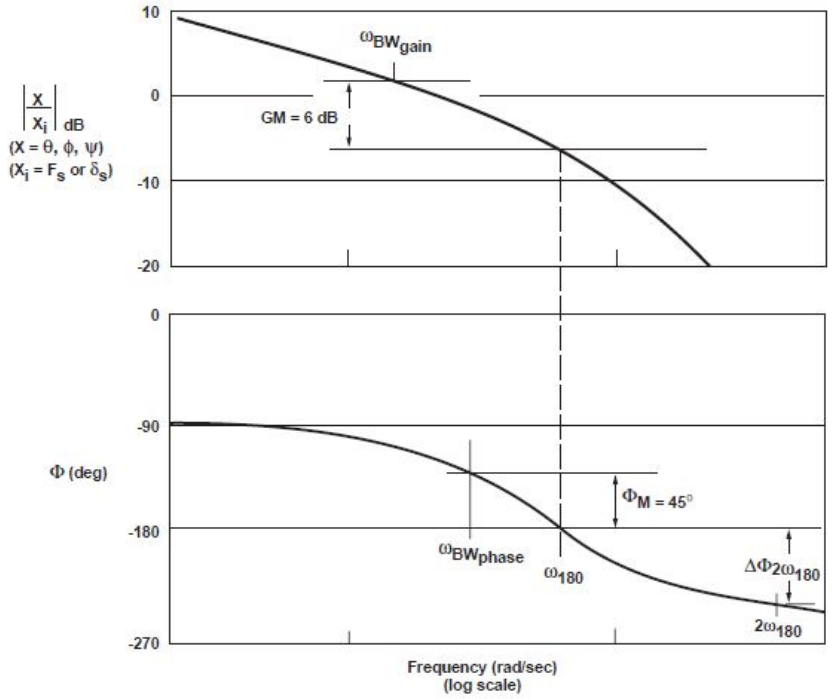

Figure III.3: Definition of bandwidth [12]

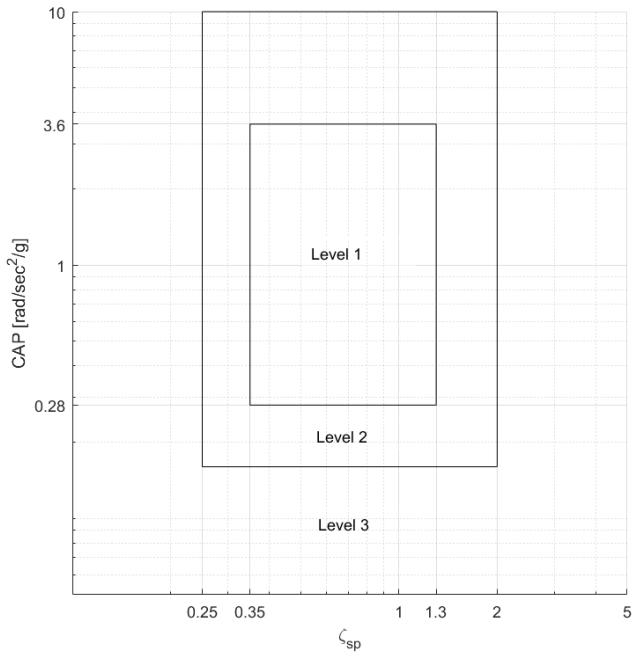

Figure III.4: CAP criterion. MIL-HDBK-1797A Category A landing and approach

Recall Equation I.10

$$CAP = \frac{\ddot{\theta}(0)}{n_z(\infty)} \approx \frac{g\omega_{sp}^2 T_{\theta 2}}{V} \tag{III.16}$$

Therefore, CAP is closely related to the incidence lag and short period responses. For category A flight, CAP must be higher than 0.28 rad/sec^2/g and lower than 3.6 rad/sec^2/g to achieve level 1 handling quality. In

Ref. [40], Gibson proposed the "Gibson Criteria", in which an upper limit of 3.6 rad/sec^2/g was considered satisfactory for gross maneuvering without a target. But it was unsatisfactory above 2 rad/sec^2/g for landing approach, above 1 rad/sec^2/g for precise tracking. In later analysis, 0.28 rad/sec^2/g to 1 rad/sec^2/g will be used as the boundaries.

3.3. DROPBACK

Dropback is a criterion used in conjunction with the CAP or bandwidth criteria as shown in Figure III.5. It compares the ratio of the peak to steady-state pitch rate with the ratio of pitch attitude dropback to the steady-state pitch rate. It is a measure of the quality of the pitch responses.

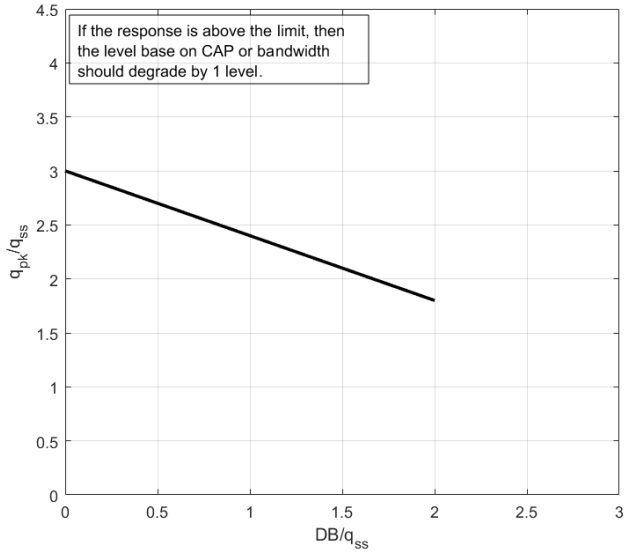

Figure III.5: Dropback criterion

The determination of dropback parameters follows the definition by Gibson as illustrated in Figure I.6.

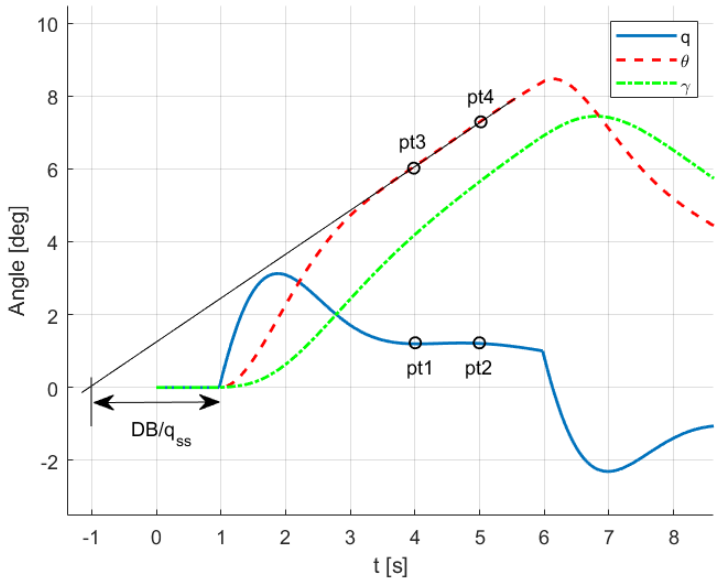

Figure III.6: Method to determine dropback parameters from pitch responses

Two parameters are needed in this criteria, the ratio of pitch dropback to steady-state pitch rate DB/q_{ss}

and the ratio of peak pitch rate to steady-state pitch rate q_{pk}/q_{ss}. Figure III.6 shows the method used to determine these two parameters when programming. It is the history of pitch rate, pitch attitude, and flight path angle after a longitudinal pulse input applied at 1s and removed at 6s. It was found that for most configurations, the pitch rate stables 3 seconds after the initial input. Hence, the pitch rate at 4s and 5s, namely the pt1 and the pt2, are taken and the average of them is considered the steady-state pitch rate. A line is drawn through the pt3 and pt4, which are the pitch angle at 4s and 5s, and its intersection point with the horizontal axis is used to determine the DB/q_{ss}.

3.4. ATTITUDE QUICKNESS

Pitch attitude quickness is a measure of the aircraft's ability to achieve rapid pitch attitude changes. It was first introduced in ADS-33 to characterize moderate-amplitude attitude changes ($5° < \theta < 30°$) for helicopter hover and low-speed flight (0-45 kts). It is defined as the ratio of peak pitch rate to changes in pitch attitude.

$$Q_\theta = \frac{q_{pk}}{\theta_{pk}} \tag{III.17}$$

ADS-33 did not define quantitative measurements of pitch agility for high-speed forward flight. In an attempt to develop a new set of consistent, complementary metrics for agility in forward flight, Pavel and Padfield defined a new quickness parameter in Ref. [41]. While the previous quickness defined in ADS-33 was named "theta quickness Q_θ", the new parameter was named "gamma quickness Q_γ" which is the peak quasi-steady normal acceleration in g units corresponding to a step change in flight path angle.

$$Q_\gamma = \frac{n_{pk}}{\Delta\gamma} \tag{III.18}$$

Pavel and Padfield also proved that for small-amplitude flight path change, the gamma quickness is a measure of the heave damping. While for large-amplitude flight path change, it characterizes more the pitch attitude control. Both quickness parameters will be computed in this study. Though the theta quickness is designed

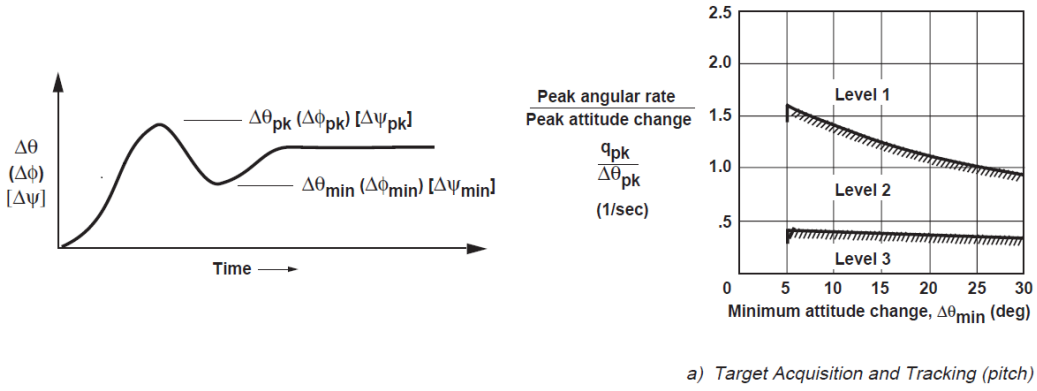

Figure III.7: Requirements for moderate-amplitude pitch attitude changes – hover and low speed, target acquisition and tracking [12]

only for low-speed flight, it will be used for all cases to compare with the gamma quickness.

3.5. PULL-UP MANEUVER

The high-speed pull-up maneuver is of great importance in situations where a sharp increase in altitude is required, such as avoiding an obstacle during the terrain following task. This is a core element in the Search and Rescue mission task. The measure of this maneuver performance is the maximum achieved normal load factor after applying a 2-second 0.5-inch longitudinal stick pull.

3.6. ACCELERATION ABILITY

The acceleration ability of the aircraft is also added as a measure of maneuverability. Unlike helicopters which can start accelerating from hover, tiltrotor aircraft have a minimum speed limit if we only consider a fixed tilt angle. The tilt angle is not changeable during this maneuver because the tilting dynamics is not modeled. Thus, for different tilt angles, this maneuver has to be initiated from a different speed.

During the acceleration, the pilot needs to push the longitudinal stick and controls the collective to maintain the altitude at the same time. A closed-loop PID control system was designed to perform this maneuver [42]. It consists of an altitude control loop and a pitch angle (attitude) control loop as shown in Figure III.8. The altitude command (h_c) and pitch angle command (theta_c) is set by the user. The altitude control loop requires two states from the dynamic mode, h_dot (vertical speed in the inertia frame, which is the same as Vz) and h (altitude). The error between h_c and h is named h_e which will go through a PI controller to get the vertical speed command (Vz_c). Vz_c then subtracts Vz to compute the error Vz_e. Again, the error goes through a PI controller and adds to the trimmed collective control to obtain the collective control command. Because the stick has its travel limit, a saturation block is added to ensure the command does not exceed the limit. Similarly, the pitch angle (theta) and the pitch rate (q) are fed into the pitch angle control loop, which uses a PID controller to compute the longitudinal stick command.

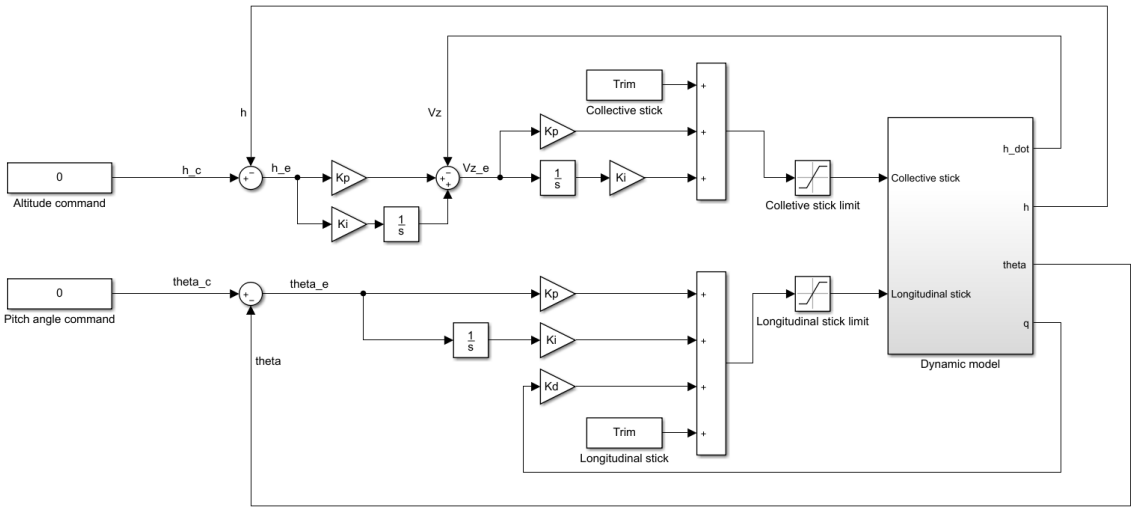

Figure III.8: Control system block diagram

In later design studies, the aircraft will arrive at a different trimmed condition after modifying the design parameters. For instance, for steady level flight at the same speed, the trimmed pitch angle will be different for different design parameters. Then how do we set the pitch angle command so that the aircraft with different design parameters can show its accelerating ability? With this simple PID controller, it is not possible. For this purpose, a more suitable method is the inverse simulation technique which has been used to calculate the control action required to achieve a specified system response [43] [44]. However, control is not the focus of this project. Therefore, we will use the PID controller above to perform the maneuvers and it can provide some insights into the acceleration ability.

To find out the maximum accelerating ability, an approximate solution to this problem is used in the program. If the power required after the aircraft reaches its steady-state after acceleration equals the power available, then this pitch angle command will be considered the maximum pitch-down angle that can help the aircraft achieve the maximum accelerating ability. Based on this assumption, the technique is to increase the pitch-down angle after each loop (every loop is a full simulation of this acceleration maneuver from the initial speed to the final speed) until the power available being exceeded. Table III.1 lists the XV-15 power rating at sea level on a standard day (density: 1.229 kg/m3; pressure: 101.325 kPa; temperature: 15 °C).

Table III.1: XV-15 power rating (sea level standard day) [27]

Contingency (2 minutes)	1802 hp
Takeoff (10 minutes)	1550 hp
Military (30 minutes)	1401 hp
Normal (max.continuous)	1250 hp

Figure III.9 shows the history of various parameters during the acceleration from 100 knots to the power-limited speed at 30 degrees tilt angle. The maximum airspeed is about 160 knots which requires a pitch-down

angle of 16 degrees. This maximum speed obtained is consistent with the limit shown in the conversion corridor in Figure III.10.

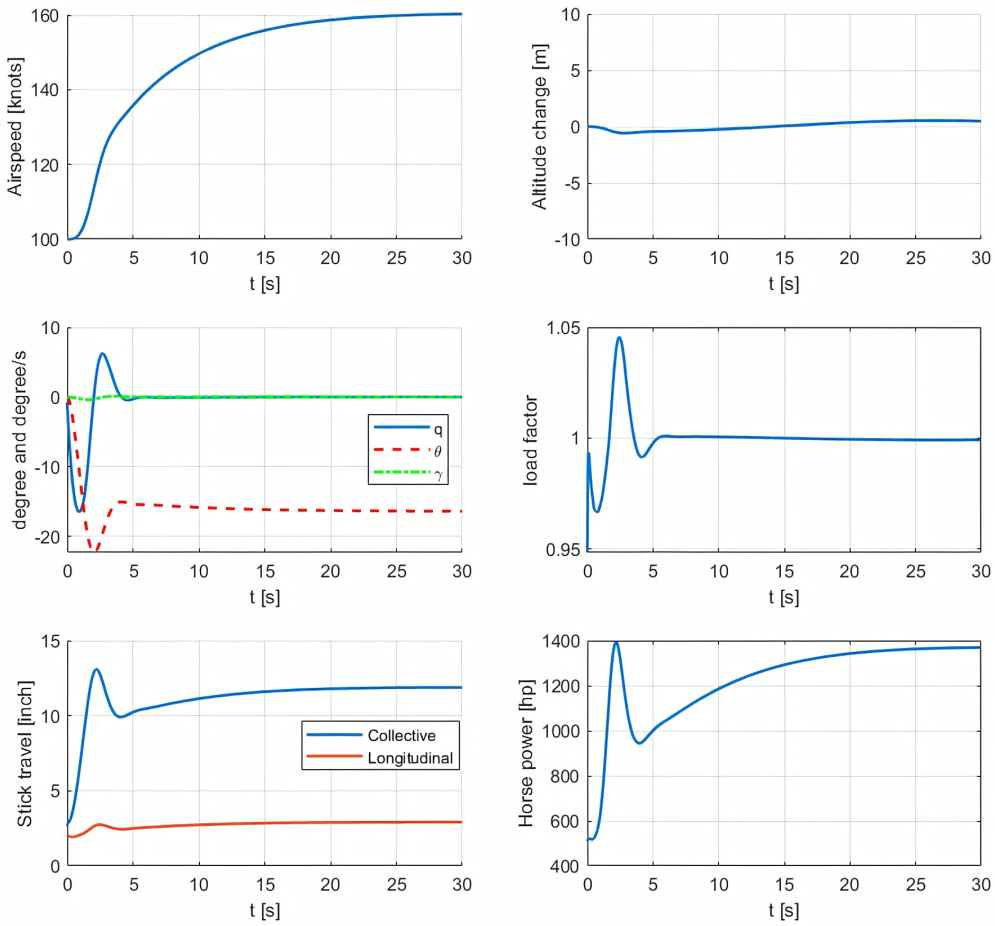

Figure III.9: Control system performance

4. HANDLING QUALITIES OVER THE FLIGHT ENVELOPE

Using the improved 3-DoF XV-15 model, the handling qualities of the XV-15 in different flight configurations are evaluated in this section to locate the deficiencies in handling qualities. The red points indicated in Figure III.10 are selected to evaluate the variation of handling qualities through the flight envelope. The plotted flight envelope follows that in Ref. [27]. These points lie near the conversion corridor boundaries. Flying near the boundaries will face critical situations, e.g., wing stall, flutter, retreating blade stall, etc. Referring to the normal operative configuration to reduce the rotor download as noted in Ref. [33], the flap/flaperon setting is 40°/25° in helicopter and conversion mode, and 0°/0° in airplane mode. (**NOTE: In Figure III.10, 0 degree tilt is the airplane mode and 90 degrees is the helicopter mode. But in the following illustrations, this follows the definition in the mathematical model, where 0 degree is the helicopter mode and 90 degrees is the airplane mode.**)

First, the short period poles of these configurations are plotted on the pole-zero map as shown in Figure III.11a. The solid black line is the 0.35 damping ratio line, which is the level 1/2 boundary defined in ADS-33E. Almost all poles fall in the level 1 area, except the 100 knots 60 degrees tilt case has a damping ratio of 0.349, which is slightly to the right of the boundary. There is a trend that the damping ratio and the undamped natural frequency will increase with airspeed. This can be more clearly observed by plotting different airspeed

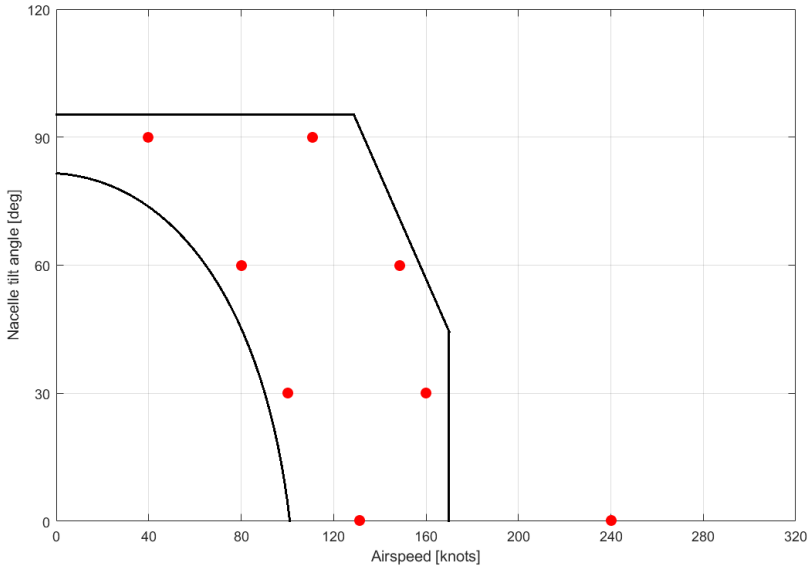

Figure III.10: Selected points inside the flight envelope. (The flight envelope is from Ref. [27])

cases for the same tilt angle, as illustrated in Figure III.11b. When flying at 30 degrees tilt angle, the pole moves to the left and farther away from the origin as the airspeed increases from 80 knots to 150 knots. Thus, in terms of short period damping, the XV-15 has a better handling quality in high-speed flight.

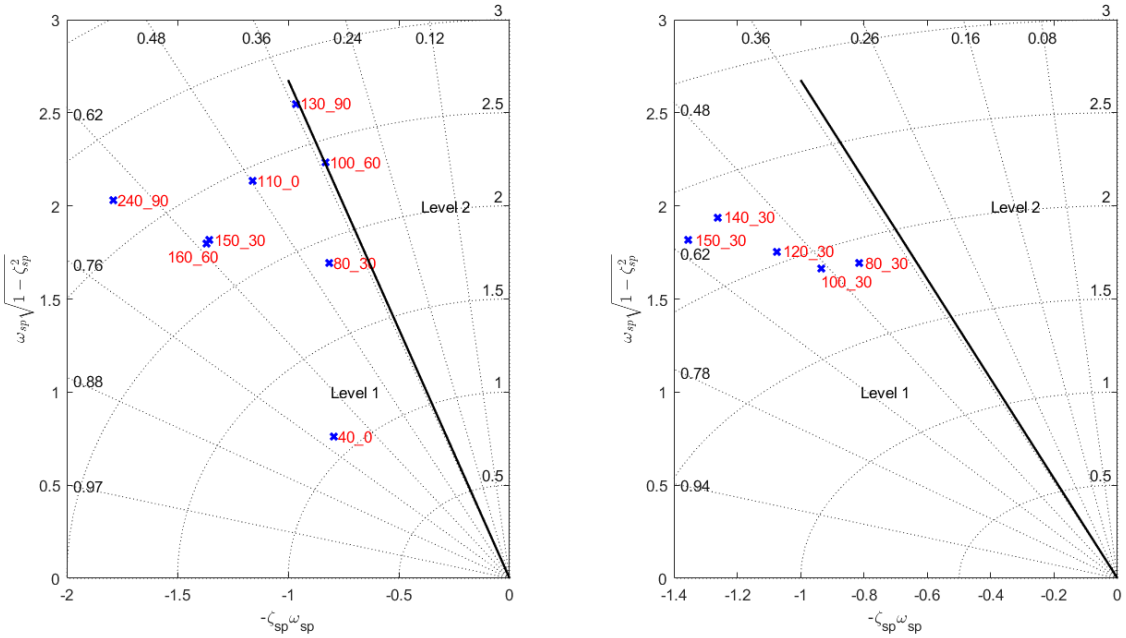

(a) Short-period damping ratio of different configurations

(b) Short-period damping ratio varying with airspeed 30 deg

Figure III.11: The results of short-period poles.
(The data tip "A_B" means "Airspeed_nacelle angle". For example, "40_0" means 40 knots flight at 0 degree nacelle angle.)

Figure III.12a shows the CAP plotted against the boundaries for Category A flight phases specified in MIL-HDBK-1797A. Due to the insufficient damping, the 100 knots 60 degrees tilt case falls in the level 2 area, while the rest are all in the level 1 area. Section 3.2 introduced that Gibson recommended an upper limit of

1 $rad/sec^2/g$ for fine tracking. According to this rule, only three cases: 150 knots 30 degrees, 160 knots 60 degrees, and 250 knots 90 degrees satisfy. These are all on the high-speed side for each tilt angle in the flight envelope. To better look at the influence of airspeed on CAP, Figure III.12b plots the CAP of different speeds at 30 degrees tilt configuration. The CAP moves below 1 $rad/sec^2/g$ as the speed increases, suggesting that for pilots, the predictability of the pitch response is better as the aircraft gains speed.

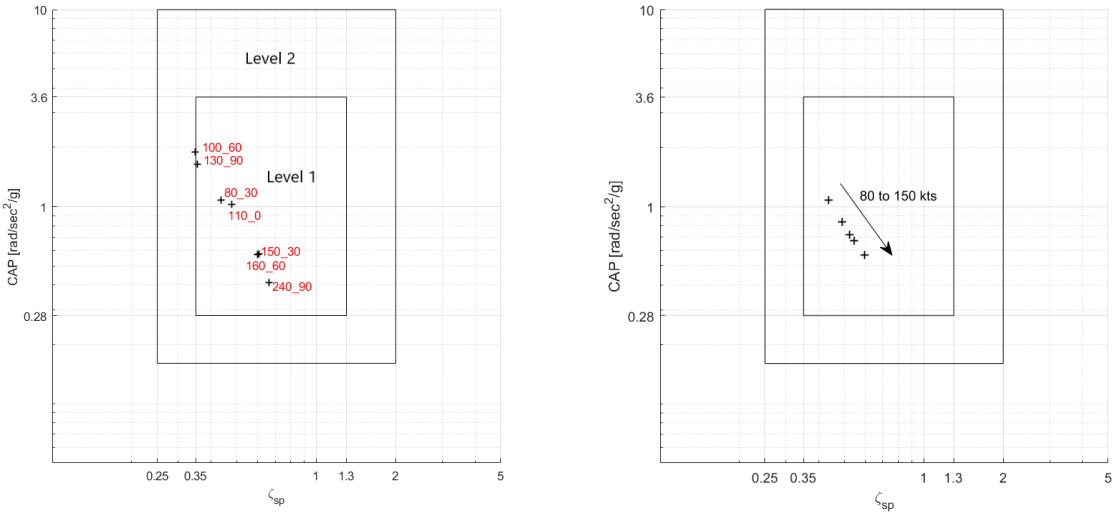

(a) Short-period damping ratio of different configurations

(b) CAP variation with airspeed 30 deg

Figure III.12: The results of CAP
(The data tip "A_B" means "Airspeed_nacelle angle". For example, "40_0" means 40 knots flight at 0 degree nacelle angle.)

Bandwidth result is shown in Figure III.13. The level 1 boundaries taken from the ADS-33E tracking and target acquisition task and MIL-HDBK-1797A Category C approach and landing task are indicated with dashed lines. Because the phase lag is zero, the bandwidth value becomes the only measure. Similar to the trend in the above two criteria, the bandwidth increases with airspeed. As the aircraft transforms from helicopter mode to airplane mode, the difference in bandwidth value between the low-speed case and the high-speed case becomes smaller. In the chart, the bandwidth of the 40 knots flight in helicopter mode does not meet the level 1 requirement of ADS-33E tracking and target acquisition task. Fixed-wing requirement is much higher than rotorcraft requirement in terms of bandwidth. The level 1 requirement in MIL for category A flight is over 6 rad/sec^2/g. None of the cases meet this level. The requirement for category C flight is 2.5 rad/sec^2/g, which excludes the case of 80 knots flight at 30 degrees tilt angle.

The pitch attitude quickness results after a 0.25-inch longitudinal stick input are drawn in Figure III.14 and III.15 with boundaries in ADS-33E for different mission tasks. Each color represents a configuration. The circular marker stands for the high-speed case in that configuration and the triangular marker stands for the low-speed case. For each line, the four markers signify the input duration of 1 second, 2 seconds, 3 seconds, and 5 seconds. It can be seen that there is a lot of overlapping for low-speed cases because the attitude change is too small. The high-speed case is more stretched for each configuration. As the airspeed increases, the line will move to the right, making it closer to the level 1/2 boundary. The black dashed lines in Figure III.14 are the boundaries for target acquisition and tracking tasks. Most parts of these lines fall inside the level 2 area. When the input duration extends, these lines can penetrate the level 2/3 boundary. A less stringent requirement is drawn in Figure III.15 which is for all other MTEs. As a result, the 240 knots flight in airplane mode meets level 1 while other cases start inside the level 1 area but stretch into the level 2 area as the input duration increases.

In comparison to the pitch attitude quickness, the results of gamma quickness are plotted in Figure III.17. The black dashed line is the proposed level 1/2 boundary determined by Pavel and Padfield [45]. In contrast to the left and right distribution for low-speed and high-speed cases seen in the theta quickness plot, the gamma quickness plot shows an up and down distribution: low-speed cases start at a high n_{zpk}/γ while high-speed cases start at a low n_{zpk}/γ. Also, they overlapped with each other in the vertical direction.

The dropback results are shown in Figure III.18. The boundary proposed by Mitchell *et al.* [23] is indicated

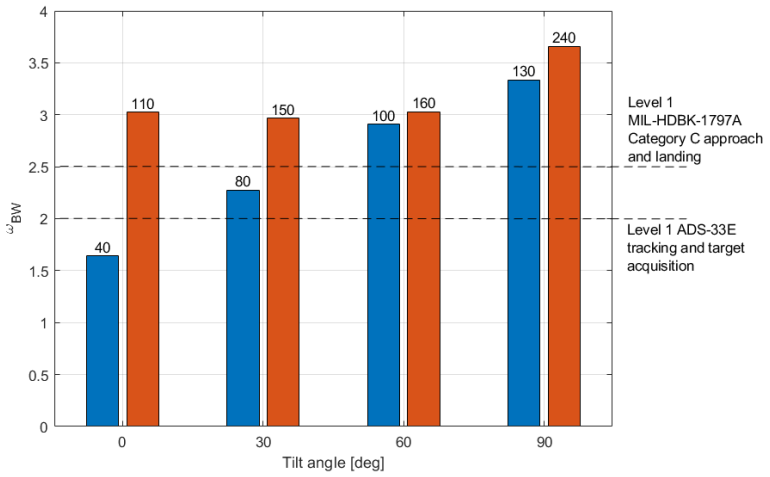

Figure III.13: Bandwidth results (The number on top of each bar is the airspeed in knots)

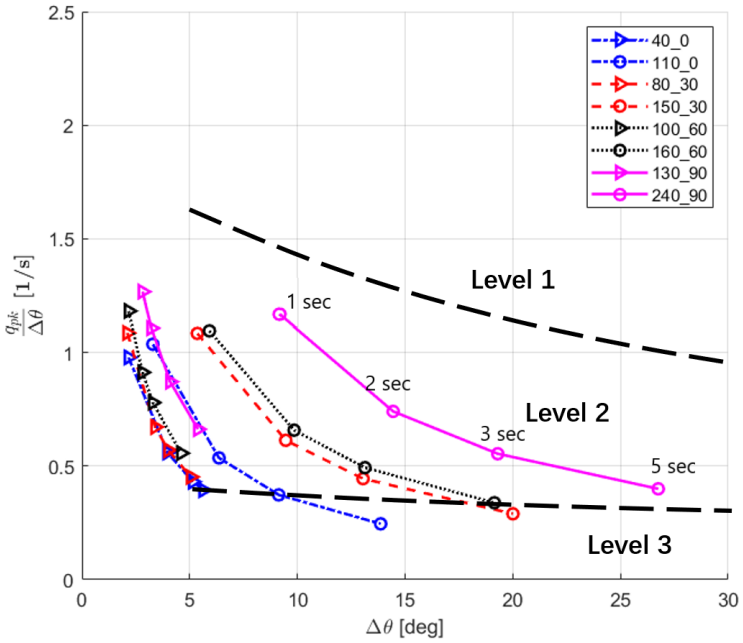

Figure III.14: Attitude quickness of the selected points in the flight envelope. Boundaries: ADS-33E target acquisition and tracking. (The legend "A_B" means "Airspeed_nacelle angle". For example, "40_0" means 40 knots flight at 0 degree nacelle angle. The data tips indicate the input pulse duration. For each line, the four markers from left to right correspond to the input duration of 1 second, 2 seconds, 3 seconds,and 5 seconds.)

with a blue line. If the response is above this line, then the level based on CAP or bandwidth should degrade by 1 level. Half of the cases lie above the line, mostly the low-speed case for each configuration. However, both the low-speed and high-speed cases in airplane mode fail to satisfy this criterion, suggesting that the XV-15 has an undesirable dropback response in airplane mode. It can also be observed that as the tilt angle increases, the point moves towards the top right. In other words, the dropback gets worse as the aircraft converts to airplane mode. Figure III.19 shows the evolution of the dropback result as the speed increases from 80 knots to 140 knots when the nacelle angle is 30 degrees. It clearly illustrates that increasing airspeed will improve the dropback.

The maximum achieved normal load factor during a 2-second longitudinal stick pulse input is plotted in Figure III.20. It aims to demonstrate the aircraft's agility during rapid obstacle avoidance maneuvers. Figure

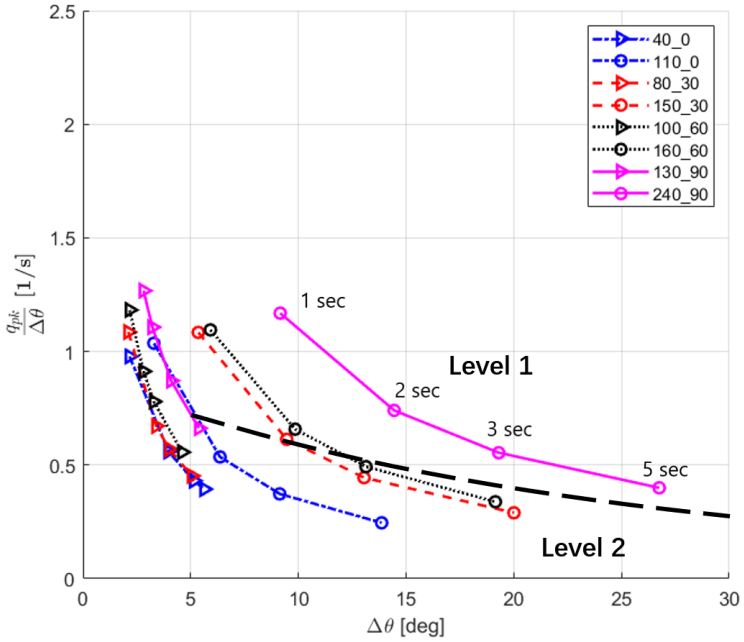

Figure III.15: Attitude quickness of the selected points in the flight envelope. Boundaries: ADS-33E All other MTEs.
(The legend "A_B" means "Airspeed_nacelle angle". For example, "40_0" means 40 knots flight at 0 degree nacelle angle. The data tips indicate the input pulse duration. For each line, the four markers from left to right correspond to the input duration of 1 second, 2 seconds, 3 seconds,and 5 seconds.)

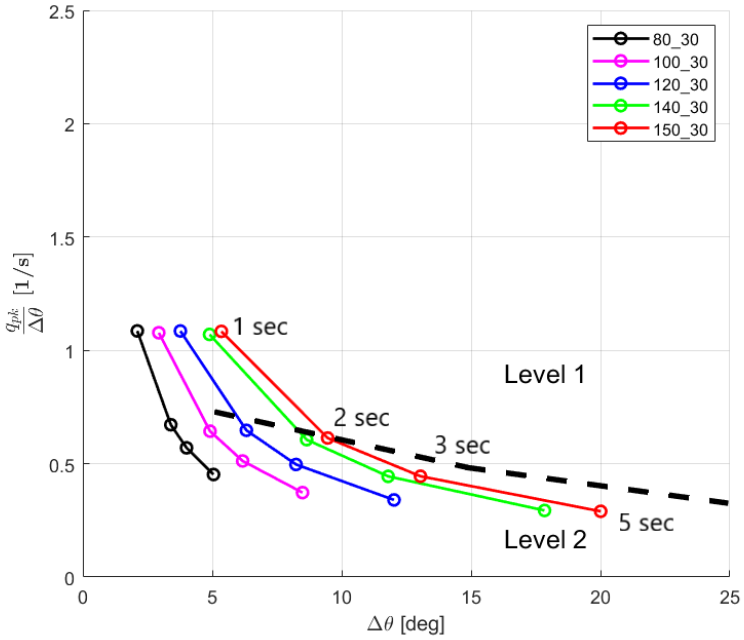

Figure III.16: Attitude quickness of different airspeed at 30 degrees nacelle angle. Boundaries: ADS-33E All other MTEs.
(The legend "A_B" means "Airspeed_nacelle angle". For example, "40_0" means 40 knots flight at 0 degree nacelle angle. The data tips indicate the input pulse duration. For each line, the four markers from left to right correspond to the input duration of 1 second, 2 seconds, 3 seconds,and 5 seconds.)

III.20a shows the results of all cases. Clearly, the peak normal load factor is a function of speed. It is also related to the configuration of the aircraft. As can be seen from the height of the bars, the peak normal

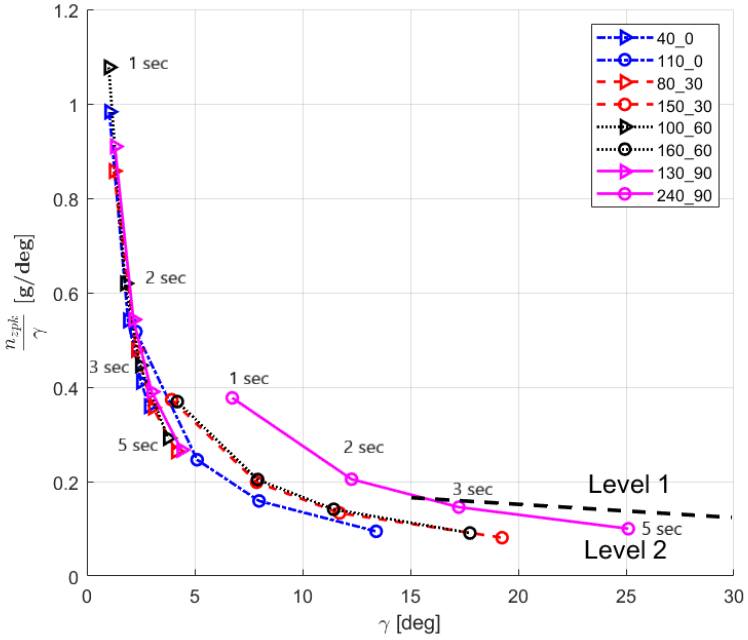

Figure III.17: Gamma quickness of the selected points in the flight envelope.
(The legend "A_B" means "Airspeed_nacelle angle". For example, "40_0" means 40 knots flight at 0 degree nacelle angle. The data tips indicate the input pulse duration. For each line, the four markers from left to right correspond to the input duration of 1 second, 2 seconds, 3 seconds,and 5 seconds.)

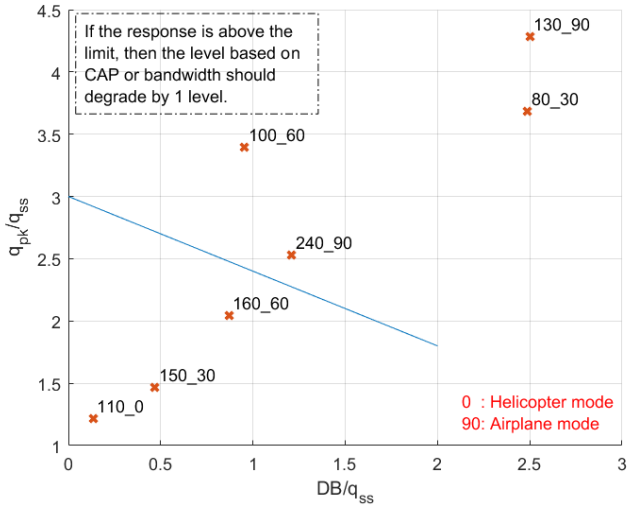

Figure III.18: Dropback results of selected points in the flight envelope.
(The data tip "A_B" means "Airspeed_nacelle angle". For example, "40_0" means 40 knots flight at 0 degree nacelle angle.)

load factor during the 110 knots 0 degree flight is higher than that during the 130 knots 90 degrees flight. Thus, flying at the right side of the conversion corridor is easier to achieve higher load factors. Figure III.20b plots the variation of the peak normal load factor with airspeed at 30 degrees tilt angle. It clearly shows the relationship between the peak normal load factor and the airspeed.

5. SUMMARY OF THE FINDINGS ON HANDLING QUALITIES DEFICIENCIES

For the short-period damping ratio, except the 100 knots 60 degrees nacelle angle had a damping ratio slightly lower than 0.35, all other cases were higher than 0.35. It was also found that the damping ratio and the un-

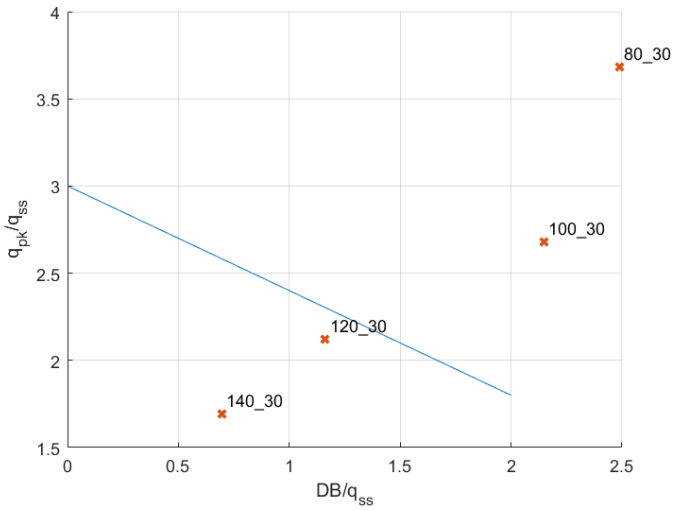

Figure III.19: Dropback results of different speed at 30 degrees nacelle angle.
(The data tip "A_B" means "Airspeed_nacelle angle". For example, "40_0" means 40 knots flight at 0 degree nacelle angle.)

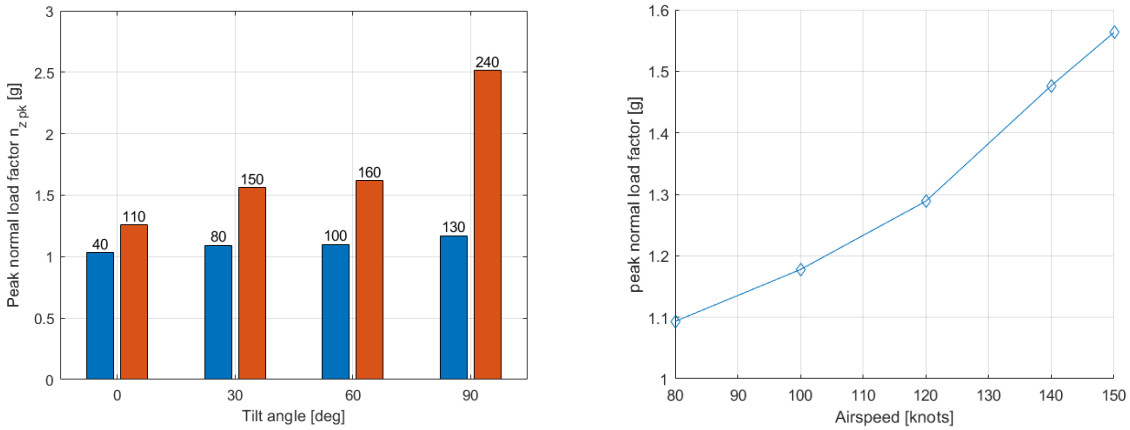

(a) Peak normal load factors of selected points in the flight envelope. The number on top of each bar is the airspeed in knots

(b) Peak normal load factors of different airspeed at 30 degrees nacelle angle

Figure III.20: Peak normal load factor during a 2-second pulse longitudinal stick input

damped natural frequency would increase with airspeed. In general, the short-period damping ratio is not a problem for this aircraft and the damping ratio will become better at high speed. For CAP, requirements are different in different standards. If using the boundaries for Category A flight specified in the MIL-HDBK-1797A, only the 100 knots 60 degrees case fell into the level 2 area due to slightly low damping. Other cases were level 1. However, if using the boundaries recommended by Gibson in Ref. [19], which is more stringent, half of the cases failed to meet level 1. It was also found that as the aircraft gains speed, the CAP would improve. In conclusion, CAP will be a problem for this XV-15 model when flying at low speed if we use the stringent criteria proposed by Gibson, but it will not be an issue if we use the less-strict criteria from the MIL-HDBK-1797A Category A flight. The results of bandwidth were compared with requirements of ADS-33E target acquisition and tracking and MIL-HDBK-1797A Category C approach and landing. The latter is more stringent. Results showed that low-speed flight in helicopter mode could not satisfy the level 1 requirement of ADS-33E. Moreover, low-speed flight in helicopter mode and conversion mode (nacelle angle below 30 degrees) could not satisfy the level 1 requirement of MIL. It was also found that the bandwidth frequency would increase with airspeed. In summary, the bandwidth frequency in low-speed flight at small nacelle angles is insufficient but it is satisfactory as the airspeed and nacelle angle increase. For the attitude quickness, none of the cases met the ADS-33E level 1 requirement of the target acquisition and tracking tasks. Some even fell

into the level 3 area as the input pulse duration increased. If using the requirement of all other MTEs, which is less stringent, only the high-speed flight in airplane mode can meet level 1. For the agility quickness, most cases started in the level 1 area using the proposed boundary in Ref. [41], but fell into the level 2 area as the input pulse duration increased. Therefore, the quickness, in general, is a problem for this aircraft throughout the flight envelope. Dropback was found to be the most critical problem for this aircraft. Results have demonstrated that very severe dropback occurred in low-speed flights. As the nacelle angle increased and the aircraft converted towards the airplane mode, dropback became worse even at high speed.

IV

Design and Optimization

1. Design parameters

Common design parameters for helicopters include disk loading, rotor solidity, blade loading, rotor tip speed, blade hinge offset, and installed power. Disk loading characterizes the hover performance and shows how loaded is the rotor. Usually, low disk loading indicates high thrust efficiency. Rotor solidity is the ratio of total blade area to disk area. It impacts the stall margin or the maneuverability potential of the rotor. Blade loading shows how loaded is the blade and indicates how close to stall is the blade operating. Rotor tip speed characterizes the noise and the performance of the rotor. Blade hinge offset is the offset of blade hinge to rotor center. This offset strongly affects the dynamic response of the blade. Blade hinge offset was left out because it was not modelled in our flight dynamic model. The installed power was also left out because varying it will cause significant changes in the weight of engines and transmission systems. Consequently, aircraft drag and weight of the tilting mechanism will change. These changes are beyond the predicting capability of our model. In the pitch axis, the tail volume coefficient is an important design parameter that affects the longitudinal stability and handling quality. It is a nondimensional parameter proportional to the tail moment arm. Finally, the design parameters selected were disk loading, solidity, blade loading, tip speed, and tail volume coefficient. Table IV.1 lists the basic data of the XV-15 tiltrotor aircraft. It is considered the baseline design.

Look-up tables are involved in the 3-DoF improved model, thus, it may come into concern that whether the validity of these tables still holds after changing the design variables. These tables describe the aerodynamics of the fuselage, the horizontal tail, and the wing. Apart from the look-up tables for the fuselage aerodynamics that contain the aerodynamic forces, what all other tables contain are aerodynamic coefficients. Hence, the resulting aerodynamic forces and moments for the horizontal tail will be reasonably scaled according to its size. Another important variable for the horizontal tail is the wing downwash angle. It remains valid because the wing is not part of the design process. The rotor is the primary subject during the design process. Its aerodynamic forces and moments are completely based on the blade element momentum theory and no look-up tables are involved. However, the significantly varied rotor will call the look-up tables for the wing, which describe the variations of wing aerodynamic coefficients with tilt angles, into question. It should be pointed out that these tables are not related to the rotor wash on the wing, but the influence of wing-pylon interference on the wing-pylon aerodynamic coefficients. They merely result from the shape change on the wing-pylon because of different nacelle angles. Therefore, their validity still holds after design changes. In summary, the look-up tables in the model will not cause problems during the design process.

1.1. Tail volume coefficient

In conventional aircraft, the primary function of the horizontal tail is to counteract the moment produced by the main wing. In tiltrotor aircraft, obviously, the moment produced by the rotor should be balanced by the horizontal tail as well. The lift generated by the horizontal tail is proportional to its area. Tail lift times the distance between aircraft CG and the tail aerodynamic center results in the tail moment. Tail volume coefficient is a nondimensional parameter proportional to the tail moment arm. It relates the tail moment arm, the wing area, and the mean aerodynamic chord of the wing.

$$V_h = \frac{S_h L_h}{S_w \cdot MAC} \tag{IV.1}$$

Table IV.1: XV-15 aircraft data

Wing	
Span	9.80 m
Chord	1.60 m
Area	15.70 m^2
Horizontal tail	
Span	3.91 m
Chord	1.19 m
Area	4.67 m^2
Proprotor	
Number of blades	3
Rotational speed	589 rpm (Helicopter mode) 517 rpm (Airplane mode)
Radius	3.81 m
Chord (constant)	0.356 m
Solidity	0.089
Disk loading	632.02 N/m^2
Weight	
Gross	5886.7 kg
Empty	4573.6 kg

S_h is the horizontal tail area.
L_h is the horizontal tail moment arm.
S_w is the wing area.
MAC is the mean aerodynamic chord of the wing.

Horizontal tail volume coefficient is a significant parameter in longitudinal stability and trim issues. As it increases, the aircraft tends to be more longitudinally stable but less controllable. Therefore, fighter aircraft usually have a low V_h to maintain the maneuverability while transport aircraft tend to have a high V_h to achieve a high degree of stability. The XV-15 has a tail volume coefficient of 1.276, which is a relatively high value. The tail volume coefficient is constrained by the longitudinal static stability requirement. The expression for the longitudinal static stability derivative C_{m_α} is shown in Equation IV.2, where C_{L_α} denotes the derivative of lift coefficient of the main wing with respect to angle of attack ($C_{L_\alpha} = dC_L/d\alpha$), $C_{L_h\alpha}$ denotes the derivative of lift coefficient of the horizontal tail with respect to angle of attack, l_{cg} is the distance of the wing aerodynamic center to the aircraft center of gravity (positive if the wing aerodynamic center is ahead of the CG), and ϵ is the wing downwash angle at the horizontal tail. The wing downwash angle ϵ is a linear function of angle of attack of the main wing before flow separation takes place. For the XV-15 aircraft, $d\epsilon/d\alpha = 0.375$. [28]

$$C_{m_\alpha} = C_{L_\alpha} \cdot \frac{l_{cg}}{c} - C_{L_h\alpha} \cdot (1 - \frac{d\epsilon}{d\alpha}) \cdot V_h \tag{IV.2}$$

A statically stable aircraft should possess a negative C_{m_α}, which leads to Equation IV.3.

$$V_h > \frac{C_{L_\alpha} l_{cg}}{c \cdot C_{L_h\alpha}(1 - \frac{d\epsilon}{d\alpha})} = \frac{4.3 \times 0.25}{1.6 \times 3.94 \times 0.625} \approx 0.273 \tag{IV.3}$$

Thus, the minimum value of V_h is 0.273. The tail volume coefficient is constrained on the high side by parasite drag and sensitivity of pitch trims to airspeed. Given a constant tail arm, a large tail will add parasite drag. Also, a large tail will move the neutral point after, which will increase the stability margin and thereby cause large (and annoying) pitch trim changes with changing airspeed. The pilot needs to apply a large elevator angle change command to restore the aircraft to level flight. In this study, the tail volume coefficient is given a small margin of ±10% to vary (1.14-1.4).

1.2. DISK LOADING

Disk loading is defined as the ratio of the aircraft weight to its rotor disk area in hovering. For tiltrotor aircraft, the rotor disk area are the sum of the two rotors' disk area. Low disk loading is an indicator of high thrust efficiency. Figure IV.1 shows the specific thrust (thrust over power) versus disk loading in hover for various VTOL configurations. As the disk loading increases, the specific thrust decreases which indicates higher energy consumption per unit of thrust. In this figure, tiltrotor aircraft has a typical disk loading of 632 N/m^2.

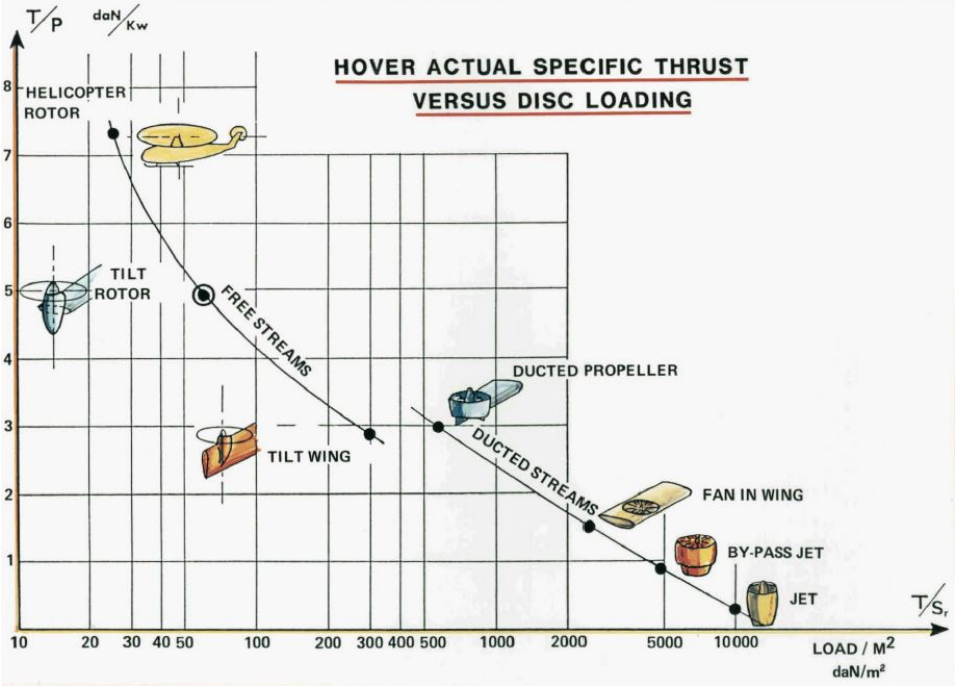

Figure IV.1: Hover lift efficiency vs disk loading [46]

$$DL = \frac{mg}{2\pi R^2} \tag{IV.4}$$

The maximum acceptable rotor size sets the lower limit of disk loading. For helicopters, the upper limit is constrained by autorotative landing capability. For tiltrotor aircraft, it is a bit different because autorotative landing capability is not a mandatory requirement for them. The XV-15 and AW609 both have demonstrated the autorotation capability, however, the V-22 was not designed with this capability. Thus, it seems that for civil applications, the autorotation capability is an additional safety requirement compared to military standards. In this study, the autorotative landing capability of the XV-15 will be preserved. Fradenburgh [47] derived the autorotative flare index which relates the energy available in descent to the energy required to perform the flare. This index is defined as:

$$AI = \frac{I_R \Omega^2}{2W \cdot DL} \tag{IV.5}$$

Higher the index is preferred because low disk loading reduces the steady-state descent rate, thus requiring less kinetic energy in the rotor. In the study carried out by Scaramuzzino *et al.* [48] to investigate the influence of this index on helicopter flight dynamics, most helicopters have an index between 5 to 40 ft^3/lb (0.31 to 2.5 m^3/kg). For the XV-15, it has an autorotative flare index of

$$AI = \frac{138 \times 3 \times 61.68^2}{2 \times 5896 \times 64.45} = 2.07$$

Due to the fact that the rotational speed Ω is also a variable, this index can not be translated to a fixed limit of the disk loading. Instead, it will act as a performance indicator at the end to evaluate the autorotative flare capability of each design. Finally, the limits of the disk loading is taken from Ref. [49]: 12-17 psf, which equal to 569-814 N/m^2.

1.3. BLADE LOADING

The definition of blade loading is

$$BL = \frac{W}{\rho A {V_T}^2 \sigma} = \frac{C_T}{\sigma} \tag{IV.6}$$

W is the aircraft gross weight in Newtons.

For tiltrotor aircraft aircraft, the W has to be divided by two because of two rotors. The design blade loading is the blade loading in hover. As the aircraft maneuvers, blade loading will change dependent of the thrust. The blade loading is constrained on the low side by structural efficiency and on the high side by the onset of blade stall. [24] Therefore, the design blade loading should not be too high in order to provide sufficient stall margin for maneuvers. The hover blade loading of the baseline XV-15 is 0.105. According to Ref. [50], certain sections may operate close to stall when the hover blade coefficient is above 0.13.

$$\overline{C}_L \approx \frac{6C_T}{\sigma} \tag{IV.7}$$

$\overline{C}_L$ is rotor mean lift coefficient.

Using Equation IV.7, the rotor mean lift coefficient is 0.78 if the blade loading equals 0.13. 0.78 is a relatively high value for mean lift coefficient, indicating that the rotor is operating close to stall. Therefore, an upper limit of 0.12 is selected for the blade loading to provide some margins for maneuvers and high-speed flight. Ref. [24] did not specify how to translate the structural efficiency to blade loading. The studies in Ref. [50][51] used 0.5 and 0.6 as the lower limit of the design blade loading. In this thesis, the lower limit of 0.8 is selected to provide the room of 20% reduction in blade loading.

1.4. TIP SPEED

The rotor tip speed is defined as:

$$V_T = \Omega R \tag{IV.8}$$

Ω is the rotor rotation speed.
R is the rotor radius.

Tip speed is constrained on the low side by an advance ratio of 0.5, where half the retreating blade side is in reverse flow. [24] It is constrained on the high side by the tip Mach number of 0.95 of the advancing blade, where the compressibility effect come into play. The rotors of XV-15 operate at 589 rpm in helicopter and conversion mode, and at 517 rpm in airplane mode. The rotor has a radius of 3.81m. According to its performance data, the XV-15 has a maximum dive speed of 300 knots (154 m/s) in airplane mode, which translates to a rotor tip speed of

$$V_T = \sqrt{154^2 + (\frac{517 \times 2\pi}{60} \times 3.81)^2} \approx 257\,\text{m/s} = 0.75\text{Ma}$$

In helicopter mode (0° tilt angle), the maximum dive speed is 132 knots (67 m/s). The tip speed is

$$V_T = 67 + (\frac{589 \times 2\pi}{60} \times 3.81) \approx 302\,\text{m/s} = 0.88\text{Ma}$$

In conversion mode (60° tilt angle), the maximum dive speed is 190 knots (98 m/s). The tip speed is

$$V_T = \sqrt{(\frac{589 \times 2\pi}{60} \times 3.81 \times \sin 60°)^2 + (\frac{589 \times 2\pi}{60} \times 3.81 \times \cos 60° + 98)^2} \approx 296\,\text{m/s} = 0.86\text{Ma}$$

In the airplane mode, there exists a considerable margin before the compressibility effect takes place. The design tip speed is the tip speed in hover. Consider the helicopter mode 140 knots flight where the tip speed mach number is the highest, the design tip speed must be lower than 259 m/s in order to keep the tip speed below 0.95 Ma when the aircraft reaches the dive speed. This corresponds to the upper limit of the design tip speed. The highest advance ratio occurs at the highest speed in helicopter mode. In order to keep the advance ratio below 0.5, the lower limit of the tip speed is 72/0.5=144 m/s.

1.5. ROTOR SOLIDITY

As defined in Equation IV.9, rotor solidity is the ratio of total blade area to disk area.

$$\sigma = \frac{Nc}{\pi R} \tag{IV.9}$$

Solidity is an important parameter in rotor design. The rotor mean lift coefficient is given in terms of the blade loading. A rotor that uses airfoil sections with a higher maximum lift coefficient can have a lower solidity. Alternatively, for the same solidity, the use of high lift airfoils allows a lower tip speed. Selecting the solidity requires careful consideration of blade stall limits, which is the rotor mean lift coefficient where the rotor is operating close to stall. The onset of stall limits the performance of a rotor. A high solidity provides a larger stall margin, which is the margin between the average operational lift coefficient and the maximum lift coefficient. Thus, rotors that are designed for high-speed flight and high maneuverability require a higher solidity for a given tip speed and radius. However, high solidity has a negative effect on profile power. To minimize the profile power, one should select a solidity as low as possible, which in turn will increase the blade loading and decrease the stall margin. In addition, high solidity comes with increased blade weight and higher overall rotor weight. Therefore, rotor solidity is constrained on the low side by hover performance and on the high side by maneuverability requirement. The baseline XV-15 uses a solidity of 0.089. In Ref. [50] and Ref. [51], the range of solidity is 0.5-0.16 and 0.06-0.12, respectively. Thus, in this study, 0.06-0.14 is used.

2. WEIGHT

To evaluate the effects of design parameters on aircraft empty weight, a standard published methodology was used [52]. These components include the rotor, wing, horizontal stabilizer, and drive system. The weights of them are estimated using empirical equations which combine analytical and empirical factors and have been well correlated with many helicopters in history. However, in the tiltrotor aircraft, some of these components have a different layout. For instance, the XV-15 has a central gearbox system that can deliver the power of one engine to the rotor on the other side in case of one engine inoperative situation. Also, the wing has to support the bending moments from the nacelles at the wingtips, which requires it to be stronger than wings on conventional aircraft. Thus, before applying these weight equations, the predictions by these equations are compared to the XV-15 data published in Ref. [27] to check if the accuracy of these equations is good. If differences are found, a correction factor will then be added to these equations to correct the deviations. The results are summarized in Table IV.2.

This weight evaluation task is different from the conventional sizing task, due to the fact that the fuel required is not considered. To simplify the analysis, the aircraft's gross weight is held constant.

2.1. ROTOR

The rotor is divided into hub and blades. The weight of the rotor controls is not included in the weight of the rotor, but belongs to the weight of flight controls and is useful when evaluating the weight of the wing.

BLADE

$$\begin{aligned} W_b &= 44 \cdot K^{0.438} \\ K &= \frac{GW}{10^4} LLF \frac{R^2}{100} \frac{R-r}{10} \cdot b \cdot c \cdot K_b \end{aligned} \tag{IV.10}$$

GW: Design gross weight
LLF: Limit load factor
R: Rotor radius
r: Blade cutout radius
b: Number of blades per rotor
c: Blade chord
K_b: Rotor type factor. Hingeless=2.2

HUB

$$\begin{aligned} W_H &= 61 \cdot K^{0.358} \\ K &= W_b \cdot R \cdot (N_R)^2 \cdot P_R \cdot r^{1.82} \cdot b^{2.5} \cdot K_{amd} \cdot 10^{-11} \end{aligned} \tag{IV.11}$$

Table IV.2: Comparison of the XV-15 components weight predicted by the empirical equations to the published data ("unknown" means the data is not published. For example, Ref. [27] does not give the hub weight and blades weight, but the rotor weight in total. The empirical equations give the hub weight and blades weight, which can be added to obtain the rotor weight. Then, the two values of rotor weight are compared (535 vs 537). Finally, the correction factor is applied to the rotor weight derived from the empirical equations, such that "Published weight = Predicted weight × Correction factor". Some correction factors are applied to the component itself, some are applied to its sub-component.)

	Published data [27]	Predicted	Correction factor
Wing	873	799	1.1
Tail	209	-	-
Horizontal Tail	unknown	138	1
Vertical Tail	unknown	-	-
Rotor	535	537	0.996
Hub	unknown	290	
Blades	unknown	247	
Drive system & Tilt Mechanism	1263	1226	
Drive system	unknown	1096	1.034
Tilt Mechanism	unknown	130	1
Fuel	1490 (Max.)	-	-
Oil and trapped fluids	138	-	-

W_H: Hub weigh per rotor
W_b: Blade weight per rotor
N_R: Rotor RPM
P_R: Rotor horsepower per rotor
K_{amd} : $a \times m \times d$
-a: Design concept: Hingeless=0.53 Other=1
-m: Material type: Steel=1 Titanium=0.54
-d: Development stage: Early=1 Developed=0.62

ROTOR CONTROLS

$$W_{RC} = 0.3 W_R \tag{IV.12}$$

According to Ref. [27], the weight of the XV-15 rotors is 1070 lbs, which gives 535 lbs per rotor. Most of the terms in the above equations are explicit and the value of them can be found in published data. Except that it is not clear which power should be used for the term rotor horsepower P_R. There are contingency power, takeoff power, military power, and normal power (max. continuous). It was decided to use the normal, maximum continuous power of 1250 hp since it is the designed power for most of the flight conditions. The term K_{amd} is determined by the rotor type, material type, and the development stage. The XV-15 features a gimballed hingeless rotor with a titanium hub. Thus, $K_{amd} = 0.53 \times 0.54 \times 0.62 = 0.177$. As a result, the equations give 247 lbs for the weight of the blades, and 289 lbs for the weight of the hub. Add these two together results in 536 lbs for each rotor, which is almost identical to the actual weight of 535 lbs.

2.2. WING

$$W_w = 377.2 K^{0.585}$$
$$K = \frac{R_M \cdot W_{XW}}{10^4} \frac{S_w}{10^2} \left(log_{10} \frac{b}{B}\right) \sqrt{\frac{1+\lambda}{2K_r}} \sqrt{N} \left(log_{10} V_D\right) \left(log_{10} AR\right) \tag{IV.13}$$

R_M: Relief term
W_{XW}: Gross weight less items at center of lift, which includes:
-Rotors

-Rotor controls
-Wing
-Fuel = 1490 lbs (Maximum)
-Oil and trapper fluids = 138 lbs
-Powerplant = 1754 lbs
-Drive system and tilt mechanism=1263 lbs

S_w: Planform wing area
b: Wing span
B: Maximum fuselage width
λ: Wing taper ratio
K_r: Wing root thickness, percent chord
N: Ultimate load factor
V_D: Dive speed
AR: Aspect ratio

It was not explained in the reference on how to derive the relief term R_M. It should be a term related to the relieving effects on the bending of the wing due to the fuel weight stored in the wing. The same value of 0.6 is used as that in the Ref. [52]. The XV-15 wing uses a modified NACA 64A223 airfoil, which indicates a maximum thickness of 23% chord. The dive speed is 300 kts. According to Ref. [27], the structural ultimate factor of safety is 1.5. Multiplying it with the limit load factor 3 gives the ultimate load factor of 4.5. In this equation, the most important term is the W_{XW}, which is the gross weight less items at the center of lift. Among those items, rotors, rotor controls, drive system and tilt mechanism are also part of the weight evaluation task. Thus, they should be evaluated before the wing. The wing weight itself is also one of the items that need to be subtracted. Thus, a while loop is created to obtain the convergence of the wing weight.

```
W_w = 1000; % initial guess of the wing weight
err = 10;   % condition to start the loop
while abs(err) > 1
    W_w_est = W_w;
    W_xw = GW - W_w_est - W_others; % W_others: weight of items at center of lift
    W_w = F(W_xw);                 % W_w is a function of W_xw
    err = W_w - W_w_est;
```

Usually, convergence can be achieved in around 3 loops. The predicted wing weight is 799 lbs, which is about 10% less than the actual weight of 873 lbs. A correction factor of 1.1 is added to the wing weight equation.

2.3. HORIZONTAL TAIL

$$
\begin{aligned}
W_{HT} &= 350 \cdot K^{0.54} \\
K &= F_H \frac{S_H}{10^2} \frac{log V_D}{T_{MA} t} \\
F_H &= \frac{GW}{10^4} \frac{K_y}{10} \frac{b_H}{10} \frac{1+2\lambda}{1+\lambda} K_{TL}
\end{aligned}
\tag{IV.14}
$$

W_{HT}: Weight of horizontal tail
S_H: Horizontal tail area
V_D: Dive speed
T_{MA}: Tail moment arm
t: Root thickness
K_y: Pitch radius of gyration. Refer to Figure IV.2
b_H: Tail span
λ: Tail taper ratio
K_{TL}: Tail load factor

Ref. [27] did not present the data of the weight of the individual horizontal tail, but the whole tail which is 209 lbs. Using the equations above the predicted weight of the horizontal tail is 138 lbs, which is a reasonable portion of the tail weight. Therefore, no correction factor is applied to the horizontal tail equation.

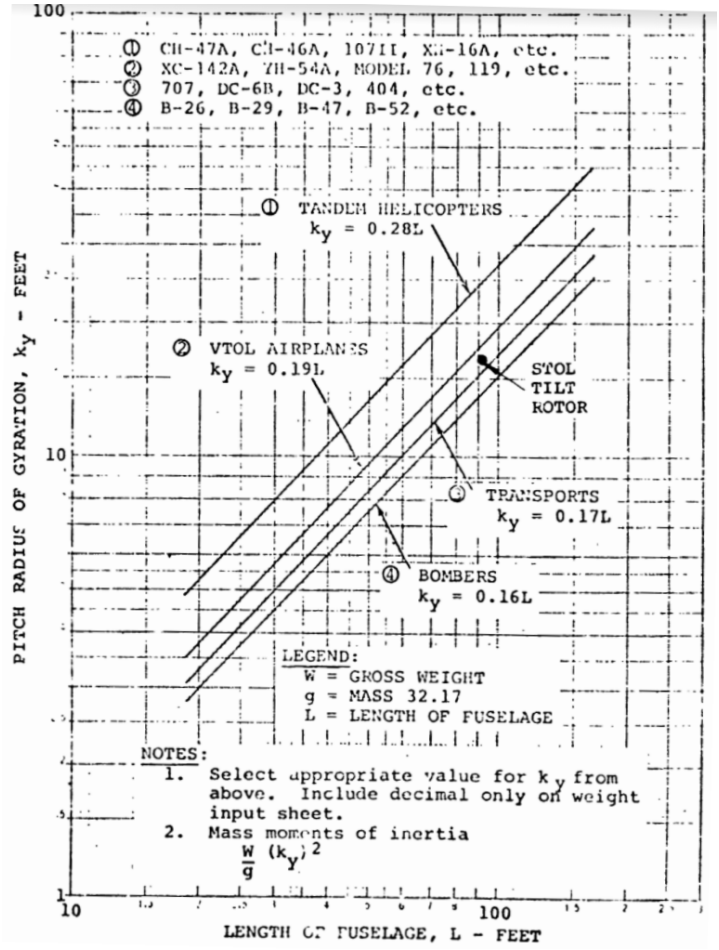

Figure IV.2: Pitch radius of gyration [52]

2.4. DRIVE SYSTEM AND TILT MECHANISM

Figure IV.3: Boeing Vertol Model 222

DRIVE SYSTEM

$$W_{DS} = 250 \cdot K^{0.67}$$
$$K = \frac{1.1 \times HP}{RPM} Z^{0.25} K_T \tag{IV.15}$$

W_{DS}: Weight of drive system
HP: Total horsepower
RPM: Rotor design RPM
Z: Number of stages in main drive
K_T: Configuration factor = 1.3

TILT MECHANISM

$$W_{TM} = 0.01 \cdot GW \tag{IV.16}$$

W_{TM}: Weight of tilt mechanism

Using the data from Ref. [27], the total weight of the drive system plus the tilt mechanism is 1263 lbs. The weight of drive system and tilt mechanism predicted by Equation IV.15 are 1096 and 130 lbs, respectively. Add them up gives 1226 lbs in total, which is very close to the actual value. Widdison *et al.* wrote in Ref. [52] that the drive system weights were based on that of the Boeing Vertol Model 222, whose engines are in fixed pods at the end of its wing, and a small rotating pod that houses the rotor is located at the inner side of the engine. Compared to it, the XV-15's engines are mounted inside the nacelles and tilt together with the rotors. The engine configuration is completely different for these two models, thus obtaining such a close result is very surprising. In the end, a correction factor of 1.034 is applied to the drive system weight to achieve consistent results.

3. DESIGN SPACE GENERATION

Design space is a multidimensional space which describes the relationship between performance parameters and design parameters. With the design space, designers can readily observe the influence of each design parameter on all performance parameters, as well as the strength of the influence. This knowledge will form the base for later optimization stage. The design parameters are disk loading, solidity, tail volume coefficient, blade loading, and tip speed. The performance parameters are handling qualities, component weight, and maneuverability. To generate the design space, an analysis tool must be developed to perform the following four tasks:

1. Translate design parameters into aircraft configuration parameters.
2. Evaluate the weight of each components.
3. Calculate the handling qualities parameters.
4. Simulate maneuvers and output the performance parameters.

This section will explain in detail how these tasks are accomplished and how they are connected to each other.

3.1. ADDITIONAL CONSTRAINTS

Apart from the individual lower and upper limit for each design parameter, there are also constraints arising from other aspects. Figure IV.4 shows the three views of the XV-15 aircraft. It should be noticed that when in airplane mode, the clearance between the blade tip and the fuselage is very small. Thus, increasing the rotor radius is not possible without increasing the wingspan simultaneously. The wing of the XV-15 features a forward sweep to provide a margin for the flapping motion of the rotor blades. Hence, increasing the wingspan will shift the nacelle forward, leading to the shift of the body CG. This change will impact the stability and overall structure of the aircraft, which exceeds the scope of this study. Therefore, the wingspan is held constant. Correspondingly, the lower limit of disk loading is fixed to 632.04 N/m^2.

The design parameters are interconnected and they cannot be varied independently. To generate the design space, the approach described in NASA's NDARC (NASA Design and Analysis of Rotorcraft) [53] is adopted. For each combination of design parameters, the rotor radius or the disk loading, the blade loading,

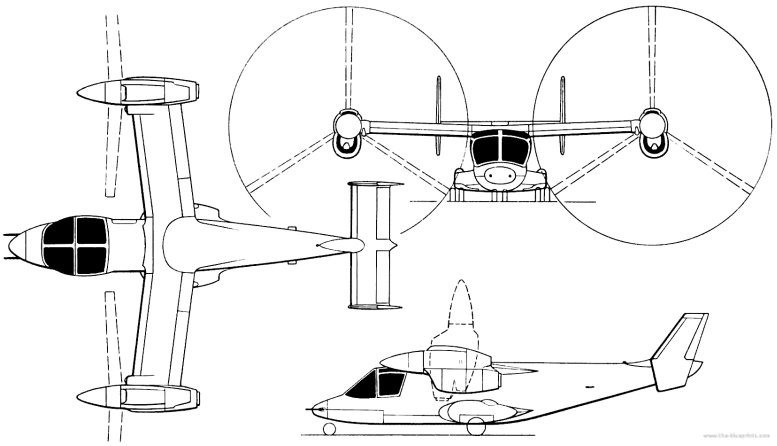

Figure IV.4: Three views of the XV-15

the rotor solidity, and the tail volume coefficient are inputs and other parameters are derived. Following the approach taken by Fradenburgh [54], this study keeps the gross weight and lifting capacity constant. The gross weight is fixed at 5897 kg. The lifting capacity is the same as the blade loading. The definition of lifting capability is:

$$NcR(\Omega R)^2 = \sigma A V_T^2 = \text{CONSTANT} \tag{IV.17}$$

This relationship is derived from the equation for the thrust force:

$$T = \frac{1}{2} a_0 \sigma \rho \pi R^2 V_T^2 = a_0 \rho \sigma A V_T^2 \tag{IV.18}$$

The blade sectional lift coefficient a_0 is always the same because the blade airfoil is not changed. Thus, the remaining part of Equation IV.18 constitutes the lifting capability described in Equation IV.17. This requirement will alter the rotor rpm. In addition, the blade number is fixed. One reason is that increasing the blade number will significantly add to the rotor weight. The other reason is that all tiltrotor aircraft (XV-3, XV-15, V-22, AW609, V-280) use a 3-blade rotor, which reflects that a 3-blade rotor is particularly suitable for tiltrotors.

3.2. SET-UP OF THE ANALYSIS TOOL

The formulation of design space requires a large number of design points. Therefore, automating the process of generating configurations, evaluating weight, computing performance parameters are essential. For each design configuration, the evaluation process is divided into five modules as illustrated in Figure IV.5: configuration generator, trim and linearization, weight evaluation, maneuver performance evaluation, and handling qualities evaluation. Each module is programmed as a function in Matlab and they are organized together in a loop. By executing the loop, the program will sequentially generate all possible configurations based on the user-specified range of the input design parameters. Then, it will perform all the calculations and save the results to a csv file.

The process starts from the configuration generator. The inputs are disk loading, tail volume coefficient, blade loading, and rotor solidity. The outputs are the aircraft configuration parameters. For the horizontal stabilizer, the aspect ratio and the tail arm are kept constant. Thus, its chord and span can be derived from the tail volume coefficient. For the rotors, with a known radius and solidity, the blade chord can be calculated. Then using Equation IV.6, the rotational speed Ω can be derived. At this step, all variables needed to calculate the tip speed have been obtained. Next, the calculated tip speed is compared against its lower and upper limits. Only if it falls into the specified range, the procedure continues. Otherwise, this combination of input parameters is discarded and the program will move to the next combination.

The second block is weight evaluation, to which the input is the aircraft configuration parameters obtained from the configuration generator. Using the empirical equations described in Section 2, the weight of those design-related components are calculated. Next, the calculated weight results are compared to their original value so that the change in the weight of each component can be obtained. Finally, adding them up gives the change in total empty weight.

For maneuver performance and handling qualities evaluation, trim and linearization results are needed. In addition to the configuration parameters, the flight condition (flight speed, air density), flap setting, and

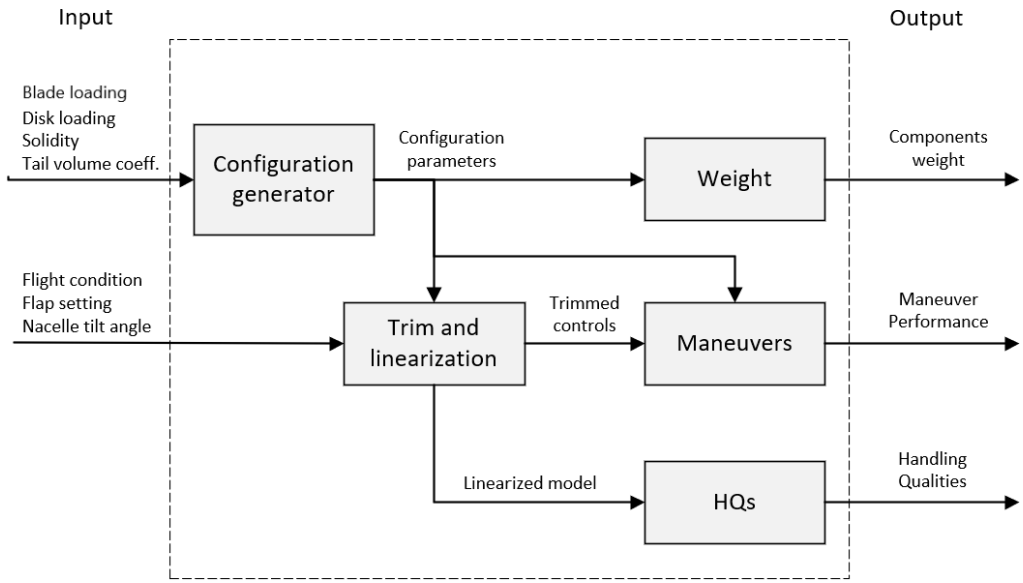

Figure IV.5: Block diagram of the program

nacelle tilt angle are also input parameters to the trim and linearization block. Following the procedure introduced in Section 3 in Chapter 2, it computes the trimmed controls in the designated flight condition and obtains the linearized state-space model. The block "HQs" computes the handling qualities parameters that can be derived directly from the linearized state-space model. The block "Maneuvers" contains those handling qualities and maneuverability parameters that can only be derived from simulation, including attitude quickness, agility quickness, peak normal load factor, and acceleration time.

4. DESIGN SPACE EXPLORATION – CASE STUDY: 100 KNOTS 30 DEGREES

The previous results show that when flying at 30 degrees with a speed of 100 knots, the original XV-15 design demonstrates insufficiency in CAP, quickness, and dropback. This case study will use the approach in Figure IV.5 to generate the design space, in the hope to find a design configuration that exhibits improved handling qualities. The inputs and their limits are shown in Table IV.3.

Table IV.3: Input parameters and their limits.
(Note: Details of how these limits were determined have been explained in Section 1. Tip speed is not an input, it is derived from other input parameters)

Inputs	Symbol	Unit	Lower limit	Upper limit	Constraint descriptions
Disk loading	DL	N/m^2	632.04	814.23	Rotor size and autorotation capability
Solidity	SIGMA	-	0.06	0.14	Hover performance and maneuverability
Blade loading	BL	-	0.08	0.12	Structural efficiency and maneuverability
Tail volume coefficient	TVC	-	1.14	1.4	Stability, parasite drag, and pitch trim

With the help of a commercial statistical analysis software *JMP* (a suite of computer programs for statistical analysis developed by the JMP business unit of SAS Institute), the influences of each design parameter on handling quality performance parameters were constructed by fitting the data into polynomial curves. The results are shown in Figure IV.6 in the form of a prediction profiler. On the horizontal axis are four design parameters (blade loading is constant thus not shown): disk loading, solidity, tail volume coefficient, and tip

speed. On the vertical axis are six handling quality parameters: short period damping ratio, short period natural frequency, CAP, bandwidth frequency, attitude dropback over steady-state pitch rate, and peak pitch rate over steady-state pitch rate. Each curve shows the predicted response of a handling quality parameter w.r.t. a design parameter. The dashed lines are user-adjustable, which intersect with the response curves at query points. All response curves are dynamically computed based on the query points. A different combination of query points will output different shapes and positions of the response curves.

The design parameters in Figure IV.6 are set to their original values. Obviously, tail volume coefficient and tip speed have much stronger influences on these handling quality parameters than disk loading and solidity. Looking at these responses curves, the following can be observed:

- A low disk loading is preferable in respect of reducing dropback, reducing CAP, increasing short period damping, and increasing the peak normal load factor. Disk loading has a minor effect on the short period natural frequency and bandwidth frequency.
- Solidity has very small influences on all these handling qualities parameters. It barely has any influence on the dropback and peak normal load factor. Decreasing solidity is favorable to increase the bandwidth frequency but will reduce the short period damping ratio and increase the CAP.
- Tail volume coefficient shows a strong influence on these handling quality parameters. Increasing the tail volume coefficient is effective in terms of elevating the bandwidth frequency and reducing the ratio of the attitude dropback to the steady-state pitch rate. However, it is not preferred because the short period damping ratio will drop and the CAP will grow.
- Similar to the tail volume coefficient, tip speed also has noticeable effects on these parameters. All curves show that lowering the tip speed is beneficial in every aspect.

From the above observations, it can be seen that disk loading and tip speed have the same effect on all handling quality parameters, improving one will not worsen the others. But the influence of solidity and tail volume coefficient is not that simple. When trying to improve one handling quality parameter by adjusting solidity or tail volume coefficient, other handling quality parameters may receive negative influences. But in view of the handling quality requirements, as long as these parameters remain in the level 1 area, the design changes are considered acceptable.

The influence of these design parameters on total weight is shown in Figure IV.7.

- The horizontal tail weight is only influenced by the tail volume coefficient. Due to the fact that the horizontal tail weight is only a small part of the total weight, the tail volume coefficient has almost no influence on the total weight.
- Disk loading affects the weight noticeably. Increasing the disk loading can significantly reduce the drive system weight because the rotor becomes smaller and the required torque is lower.
- Solidity has a medium influence on the total weight mainly through its influence on the drive system weight, because higher solidity will require more torque to overcome the profile drag.
- Tip speed has a comparable influence on weight as disk loading does and their influences on the weight of each component share the same trends.

It is worth noticing that the decrease of tip speed will significantly increase the total weight, although lowering the tip speed is beneficial in every aspect.

The CAP variation with tip speed and tail volume coefficient is plotted in Figure IV.8. All configurations demonstrate satisfactory CAP values between 0.28 and 1. Only the lowest and the highest tip speed are indicated because the points are very dense. From left to right, the tip speed varies from 267 to 202 m/s. Also, three different values of tail volume coefficient are marked with different colors as illustrated in the legend. This plot is a more concrete illustration of the curves in the prediction profiler for CAP: decreasing the tail volume coefficient and the tip speed both contribute to the decline of CAP.

Apart from the tail volume coefficient, other parameters have negligible effects on the bandwidth frequency. The bandwidth frequency varies linearly with the tail volume coefficient. Figure IV.9 shows the bandwidth frequency vs. tail volume coefficient when other design parameters are fixed (DL=632.04, SIGMA=0.085, VT=202). The level 1 boundaries from ADS-33E and MIL-HDBK-1797A are drawn in dashed lines. The baseline design has a tail volume coefficient of 1.276, which falls below the level 1 boundary of the fixed-wing

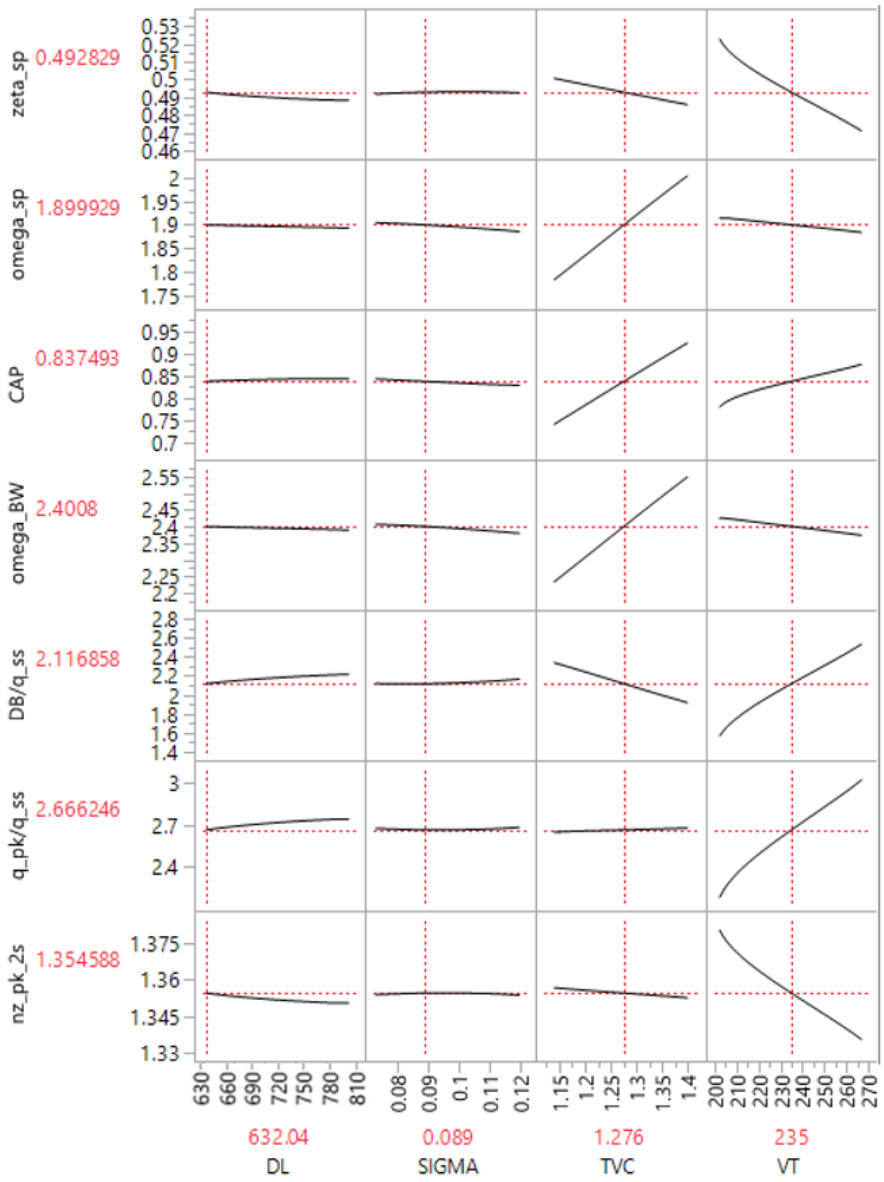

Figure IV.6: Predication profiler of handling qualities parameters – 100 knots 30 degrees

requirement for approach and landing tasks, but satisfies the rotorcraft requirement. By increasing the tail volume coefficient, the level 1 boundary of the MIL requirement can be met.

Figure IV.10a shows the evolution of dropback when the tip speed changes. The disk loading is set to 632.04 and solidity to 0.085. Three cases with different tail volume coefficients are shown here. By increasing the tail volume coefficient by 10%, a low tip speed down to 202 m/s can move the dropback response to the boundary of the preferred zone. Increasing the tail volume coefficient will shift the curve to the left, making it closer to the boundary. It can be expected that if more freedom were given to the tail volume coefficient and the tip speed, a dropback point inside the preferred zone can be obtained.

The dropback criterion requires two parameters, which constitute the two coordinates to determine the point on the dropback plot. It is inconvenient to use two parameters in the analyzing process. Additionally, two parameters make it difficult to show dropback together with the other results on a 2D plot. Hence, it was decided to use a new parameter, namely the "dropback distance", to express the dropback quantitatively. It is basically the distance between the resulting point to the dropback boundary line. The expression of the boundary line in the dropback plot is

$$y = -0.6x + 3 \tag{IV.19}$$

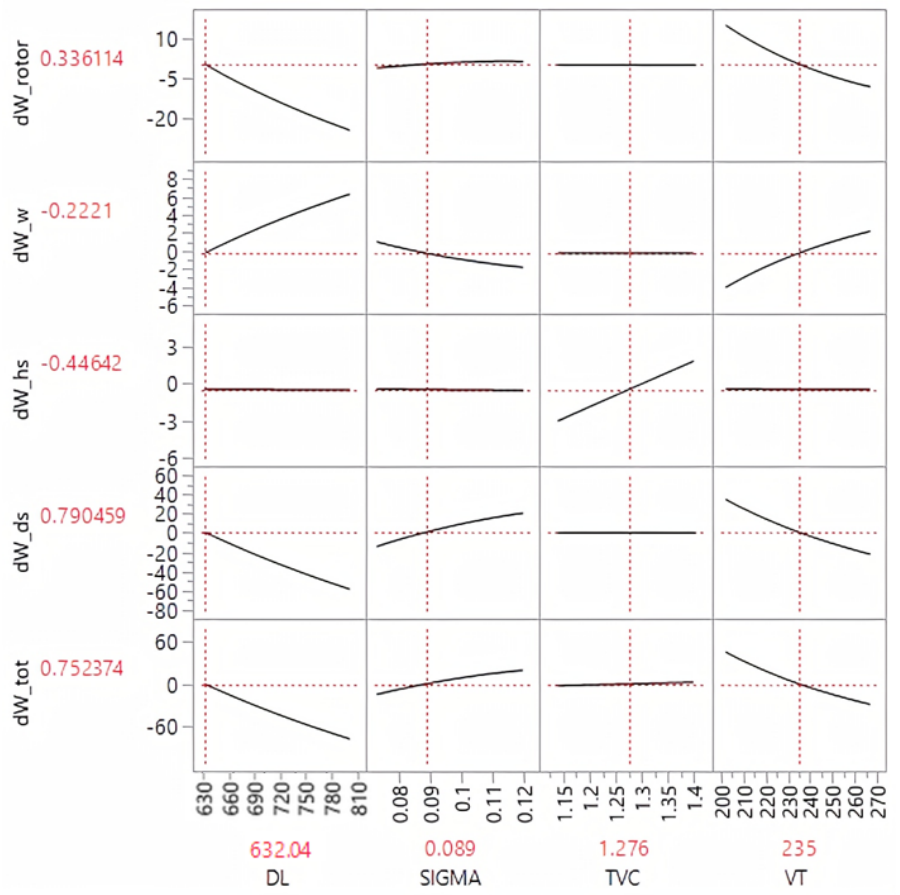

Figure IV.7: Prediction profiler of weight – 100 knots 30 degrees

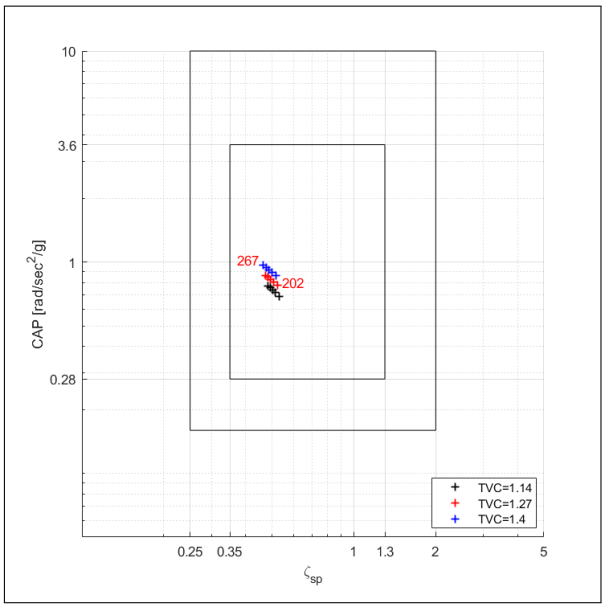

Figure IV.8: The results of CAP for different TVC and VT (DL=632.04, SIGMA=0.085). From left to right, the tip speed varies from 267 to 202 m/s. The data tips indicate the tip speed

The distance of a point (x_0, y_0) to a line $y = kx + b$ can be calculated via

$$d = \frac{|kx_0 - y_0 + b|}{\sqrt{k^2 + 1}} \tag{IV.20}$$

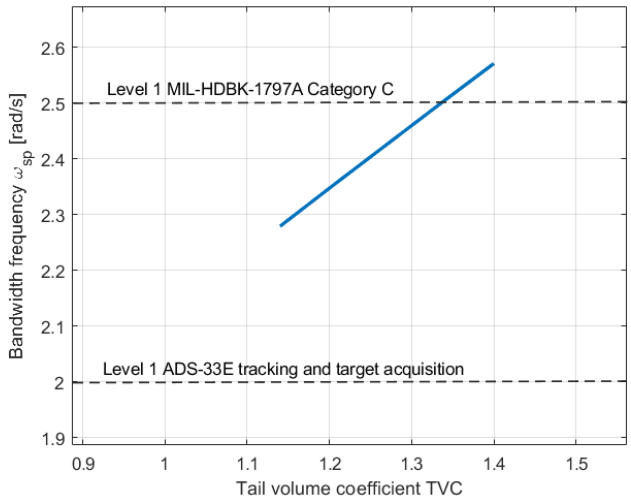

Figure IV.9: Bandwidth frequency vs. tail volume coefficient (DL=632.04, SIGMA=0.085, VT=202)

Thus, the distance of a point (x_0, y_0) on the dropback plot to the boundary line is

$$d = \frac{-0.6x_0 - y_0 + 3}{\sqrt{0.6^2 + 1}} \tag{IV.21}$$

If d is positive, the point lies below the line. Otherwise, it lies above the line. Therefore, the larger the d is, the better the dropback response. And a positive d is preferred.

By applying the "dropback distance", the effect of the variation of dropback, tail volume coefficient, and tip speed on the empty weight is plotted in Figure IV.10b. Dropback distance is on the vertical axis. The larger the better. This plot shows the variation of tip speed from 202 m/s to 267 m/s under three values of tail volume coefficient and the resulting change in the empty weight. Each curve consists of five points. From left to right, they represent tip speed values of 267, 251, 235, 218, and 202 m/s. As the tail volume grows, the curve moves upwards and the points move rightwards. The former means an improvement of dropback and the latter means an increase in empty weight. At high tip speed, the three lines converge, indicating that the tail volume coefficient no longer influences the dropback too much. As the tip speed decreases, the dropback improves but the empty weight rises as well. When the tip speed equals 202 m/s at a tail volume coefficient of 1.4, the dropback distance becomes zero, which corresponds to the point lying on the boundary line in Figure IV.10a. However, the empty weight is also the highest at this point.

The attitude quickness of all configurations and the requirements for target acquisition and tracking are drawn in Figure IV.11a. Correspondingly, the agility quickness results of all configurations are plotted in Figure IV.11b. It shows that these design parameters have nearly no effect on attitude quickness and agility quickness.

Finally, the curves showing the change in the power required (100 knots 30 degrees) vs. change in design parameters are plotted in Figure IV.12. All parameters are scaled to percentages. The slope of the curve indicates the sensitivity of the power w.r.t. the design parameter. Clearly, the power required is most sensitive to the variation in tip speed because increasing tip speed will lead to the rapid growth of rotor drag. Secondly, disk loading and solidity have almost identical effects on the power required. Lastly, the tail volume coefficient barely influences the power required. This is due to the fact that this parameter only changes the tail surface area, which is a very small contribution to the overall drag of the aircraft.

4.1. COMPARISON WITH THE 140 KNOTS 60 DEGREES CASE

A tiltrotor can fly at different configurations than the 100 knots 30 degrees. Then the question comes: are the trends obtained above also applicable to other configurations? In order to answer this question, the same process was run again for the 140 knots 60 degrees case to generate another prediction profiler. By comparing the trends of the curves to those of the 100 knots 30 degrees case, it can be found that

- For disk loading and solidity, the slopes of the curves remain small. There are minor differences in the

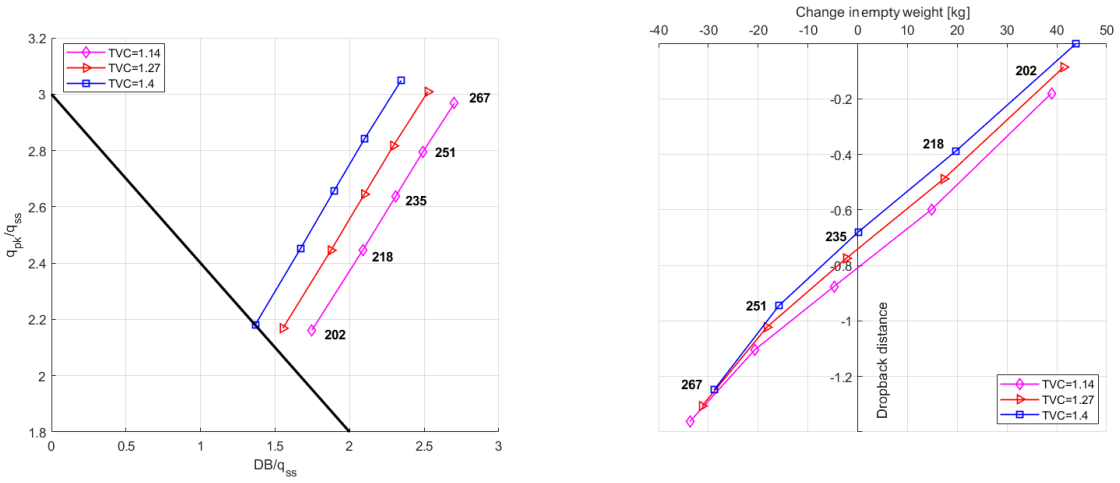

(a) Dropback at different tail volume coefficient

(b) Dropback at different tail volume coefficient

Figure IV.10: Dropback at different tail volume coefficient (DL=632.04, SIGMA=0.085)
(The number next to each point is the tip speed in m/s)

directions of these curves, but the majority shows a consistent result. These minor differences may also source from the errors during the fitting.

- The major differences are the effects of tip speed on bandwidth frequency and short-period frequency. In the 100 knots 30 degrees case, the two frequencies increase with tip speed. While in the 100 knots 60 degrees case, the two frequencies slightly decrease with tip speed.

Therefore, even though most of the trends are similar, the results of the 100 knots 30 degrees alone cannot represent the influences of the design parameters in other configurations. In order to make the design study more comprehensive, more configurations should be included in the future.

4.2. REMOVE THE CONSTRAINT OF CONSTANT BLADE LOADING

In previous design changes, the dropback point cannot be moved into the preferable region. In this section, the constant blade loading constraint will be removed to give the design more freedom in the hope to obtain a better dropback performance. The blade loading then becomes another design parameter. In the configuration generator, the tip speed will be derived from these four inputs. Same as before, the derived tip speed will be compared against its lower and upper limits, out-of-bounds tip speed will cause this combination of inputs to be rejected.

Figure IV.14 and IV.15 shows the predication profiler of handling qualities parameters and weights, respectively. It can be found that the blade loading does have an influence on the dropback parameters, as well as the bandwidth frequency. A higher blade loading causes the bandwidth frequency to decrease and the dropback to degrade. Its influences are only next to the tip speed's. The biggest benefit of increasing the blade loading is that it permits a wider range for the tip speed. From the definition of blade loading, it can be seen that a higher blade loading can lead to a lower tip speed when fixing disk loading and solidity. Figure IV.10a already demonstrated the huge impact the tip speed has over the dropback — a lower tip speed is very helpful in improving the dropback. Though the increase in blade loading will worsen the dropback, it will eventually produce a much better dropback result due to the extra decreasing room for the tip speed. This will be proven in the following sections. In terms of weight, blade loading has a large influence on the rotor weight but overall a relatively small influence on the total weight. Reducing the blade loading will increasing the rotor weight, thereby increasing the total empty weight.

5. OPTIMIZATION

5.1. PROBABILISTIC DESIGN INCORPORATING HANDLING QUALITY REQUIREMENTS

Section 4.2 in Chapter I introduced the Joint Probabilistic Decision Making technique. This technique is applied here to investigate how easy is it to obtain a design with desired handling qualities. The correlating equations are repeated here. As given in Equation IV.22 and IV.23, $F(x_1, x_2, ..., x_m)$ denotes the probability

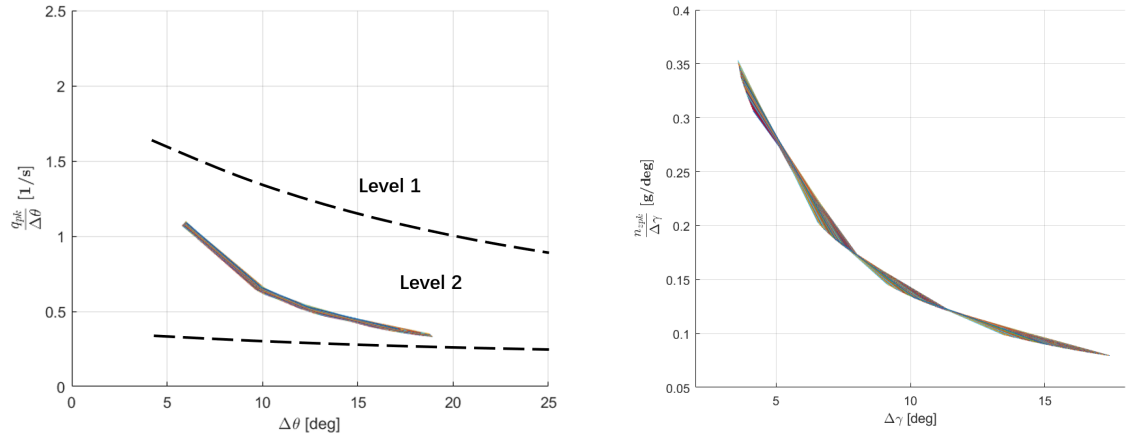

(a) Attitude quickness of all configurations

(b) Gamma quickness of all configurations

Figure IV.11: Quickness results of all design configurations
(The quickness results of all design configurations are plotted together. The input pulse duration increases from 1 sec to 5 sec from left to right. The results contain thousands of lines overlapping with each other. No data tips and legends are provided because it is not necessary and not feasible. These two plots are to demonstrate the finding that the design parameters almost have no influence on the quickness parameters.)

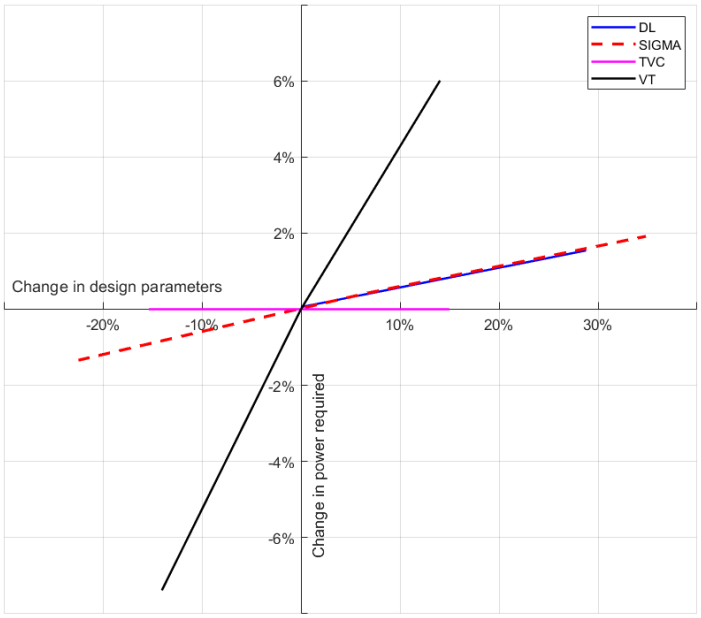

Figure IV.12: The variation of power required with individual design parameters

of the events $X_1 = x_1, X_m = x_m, ..., X_m = x_m$ happening simultaneously. x_{imin} and x_{imax} denote the lower and upper limit of the handling qualities, which are selected according to the observations from Section 4 and 4. a_i stands for the sample values of the design metrics, which are the points in the design space. The probability of success (POS) (Equation IV.24) reflects the feasibility of a design. Too big a POS indicates the design goal is too low while too small a POS indicates the design goal is too stringent, meaning that a small design change could lead to an infeasible design. In the end, a gradient-based method will be used to obtain a set of design parameters that bring about the desired handling qualities within the achievable range.

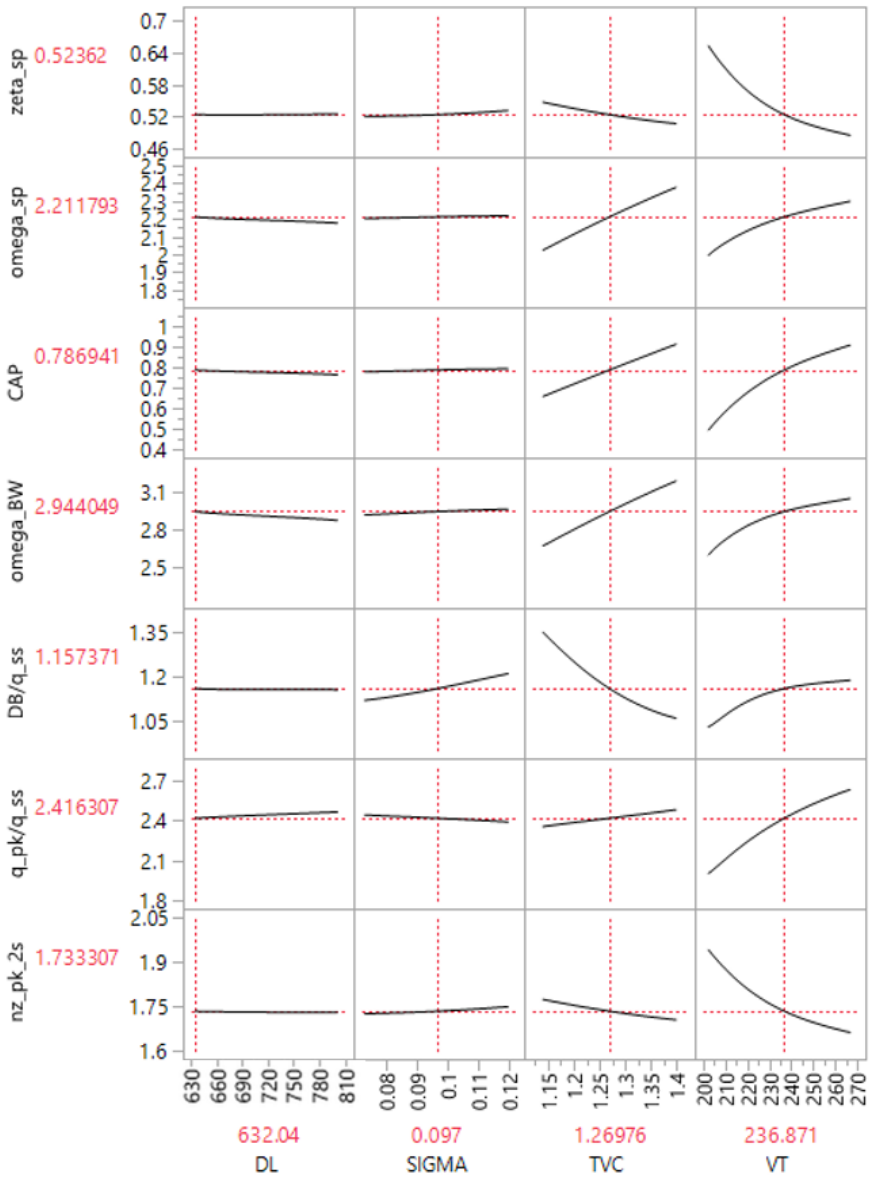

Figure IV.13: Predication profiler of handling qualities parameters – 140 knots 60 degrees

$$F(x_1, x_2, ..., x_m) = \frac{1}{m}\sum_{i=1}^{m} I(a_{i1} \le x_1, a_{i2} \le x_2, ..., a_{im} \le x_m) \tag{IV.22}$$

$$\frac{1}{m}\sum_{i=1}^{m} I(a_{i1} \le x_1, a_{i2} \le x_2, ..., a_{im} \le x_m) = \begin{cases} 1, for(a_{i1} = x_1, a_{i2} = x_2, ..., a_{im} = x_m) \\ 0, otherwise \end{cases} \tag{IV.23}$$

$$POS = \frac{1}{m}\sum_{i=1}^{m} I(x_{imin} \le a_i \le x_{imax}) \tag{IV.24}$$

Continuing with the 100 knots 30 degrees case, the key to this technique is a design space containing a large number of design points. Hence, 5541 feasible points were first generated using the approach presented in Figure IV.5. Next, the limits of handling qualities parameters need to be determined. According to previous findings, the 100knots 30 degrees case fails to meet the following requirements:

- Level 1 bandwidth frequency requirement specified in MIL-HDBK-1797A Category C flight
- Level 1 Attitude quickness

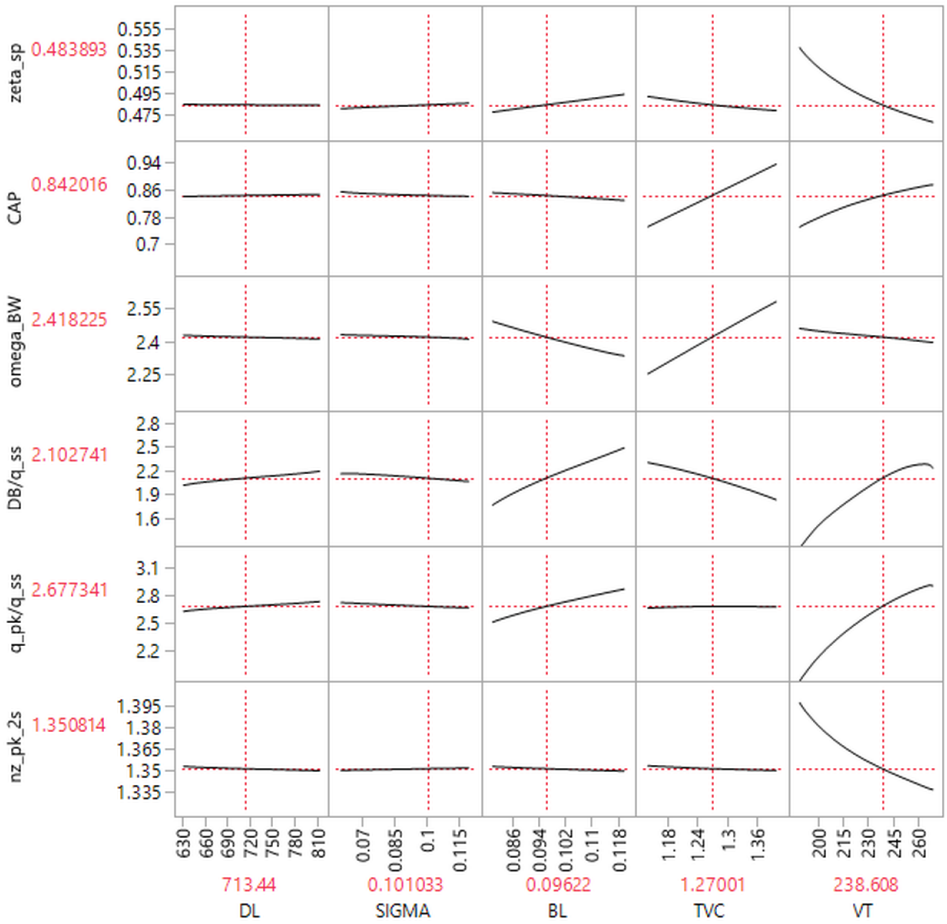

Figure IV.14: Predication profiler of handling qualities parameters – 100 knots 30 degrees. Constant blade loading constraint removed

- Level 1 Agility quickness
- Dropback criteria

Table IV.4: Ideal design metrics.
(Note: the limits here are ideal values according to handling qualities specifications ADS-33E and MIL-HDBK-1797A. In later design optimization, these limits will change because it is not possible to satisfy them all at the same time)

Parameters	Symbol	Unit	Lower limit	Upper limit
Short-period damping ratio	ζ_{sp}	-	0.35	1.3
Control anticipation parameter	CAP	rad/s^2/g	0.28	1
Bandwidth frequency	ω_{BW}	rad/s	2.5	-
Dropback distance	d	-	0	-
Autorotative index	AI	m^3/kg	2.0	-
Acc. time (100 to 150 kts)	t_150kts	s	-	10.2
Weight investment	dW	kg	-	0

It has been demonstrated in Figure IV.11 that the design parameters have no effect on both quickness parameters, hence these two quickness parameters will be dropped out during the optimization. Table IV.4 lists the handling quality parameters that will act as constraints during optimization. The upper and lower limits are their ideal values. For example, it is desired that the CAP is below 1 rad/s^2/g even though below 3.6 rad/s^2/g already meets the level 1 requirement. It is also desired that the bandwidth frequency can be higher than 2.5 rad/s to satisfy the level 1 requirement for category C flight specified by the MIL, which is more stringent than the ADS-33E level 1 requirement for target acquisition and tracking. Also, the dropback

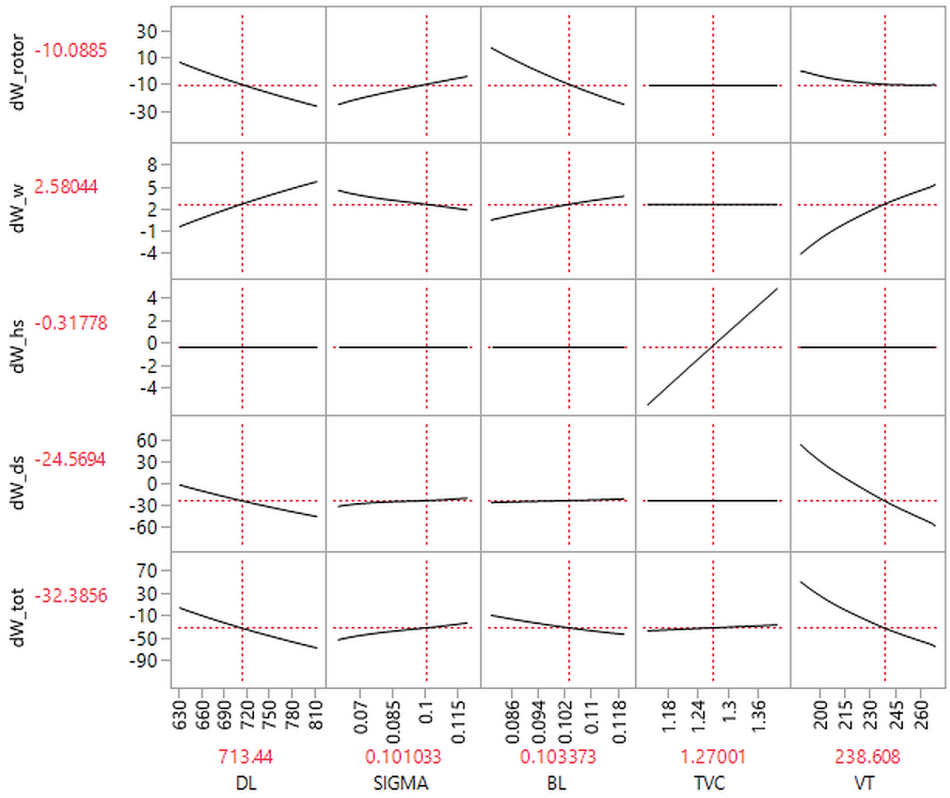

Figure IV.15: Predication profiler of components' weight – 100 knots 30 degrees. Constant blade loading constraint removed

distance should be larger than 0 for the dropback point to fall below the boundary line. For the autorotative index, the baseline model has an AI of 2.088 m^3/kg. This index ranges from 0.31 m^3/kg to 2.5 m^3/kg for most helicopters. [48] The main wing lies below the rotor in tiltrotor aircraft, which may have a negative effect during autorotation. Thus, it is preferred not to decrease the original value too much in order to retain its autorotation capability. Thus, the lower limit is 2 in this case. The baseline model takes 10.2 seconds to accelerate from 100 kts to 150 kts. Ideally, the modified design should possess the same or even better acceleration ability. Thus, 10.2 seconds is the upper limit of t_150kts. The last parameter is the amount of weight investment. Usually, the weight always increases on one's way to better performance. The amount of weight investment means how much increase in weight is acceptable for the designer. Its ideal upper limit is 0.

The resulting POS, however, is zero if using the ideal values in Table IV.4. This implies that by modifying disk loading, solidity, tail volume coefficient, and tip speed, it is not possible to find a design that can satisfy all these ideal constraints. Therefore, there must be trade-offs and the "optimal" is up to the designer to define. To illustrate the feasibility of each design under different constraints, Table IV.5 shows the resulting POS of various constraints. The first row lists the values of these parameters for the baseline design. It can be concluded from this table that while meeting the damping ratio and CAP constraints is easy, finding a design that is better than the baseline design in other these aspects is very difficult. Especially the dropback distance which, if improves a bit, can rapidly reduce the POS. Also, the POS will drop evidently once the required bandwidth frequency is set to 2.5 rad/s. Another parameter to look at is the time required to accelerate from 100 kts to 150 kts. It seems that when trying to satisfy other constraints, the design will always face a decrease in the acceleration ability. Meeting other constraints while trying to keep the same acceleration ability is extremely difficult. The last parameter is the weight investment. It is almost inevitable if one wants to make design changes.

5.2. OPTIMIZATION CASES

With the knowledge gained in the previous discussion, the study now can now move forward to the optimization part. Still continuing with the 100 knots 30 degrees case, the study will make use of the fmincon function

Table IV.5: POS experiments – 100 knots 30 degrees

ζ_{sp}	CAP	ω_{BW}	d	AI	t_150kts	dW	POS (%)
0.49	**0.835**	**2.4**	**-0.82**	**2.088**	**10.2**	**0**	**Baseline**
(0.35, 1.3)	(0.28, 1.0)	(2.0, Inf)	(-0.5, Inf)	(2.0, Inf)	(0, 15.0)	(-Inf, 100)	5.52
(0.35, 1.3)	(0.28, 1.0)	(2.5, Inf)	(-0.5, Inf)	(2.0, Inf)	(0, 15.0)	(-Inf, 100)	2.00
(0.35, 1.3)	(0.28, 1.0)	(2.0, Inf)	(-0.5, Inf)	(2.0, Inf)	(0, 14.0)	(-Inf, 100)	4.80
(0.35, 1.3)	(0.28, 1.0)	(2.5, Inf)	(-0.5, Inf)	(2.0, Inf)	(0, 14.0)	(-Inf, 100)	1.79
(0.35, 1.3)	(0.28, 1.0)	(2.0, Inf)	(-0.5, Inf)	(2.0, Inf)	(0, 14.0)	(-Inf, 50)	3.90
(0.35, 1.3)	(0.28, 1.0)	(2.5, Inf)	(-0.5, Inf)	(2.0, Inf)	(0, 14.0)	(-Inf, 50)	1.32
(0.35, 1.3)	(0.28, 1.0)	(2.0, Inf)	(-0.2, Inf)	(2.0, Inf)	(0, 14.0)	(-Inf, 100)	0.14
(0.35, 1.3)	(0.28, 1.0)	(2.5, Inf)	(-0.2, Inf)	(2.0, Inf)	(0, 14.0)	(-Inf, 100)	0.11
(0.35, 1.3)	(0.28, 1.0)	(2.5, Inf)	(-0.11, Inf)	(2.08, Inf)	(0, 16.0)	(-Inf, 100)	0.02
(0.35, 1.3)	(0.28, 1.0)	(2.5, Inf)	(-0.11, Inf)	(2.08, Inf)	(0, 10.2)	(-Inf, 100)	0.00

from the Optimization Toolbox in Matlab. Ideally, the design space should be constrained by the limits listed in Table IV.4. But in practice, these ideal limits cannot be satisfied simultaneously. Thus, trade-offs need to be made when selecting the optimization constraints. The dropback parameter has been chosen as the target parameter to improve because the excessive dropback is found to be the most serious and common problem in previous studies. The dropback, which originally needs two parameters to describe, has been represented by the dropback distance (d). Referring to its definition in Equation IV.21, a negative d means the point lies above the boundary line which is not preferred. Additionally, the d may change its sign during the optimization. In order to formulate a minimization problem, it is required that the objective function value stays positive and preferably, be normalized. Therefore, the positive and normalized d', which is defined in Equation IV.25, will be used during optimization.

$$d' = (-d + 10)/10; \tag{IV.25}$$

For the 100 knots 30 degrees case, requirements like short-period damping ratio, CAP can be met easily. To give the design more freedom, the bandwidth will be constrained by the boundary specified by the ADS-33E target acquisition and tracking instead of the MIL-HDBK-1797A category C flight. The autorotative index is not constrained. The time required to accelerate from 100 kts to 150 kts and the weight investment are two constraints to be varied. Several experiments were done to determine the limit of the acceleration time. It was found that 12 seconds and 16 seconds were two values that can represent two levels of acceleration ability while provide other design parameters enough space to change. Finally, xix cases are studied with different conditions, as listed in Table IV.6.

Table IV.6: Conditions of the six optimization cases

Cases	BL	ζ_{sp}	CAP	ω_{BW}	AI	**dW**	**t_150kts**
1	0.105	>0.35	<1.0	>2.0	Free	0	<16
2	0.105	>0.35	<1.0	>2.0	Free	<20	<12
3	0.105	>0.35	<1.0	>2.0	Free	<50	<12
4	0.105	>0.35	<1.0	>2.0	Free	Free	<16
5	0.08-0.12	>0.35	<1.0	>2.0	Free	Free	Free
6	0.08-0.12	>0.35	<1.0	>2.0	Free	<100	<16

The results of these optimization cases will be shown in bar plots. Appendix A contains the complete and detailed results. In the bar plots, the percentage changes of each parameter compared to their baseline values are plotted. The design parameters are placed at the beginning, including disk loading (DL), solidity (SIGMA), blade loading (BL), tail volume coefficient (TVC), and tip speed (VT). The rest are performance parameters,

from left to right are AI (autorotative index), CAP (control anticipation parameter), ω_BW (bandwidth frequency), d (dropback distance), P_100kts (power required to fly at 100 kts), nz_pk (peak normal load factor during a 2-second pulse longitudinal stick input), t_150kts (time required to accelerate from 100 kts to 150 kts), P_150kts (power required to fly at 150 kts). Note that the d in these diagrams is the original d, not the d' defined in Equation IV.25. Thus, the more it decreases, the more close it is to the boundary line, which can be interpreted as milder dropback. The resulting dropback points are summarized in Figure IV.22.

CASE 1: CONSTANT BLADE LOADING, $dW = 0$, t_150kts<16

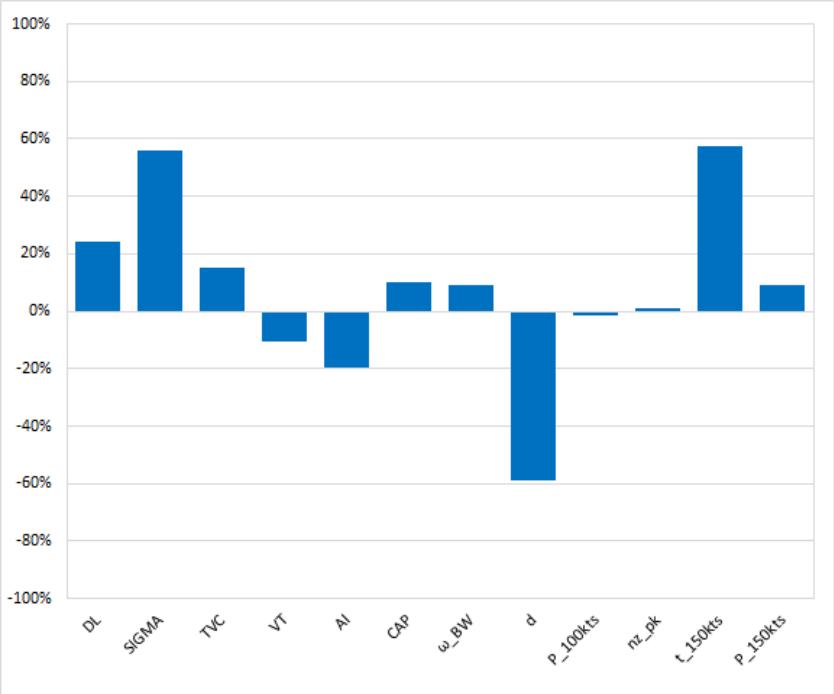

Figure IV.16: Optimization Case 1: dW=0 kg, t_150kts<16 seconds

In the first case, the constraints are dW<0 and t_150kts<16. As a result, disk loading, solidity, and tail volume coefficient are all increased. Only the tip speed is decreased by 10%. It shows that with 0 weight investment, the dropback distance can be decreased by 60%. The bandwidth frequency is also increased. However, there are performance parameters that become worse. Firstly, the autorotative index is reduced by 20%, which may cause the autorotative landing capability to degrade. Secondly, the CAP is slightly increased but still remains between 0.28 and 1 rad/s^2/g. Thirdly, the time required to accelerate from 100 kts to 150 kts is significantly increased from 10.2 seconds to 16 seconds (upper limit). This indicates a noticeable degradation in the aircraft's accelerating ability. Lastly, 10% more power is now required to fly at 150 kts, which can lead to a drop in the maximum speed since the aircraft will hit the power limit earlier. The data in Appendix A point out that 1300 hp is now required to fly at 150 kts, which has already exceeded the normal power of 1250 hp. Thus, the endurance of the aircraft in high-speed flights will be limited.

CASE 2: CONSTANT BLADE LOADING, $dW < 20$, $t\_150kts < 12$

In the second case, with 20 kg weight investment and the limit of acceleration time adjusted to 12 seconds, the optimal design is obtained as shown in Figure IV.17. Compared to the first case, the directions of change of the four design parameters are the same, except that the magnitude is reduced. The result is encouraging because a 45% reduction of the dropback distance is obtained at the cost of only a small drop in the autorotative index and a small rise in the acceleration time and the power required to fly at 150 kts. The bandwidth is also increased which is good. In the meantime, the CAP grows more than that in the previous case, which brings it closer to the upper limit of 1 rad/s^2/g.

CASE 3: CONSTANT BLADE LOADING, $dW < 50$, $t\_150kts < 12$

The allowable weight investment is 50 kg and the upper limit of the acceleration time is 12 seconds in Case 3. The optimization converged at 35 kg weight investment. The relative changes of these parameters are very

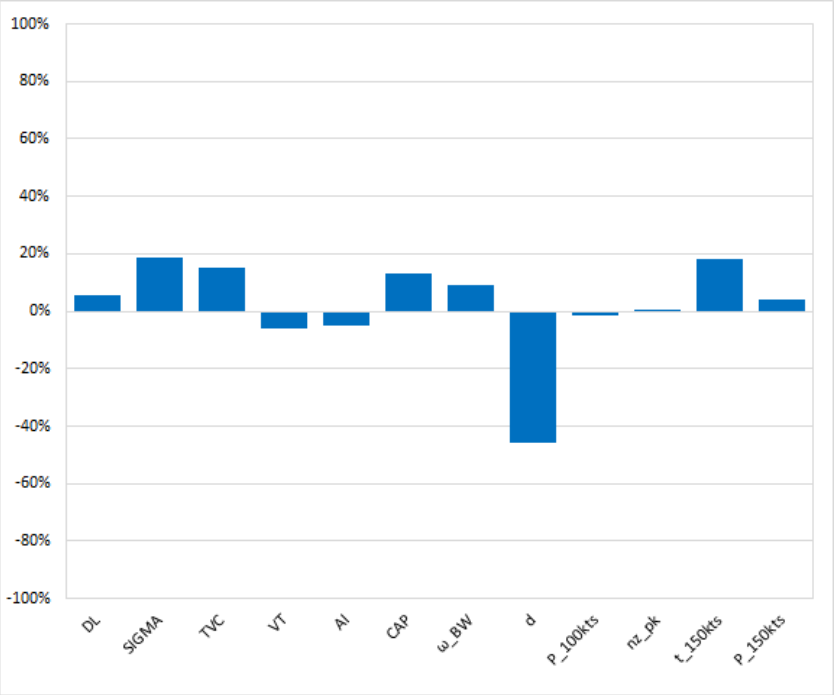

Figure IV.17: Optimization Case 2: dW<20 kg, t_150kts<12 seconds

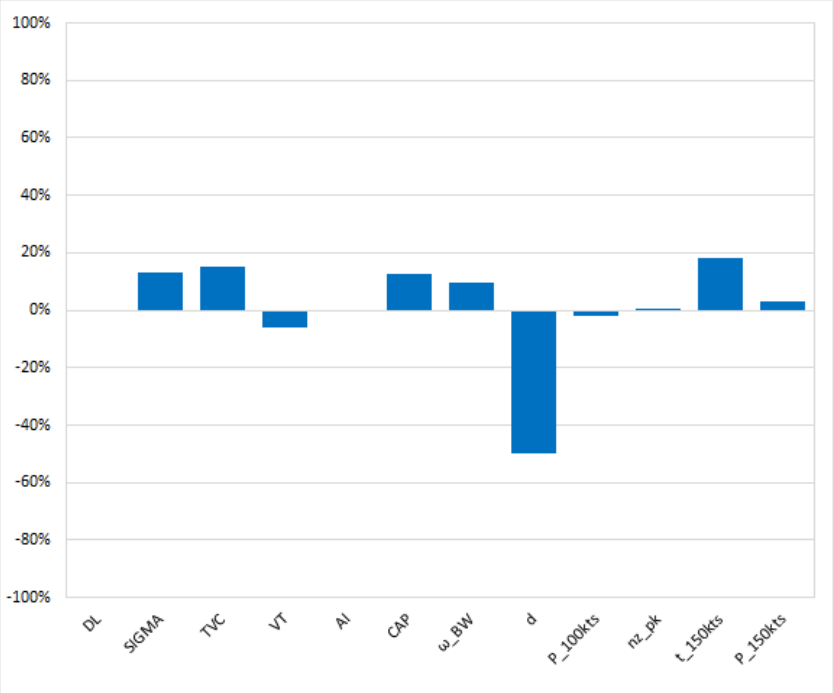

Figure IV.18: Optimization Case 3: dW<50 kg, t_150kts<12 seconds

similar to Case 2. The disk loading is not modified here, allowing the autorotative index to remain unchanged. This time the dropback distance is decreased by 50%. Compared to the last case where a 20 kg weight investment achieves a 45% reduction in the dropback distance, a 50% reduction is not comparable to the increase in weight. In other words, more investment in weight results in only a small improvement in the dropback, which is obviously not cost-effective.

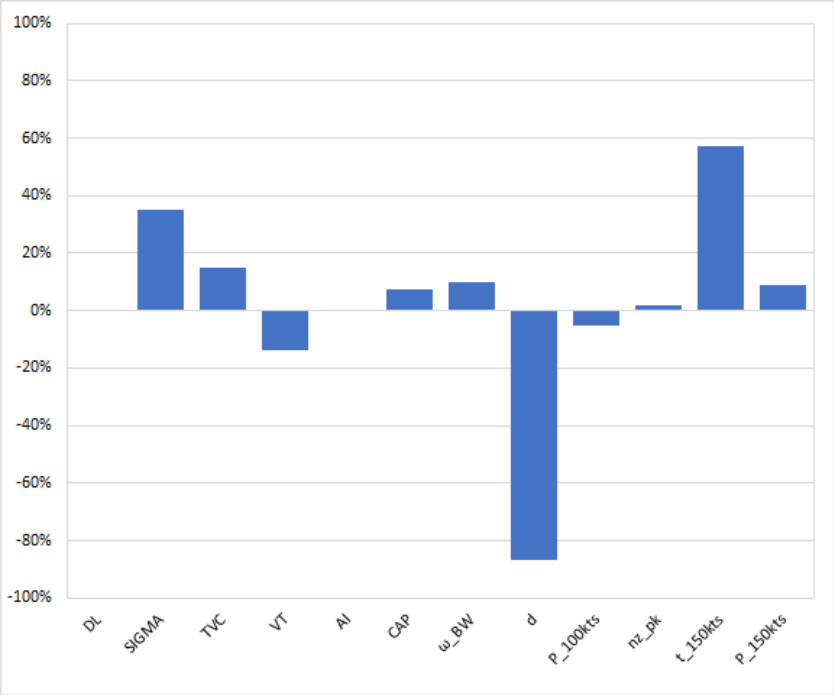

Figure IV.19: Optimization Case 4: unlimited dW, t_150kts<16 seconds

CASE 4: CONSTANT BLADE LOADING, dW UNLIMITED, $t\_150kts < 16s$

The fourth optimization case presented here is the dW-free case, where the weight investment is not constrained. The acceleration time is set to its upper limit of 16 seconds. An 87% reduction in the dropback distance is obtained, representing the biggest dropback improvement one can obtain with a fixed blade loading. However, the biggest improvements come with the largest side-effects: 74 kg additional weight. The acceleration time again hits its upper limit of 16 seconds. Apart from the improvement in dropback, the improvements in bandwidth frequency and power required to fly at 100 kts can be observed. It is worth mentioning that the power required to fly at 100 kts is the least in all four cases, which can to some extent compensate for the addition in weight. However, the power required to fly at 150 kts is higher.

CASE 5: VARIED BLADE LOADING, dW UNLIMITED, t_150kts UNLIMITED

In previous optimization cases, the dropback could not be improved to the satisfied level. Referring to the definition of dropback distance in Equation IV.21, a positive d is the target of the design optimization. This corresponds to more than -100% decrease of d. It was decided to remove the constraint of constant blade loading to give more freedom to the design. Now, blade loading is a design parameter. Figure IV.21 shows the optimization results of the new design case, where both weight investment dW and acceleration time t_150kts are not limited. This condition will give the extreme value of the dropback distance. The outcome is a decrease of -176% in the dropback distance. The dropback point is plotted in Figure IV.22. The design hits the upper limit of solidity and blade loading in order to reach the lowest tip speed possible. Aside from the improvement in dropback, the peak normal load factor is the highest among all cases, and the power required to fly at 100 knots is reduced.

However, the cost is not negligible. The autorotative index is reduced; the bandwidth frequency is reduced (almost arrives at the level 1/2 boundary of the ADS-33E target acquisition and tracking. See Table A.1); 111 kg of additional weight; the maximum speed at 30 degrees is now 136 knots. The decrease in maximum speed is unaffordable. A higher design blade loading means a smaller blade stall margin. The blade will enter stall more quickly as the thrust increases. Also, the maneuverability of the aircraft will be influenced because a less-rapid maneuver now can trigger stall in the rotor, which will cause strong vibrations and decrease control effectiveness.

CASE 6: VARIED BLADE LOADING, $dW < 100$, $t\_150kts < 16$

In Case 6, the blade loading is also adjustable. But different from the last case, an upper limit of 100kg and 16s is now applied to the allowable investment and maximum acceleration time, respectively. The goal is to ob-

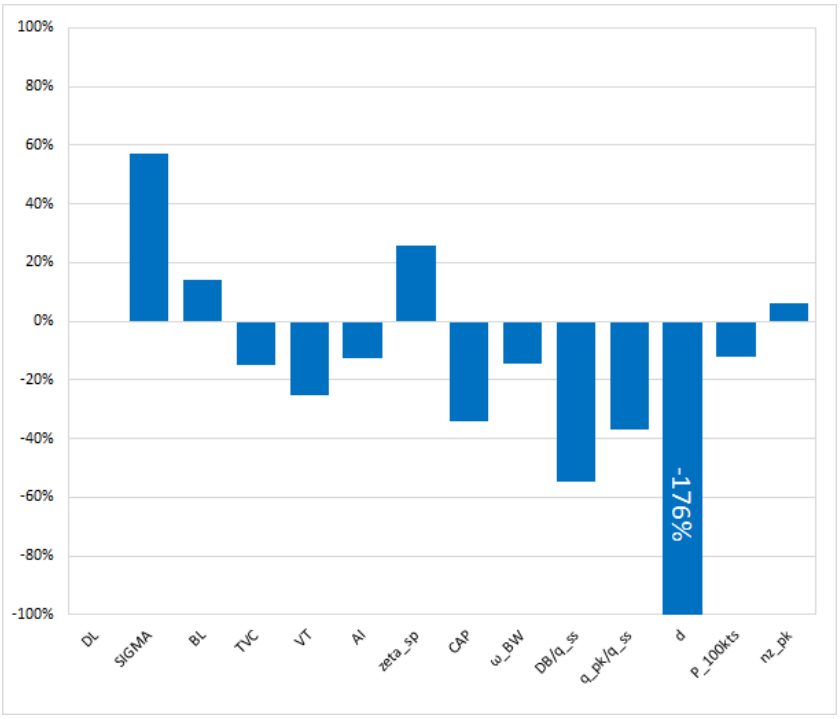

Figure IV.20: Optimization Case 5: unlimited dW, unlimited t_150kts, varied BL

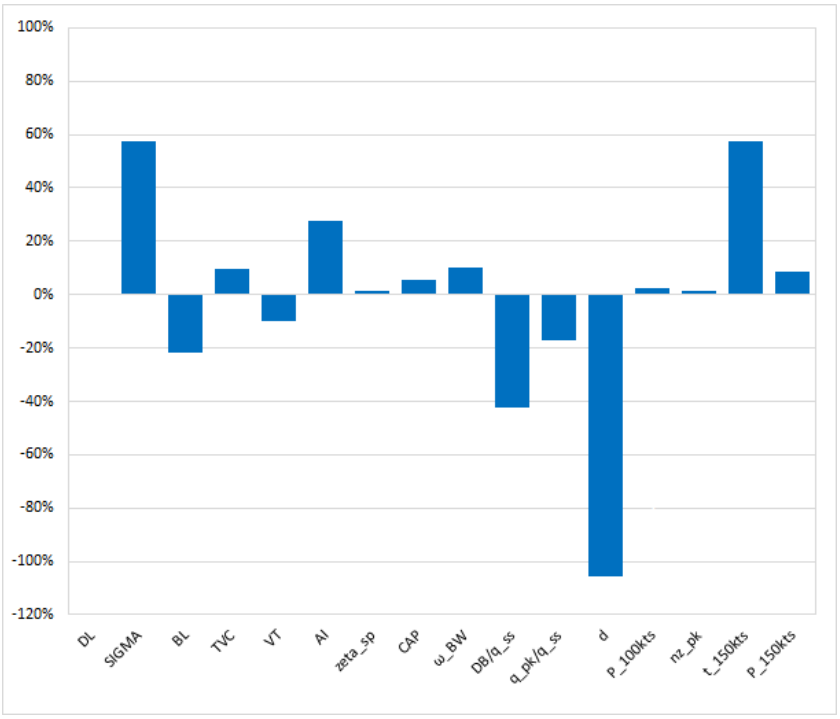

Figure IV.21: Optimization Case 6: dW<100, t_150kts<16, varied BL

tain a design that results in a good dropback while keeping the weight and maneuverability at an acceptable level. Finally, a decrease of 105% in the dropback distance is obtained. As shown in Figure IV.22, the dropback point just falls into the preferred area. It comes with 85kg of additional weight. Contrary to Case 5 where the blade loading was changed to the upper limit, the blade loading here is close to the lower limit of 0.08. This can be explained by the curves in Figure IV.14. It has already been known that the dropback distance is most sensitive to the tip speed. In Case 5, the optimization program did everything to achieve the lowest

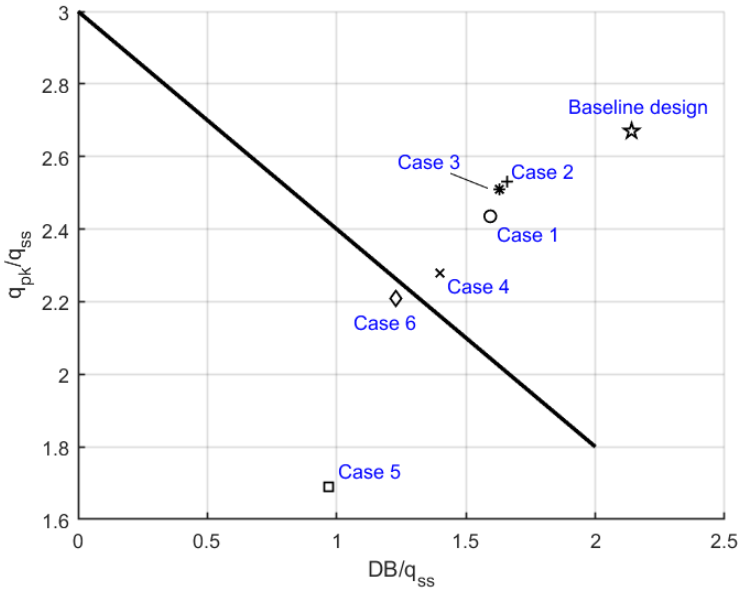

Figure IV.22: Optimized dropback results

tip speed to improve the dropback. But in Case 6, due to the constraints of weight and maneuverability, the optimization program chose to reduce the blade loading in addition to a low tip speed. This way not only can it further improve the dropback distance compared to the first 4 cases, but also keep a reasonable weight and maneuverability.

5.3. SHORT SUMMARY OF THE OPTIMIZATION RESULTS

Although the magnitudes of the changes differ, the results of the first four cases display the same design trend: decreasing the tip speed, increasing the solidity, increasing the tail volume coefficient, and increasing the disk loading (when the weight investment is low). The directions of change in these four design parameters are closely related. In previous discussions, the large benefit of decreasing the tip speed has been illustrated. Due to the requirement of keeping the lifting capability constant, the lift lost because of a lower tip speed is compensated by a higher rotor solidity. Also, a lower tip speed requires higher torque, which gives rise to the drive system weight. In case the weight investment is low, the disk loading has to be increased to prevent the weight from growing too much. In Case 5 and 6, the blade loading becomes a design parameter. It can be increased or decreased depending on the constraints of weight and acceleration time. Case 5 shows that a high design blade loading can give considerable space for the tip speed to decrease further. But it is hardly acceptable because the blade stall margin will be largely squeezed, thereby limiting the flight envelope. After applying the constraints on weight and acceleration time, Case 6 gives a better result by decreasing the blade loading. Not only the dropback has been improved to the desired region while satisfying other handling quality requirements, the resulting weight and acceleration ability are also within the acceptable range.

It can be seen that the improvement in dropback after applying these design changes always comes with the cost of longer acceleration time and more power required to fly at high speed. To investigate this phenomenon, the power curves of the baseline design and the fourth optimization case are plotted in Figure IV.23. The largest contribution to the increase in total power is the parasite power. This is due to a larger tail surface resulting from a higher tail volume coefficient, causing an increased portion of power to be diverted to overcome the parasite drag of the horizontal tailplane. In addition, the induced power also plays a part in the increase in total power. Typically for helicopters, the induced power will decrease continuously as the airspeed increases. But a noticeable rise in the induced power from 100 knots to 150 knots is clearly shown in Figure IV.23. This is mainly because of the decrease in the angle of attack of the wing when airspeed increases. The trimmed pitch angle in steady level flight of the XV-15 always decreases with speed, as illustrated in the pitch trim curves in Figure II.4. Thus, the angle of attack of the main wing decreases as well. As a consequence, the rotors need to generate more lift to compensate for the loss in the wing lift, which causes the induced power to rise. This process is illustrated in Figure IV.24.

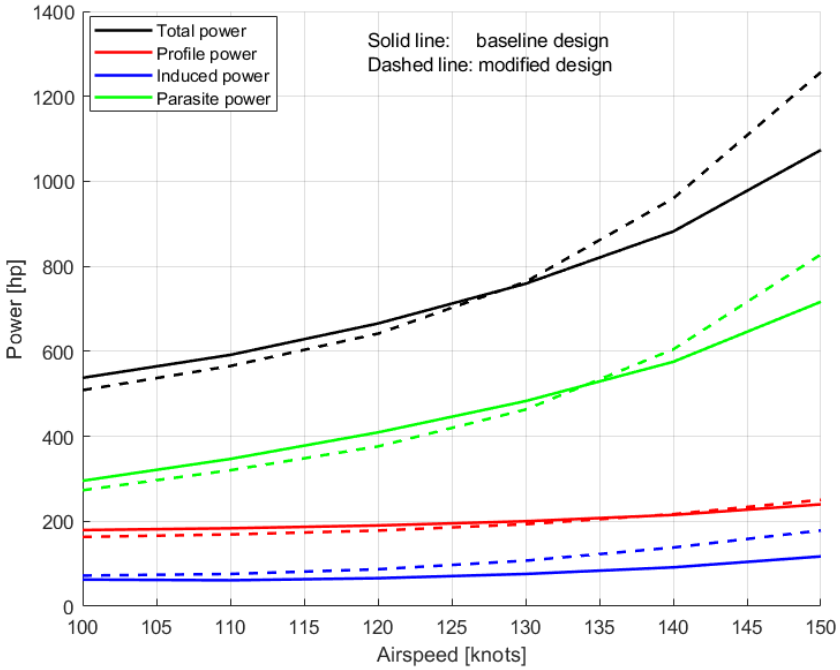

Figure IV.23: Power curves of baseline design vs. optimized design (unlimited dW, t_150kts<16 seconds)

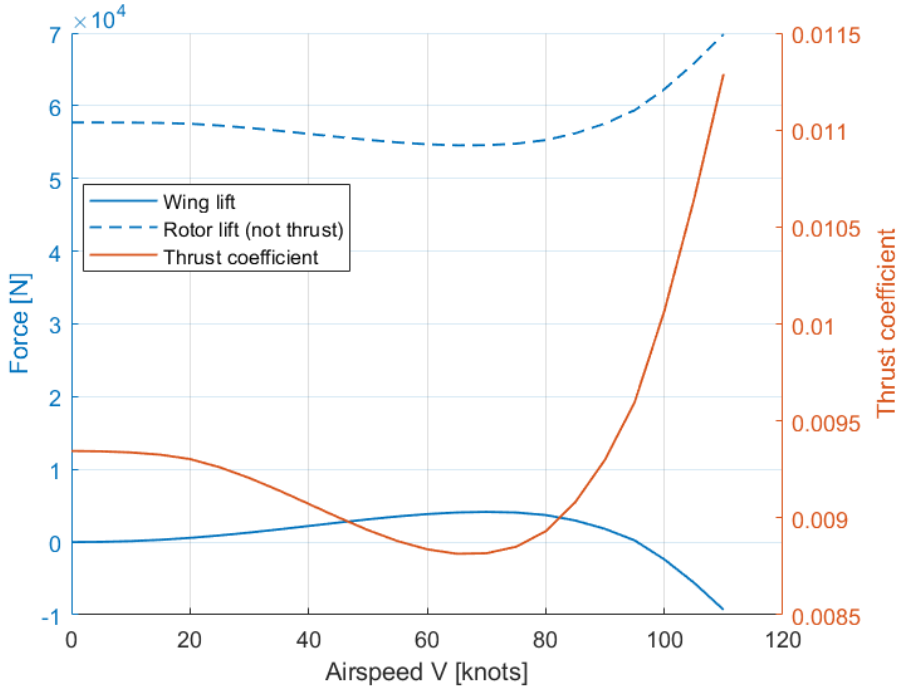

Figure IV.24: The variations of rotor lift, wing lift, and thrust coefficient with airspeed (helicopter mode, flap/flaperon=40/25)

V

CONCLUSIONS AND RECOMMENDATIONS

1. CONCLUSIONS

The main research question of this thesis is:

How to improve the bare-airframe handling qualities of the XV-15 tiltrotor aircraft in conversion mode?

The main research question was divided into three sub-questions. This thesis was ordered in such a way that these sub-questions were answered consecutively. Chapter 1 and 2 serve as the preparation phase of this thesis. In Chapter 1, relevant literature was reviewed to gather information about the features of the tiltrotor aircraft, the handling quality standards, the development of tiltrotor handling quality studies, and methods that can be applied for design and optimization. They form the theoretical base of this thesis. In Chapter 2, a TU Delft in-house 3-DoF XV-15 flight dynamic model was selected as the baseline model of this study. The baseline model was improved by implementing look-up tables to model various aerodynamic effects. Some errors in the baseline model were also corrected. Then the trim and linearization functions were implemented, using which the trimmed curves of the improved model and the baseline model were obtained. The trimmed curves were compared to the published data. The comparisons showed an obvious improvement in matching the real pitch trim curves. Besides, the short period and phugoid poles calculated by the improved model also compared well with the published data. The results of these comparisons demonstrated that the improved model has good accuracy in predicting pitch dynamics. In the following part, the answers to each sub-question are summarized.

1. What are the existing problems of the handling qualities of the XV-15 tiltrotor aircraft in conversion mode?

The handling quality parameters, including short-period damping ratio, control anticipation parameter (CAP), bandwidth, attitude quickness, agility quickness, and pitch dropback across the flight envelope were investigated. 4 nacelle tilt angles were selected, each of which was studied for a low-speed case and a high-speed case. The results were plotted against boundaries from rotorcraft standard ADS-33E and fixed-wing standard MIL-HDBK-1797A.

Short-period damping ratio The short-period damping ratio requirement specifies that the damping ratio needs to be higher than 0.35 to meet the level 1 requirement. Except for the 100 knots 60 degrees nacelle angle had a damping ratio slightly lower than 0.35, all other cases were higher than 0.35. It was also found that the damping ratio and the undamped natural frequency will increase with airspeed. In general, the short-period damping ratio is not a problem for this aircraft and it becomes better at high speed.

CAP Control anticipation parameter is a measure of predictability of the pitch response. Requirements are different in different standards. If using the boundaries for Category A flight specified in the MIL-HDBK-1797A, only the 100 knots 60 degrees case fell into the level 2 area due to slightly low damping. Other cases were level 1. However, if using the boundaries recommended by Gibson in Ref. [19], which is more stringent, half of the cases failed to meet level 1 requirement. It was also found that as the aircraft gains speed, the CAP improves. In conclusion, CAP will be a problem for this XV-15 model when flying at low speed if we use the

stringent criteria proposed by Gibson, but it will not be a problem if we use the less-strict criteria from the MIL-HDBK-1797A Category A flight.

Bandwidth Bandwidth is an indication of the highest frequency at which the pilot-aircraft loop can be closed without introducing instability. The results of bandwidth were compared with requirements of ADS-33E target acquisition and tracking and MIL-HDBK-1797A Category C approach and landing. The latter is more stringent. Results showed that low-speed flight in helicopter mode can not satisfy the level 1 requirement of ADS-33E. Moreover, low-speed flight in helicopter mode and conversion mode (nacelle angle below 30 degrees) could not satisfy the level 1 requirement of MIL. It was also found that the bandwidth frequency will increase with airspeed. In summary, the bandwidth frequency in low-speed flight at a small nacelle angle is insufficient but it is satisfactory as the airspeed and nacelle angle increase.

Quickness Quickness is a measure of the aircraft's ability to achieve rapid attitude changes. For the attitude quickness, none of the cases met the ADS-33E level 1 requirement of the target acquisition and tracking tasks. Some even fell into the level 3 area as the input pulse duration increased. If using the requirement of all other MTEs, which is less stringent, only the high-speed flight in airplane mode can meet level 1 requirement. For the agility quickness, most cases started in the level 1 area using the proposed boundary in Ref. [41], but fell into the level 2 area as the input pulse duration increased. Therefore, quickness, in general, is a problem for this aircraft throughout the flight envelope.

Dropback Dropback is a criterion used in conjunction with the CAP or bandwidth criteria. It compares the ratio of the peak to steady-state pitch rate with the ratio of pitch attitude dropback to the steady-state pitch rate. It is a measure of the quality of the pitch responses. Dropback was found to be the most critical problem for this aircraft. Results demonstrated that large dropback occurred in low-speed flights. As the nacelle angle increases and the aircraft converts towards the airplane mode, dropback becomes worse even at high speed.

2. What are the design parameters to be selected and how do they influence the handling qualities?

Common design parameters for helicopters include disk loading, rotor solidity, blade loading, rotor tip speed, blade hinge offset, and installed power. Disk loading characterizes the hover performance and shows how loaded is the rotor. Usually, low disk loading indicates high thrust efficiency. Rotor solidity is the ratio of total blade area to disk area. It impacts the stall margin or the maneuverability potential of the rotor. Blade loading shows how loaded is the blade and indicates how close to stall is the blade operating. Rotor tip speed characterizes the noise and the performance of the rotor. Blade hinge offset is the offset of blade hinge to rotor center. This offset strongly affects the dynamic response of the blade. Blade hinge offset was left out because it was not modelled in our flight dynamic model. The installed power was also left out because varying it will cause significant changes in the weight of engines and transmission systems. Consequently, aircraft drag and weight of the tilting mechanism will change. These changes are beyond the predicting capability of our model. In the pitch axis, the tail volume coefficient is an important design parameter that affects the longitudinal stability and handling quality. It is a nondimensional parameter proportional to the tail moment arm. Finally, the design parameters selected were disk loading, solidity, blade loading, tip speed, and tail volume coefficient. The first four are helicopter design parameters and the last one is the fixed-wing design parameter. Disk loading is constrained on the low side by the maximum allowable rotor radius. In this study we do not modify the wing, hence, the rotor cannot be larger than the original one to prevent it from hitting the fuselage. In practice, the disk loading is constrained on the high side by the autorotative landing capability, which is defined by the autorotative index. Since this index's expression includes the rotor rotational speed, which is also a variable, the autorotative index cannot be determined in advance. Hence, it was selected as a performance indicator during the analysis. Selecting solidity is in practice a process of finding a balance between maximizing maneuverability and minimizing drag. It is constrained on the low side by maneuverability requirement and on the high side by hover performance. Tip speed is constrained on the low side by the retreating blade stall and on the high side by the compressibility effect on the advancing blade. In terms of the tail volume coefficient, its lower limit is determined by the static stability requirement. The higher the tail volume coefficient, the more stable the aircraft will be. But too stable means less controllable. Additionally, a high tail volume coefficient will make the pitching moment to be very sensitive to the change in airspeed, thus causes problems in the pitch trim.

In order to automate the analysis process, an analysis tool was developed. It integrates the process of configuration generation, trim and linearization, weight calculation, handling quality analysis, and simple maneuver simulation based on a PID controller. With the help of this tool, a design space was created with design parameters as inputs and handling quality parameters, maneuverability parameters, plus components'

weight as outputs. The resulting data was then processed by the statistical analysis software *JMP* to generate the prediction profilers. The prediction profiler is a plot that shows the response curves of each performance parameter with respect to each design parameter. In addition, these design parameters' influences on hover power were plotted. The results showed that the tail volume coefficient and the tip speed had a large influence on handling qualities and maneuverability; disk loading and tip speed had a large influence on empty weight; disk loading had the most pronounced influence on hover power. These design parameters had no effect on quickness. The dropback, which is determined by two parameters, was represented by one parameter: "dropback distance", defined by the author for easier illustration. As the most critical problem, the dropback parameter can be improved by increasing the tail volume coefficient, decreasing the blade loading, and decreasing the tip speed. But with a fixed blade loading, the room for improving the dropback parameter was limited. Later results showed that increasing the blade loading can produce a much better dropback result because higher blade loading permits a much lower tip speed.

3. How to find the optimal values of design parameters?

Through the probabilistic design, the probability of success under different constraints was studied. The result showed that it is impossible to find a design that can satisfy all requirements. The probability of success (POS) was very low when constraints were set close to the desired values. Also, it was found that the dropback problem can be improved but cannot be cured if the blade loading was kept constant. Most importantly, almost all preferred design changes contribute to additional weight. Next, fmincon, the gradient-based method provided by the Optimization Toolbox in Matlab, was used to find the optimal design based on different constraints. The quickness requirement was left out because it was independent of all design changes. The bandwidth requirement and autorotative requirement were loosened to provide the optimization with more freedom. The amount of weight investment and the allowable acceleration time were the two adjustable constraints during the optimization. With a fixed blade loading, four cases with different combinations of these two constraints were presented. They showed that the dropback can be improved but cannot be improved to the desired region. After adding the blade loading as a design parameter, another two optimization cases were studied. These two cases with adjustable blade loading showed that the dropback parameter can be improved further to the desired region by modifying the blade loading. This is because a higher blade loading permits more room for the tip speed to reduce and the blade loading itself has a relatively large influence on the dropback parameter. Decreasing the blade loading combining with a low tip speed could help to improve the dropback further. However, the blade loading would influence the flight envelope and power required significantly, thus it should be careful when increasing the blade loading. It was observed that the improvement in dropback after applying these design changes always came with the cost of longer acceleration time and more power required to fly at high speed. To investigate the reason why more power is required to fly at high speed after these design changes, the power curves were plotted. It was found that the parasite power was the largest contribution to the increase in total power, which was due to a larger tail surface resulting from a higher tail volume coefficient. In addition to parasite power, the induced power also increased because of the higher thrust coefficient. The induced power was found to increase with airspeed. This is mainly because of the decrease in the angle of attack of the wing when airspeed increases. The trimmed pitch angle in steady level flight of the XV-15 always decreases with speed, thus, the angle of attack of the main wing decreases as well. As a consequence, the rotors need to generate more lift to compensate for the loss in the wing lift, which causes the induced power to rise.

2. RECOMMENDATIONS FOR FUTURE WORK

The aircraft dynamic model was constructed based on some assumptions. Future work can be done to reduce the number of assumptions to make this model more accurate. For example, the articulated rotor can be substituted by a gimballed rotor to improve the accuracy of the rotor dynamic response; the beta-governor model can be added to mimic the real collective control system; the tilting dynamics can be modeled to enable the simulation of the transition process; the rotor inflow dynamics can be modelled to improve the accuracy of the rotor dynamic response. In addition, the rotor wash on the wing and the horizontal tail is not a negligible factor for tiltrotor aircraft, so it is better to include it in future work. Also, the look-up tables are not very suitable for dealing with design changes. The best practice is to model these interference effects analytically.

In this study, only five design parameters that concern the rotor and the horizontal tail were included. To make the design analysis more comprehensive, the wing, the airfoils, and different tail configurations can

also be part of the design parameters. For instance, XV-15 and V-22 both use an H-tail configuration. But the newly developed Bell V-280 features a V-tail configuration. What does this imply in terms of the handling qualities? Another important factor that was omitted in this study is the fuel or range requirement. In this study, the amount of fuel was assumed to be constant, therefore the resulting design may fail to meet the original mission requirement. Sizing of the aircraft requires it to carry sufficient fuel in order to accomplish a certain mission. A parametric model will be needed to estimate the volume of the fuel tanks.

In the maneuver simulation part, a PID controller and an approximate solution were used to find the maximum acceleration ability. Instead, an inverse simulation approach can be used to simulate specific maneuvers, which will yield results that are more close to the real pilot-in-the-loop simulation.

In the design and optimization stage, we mainly focused on one case: 100 knots 30 degrees. The 140 knots 60 degrees case was briefly studied by showing that the trends in its prediction profiler were similar to those of the 100 knots 30 degrees case. Moreover, the optimization was merely based on the 100 knots 30 degrees case. But the tiltrotor performance can vary in other configurations because its CG, its shape, and aerodynamics will change notably. It is possible that the optimized design in the 30 degrees nacelle configuration will worsen the performance in other configurations. A complete and reliable design and optimization study should include all modes. But the effort and time required would dramatically exceed what is tolerable for this thesis. However, it can be very meaningful to perform such inclusive work in future studies.

A

OPTIMIZATION RESULTS

Table A.1: Optimization results

	Units	Baseline	Case 1	Case 2	Case 3	Case 4	Case 5	Case 6
DL	N/m^2	632.04	784.52	665.94	632.04	632.04	632.040	632.040
SIGMA		0.089	0.139	0.106	0.101	0.120	0.140	0.140
BL		0.105	0.105	0.105	0.105	0.105	0.120	0.082
TVC		1.276	1.467	1.467	1.467	1.467	1.085	1.400
VT	m/s	234.834	209.515	221.046	220.685	202.235	175.247	211.617
AI	m^3/kg	2.087	1.682	1.982	2.087	2.087	1.829	2.667
ζ_{sp}		0.489	0.505	0.492	0.493	0.512	0.616	0.497
ω_{sp}	rad/s	1.910	2.029	2.057	2.063	2.055	1.628	2.120
$T_{\theta 2}$	s	1.201	1.172	1.171	1.161	1.115	1.086	1.029
CAP	$rad/sec^2/g$	0.835	0.920	0.945	0.942	0.897	0.549	0.881
ω_{BW}	rad/s	2.402	2.621	2.626	2.631	2.639	2.051	2.643
DB/q_{ss}	s	2.144	1.594	1.657	1.628	1.403	0.969	1.231
q_{pk}/q_{ss}		2.673	2.435	2.527	2.506	2.284	1.691	2.210
d		-0.822	-0.336	-0.447	-0.414	-0.108	0.624	0.044
P_100kts	hp	537.560	530.900	529.520	526.100	508.500	472.440	551.256
n_{zpk}	g	1.354	1.367	1.360	1.361	1.377	1.438	1.370
t_150kts	s	10.166	16.000	12.000	12.000	16.000	-	16.000
P_150kts	hp	1190.382	1300.936	1236.639	1228.030	1294.572	-	1295.800
dW_rotor	kg	0.358	-11.074	0.790	6.512	16.625	16.035	48.842
dW_wing	kg	0.190	0.588	-1.193	-2.006	-5.315	-9.652	-6.844
dW_hs	kg	-0.080	7.413	7.413	7.413	7.413	-7.791	4.797
dW_ds	kg	0.932	3.073	12.990	22.822	55.154	112.476	38.125
dW_tot	kg	0.000	0.000	20.000	34.741	73.878	111.068	84.919

BIBLIOGRAPHY

[1] M. Maisel, D. Giulianetti, and D. Dugan, *The History of the XV-15 Tilt Rotor Research Aircraft: From Concept to Flight* (National Aeronautics and Space Administration, Office of Policy and Plans, NASA History Division, Washington, D.C., 2000).

[2] L. George, *Flying machine,* (U.S. Patent US1775861A, Sept. 1930).

[3] A. Straubinger, R. Rothfeld, M. Shamiyeh, K.-D. Büchter, J. Kaiser, and K. O. Plötner, *An overview of current research and developments in urban air mobility – setting the scene for uam introduction,* Journal of Air Transport Management **87**, 101852 (2020).

[4] M. A. Meyer and G. D. Padfield, *First steps in the development of handling qualities criteria for a civil tilt rotor,* Journal of the American helicopter society **50**, 33 (2005).

[5] W. H. Phillips, *Flying qualities from early airplanes to the space shuttle,* Journal of Guidance, Control, and Dynamics **12**, 449 (1989).

[6] G. E. Cooper and R. P. Harper, *The use of pilot rating in the evaluation of aircraft handling qualities*, Tech. Rep. (Advisory group for aerospace research and development, 1969).

[7] B. Lawrence, C. R. Theodore, W. Johnson, and T. Berger, *A handling qualities analysis tool for rotorcraft conceptual designs,* The Aeronautical Journal **122**, 960 (2018).

[8] G. D. Padfield, *Rotorcraft handling qualities engineering: Managing the tension between safety and performance,* Journal of the American Helicopter Society **58**, 1 (2013).

[9] R. R. Gilruth, *Requirements for satisfactory flying qualities of airplanes*, Tech. Rep. (National Advisory Committee for Aeronautics, 1943) [Online]: https://ntrs.nasa.gov/citations/19930091834 [Dec. 2020].

[10] *Final Report: Accident occurred to the AgustaWestland AW609 Aircraft Registration Marks N609AG*, Tech. Rep. (Agenzia Nazionale Per La Sicurezza Del Volo (ANSV), 2017).

[11] *Flying Qualities of Piloted Aircraft, MIL-HDBK 1797*, Standard (US Dept. of Defence Handbook, 1997).

[12] *Handling Qualities Requirements for Military Rotorcraft, Performance Specification, ADS-33-PRF*, Standard (USAAMC, Aviation Engineering Directorate, 2000).

[13] D. G. Mitchell, D. B. Doman, D. L. Key, D. H. Klyde, D. B. Leggett, D. J. Moorhouse, D. H. Mason, D. L. Raney, and D. K. Schmidt, *Evolution, revolution, and challenges of handling qualities,* Journal of guidance, control, and dynamics **27**, 12 (2004).

[14] G. D. Padfield, *The making of helicopter flying qualities: a requirements perspective,* The Aeronautical Journal **102**, 409 (1998).

[15] G. D. Padfield and M. A. Meyer, *Progress in civil tilt-rotor handling qualities,* Journal of the American Helicopter Society **51**, 80 (2006).

[16] G. Padfield, *Capturing requirements for tiltrotor handling qualities–case studies in virtual engineering,* The Aeronautical Journal **112**, 433 (2008).

[17] P. Rollet, F. Sandri, and T. Roudaut, *Latest european achievements in tilt rotor piloted simulation and handling qualities assessments,* (2003) [Online] https://dspace-erf.nlr.nl/xmlui/handle/20.500.11881/374 [Dec. 2020].

[18] N. Cameron and G. D. Padfield, *Tilt rotor pitch/flight-path handling qualities,* Journal of the American Helicopter Society **55**, 42008.1 (2010).

[19] J. C. Gibson, *Development of a design methodology for handling qualities excellence in fly by wire aircraft* (Delft University Press, 1999).

[20] M. C. Cotting, *Evolution of flying qualities analysis: Problems for a new generation of aircraft*, Ph.D. thesis, Virginia Polytechnic Institute and State University (2010), [Online] https://vtechworks.lib.vt.edu/handle/10919/26781 [Dec. 2020].

[21] W. Bihrle, *A Handling Qualities Theory for Precise Flight-Path Control*, Tech. Rep. AFFDL-TR-65-198 (Aif Force Flight Dynamics Laboratory, 1966) [Online] https://apps.dtic.mil/dtic/tr/fulltext/u2/801498.pdf [Dec. 2020].

[22] D. E. Bischoff, *The Control Anticipation Parameter for Augmented Aircraft.*, Tech. Rep. (Naval Air Development Center - Aircraft And Crew Systems, 1981) [Online] https://apps.dtic.mil/dtic/tr/fulltext/u2/a102626.pdf [Dec. 2020].

[23] D. G. Mitchell, R. H. Hoh, B. L. Aponso, and D. H. Klyde, *Proposed Incorporation of Mission-Oriented Flying Qualities into MIL-STD-1797A*, Tech. Rep. WL-TR-94-3162 (Air Force Flight Dynamics Laboratory, 1994) [Online] https://apps.dtic.mil/dtic/tr/fulltext/u2/a294211.pdf [Dec. 2020].

[24] J. R. Oslon and M. W. Scott, *Helicopter design optimization for maneuverability and agility,* in *45th Annual Forum AHS Proceedings* (1989) pp. 803–814.

[25] F. Patterson, R. Lamour, and D. Schrage, *A conceptual design methodology for rotorcraft maneuverability,* in *39th European Rotorcraft Forum* (2013) [Online] https://dspace-erf.nlr.nl/xmlui/handle/20.500.11881/617 [Dec. 2020].

[26] O. Bandte, D. N. Mavris, and D. A. DeLaurentis, *Viable designs through a joint probabilistic estimation technique,* SAE transactions **108**, 1365 (1999).

[27] M. Maisel, D. Borgman, and D. Few, *Tilt rotor research aircraft familiarization document,* NASA TN X-62 **407** (1975).

[28] S. W. Ferguson, *A mathematical model for real time flight simulation of a generic tilt-rotor aircraft,* NASA CR-166536 **1** (1988).

[29] A. Desopper, O. Heuzé, V. Routhieau, S. Baehrel, G. Roth, W. von Grünhagen, and H. Haverdings, *Study of the low speed characteristics of a tiltrotor,* in *28th European Rotorcraft Forum, Bristol (uk), 17-20 September, 2002* (2002) pp. 16.1–16.14, lIDO-Berichtsjahr=2002,.

[30] A. Filippone, *Aerodynamic modelling of tilt rotor aircraft,* (2019).

[31] D. F. Kimball, *Recent tilt rotor flight control law innovations,* Journal of the American Helicopter Society **32**, 33 (1987).

[32] P. Harendra, M. Joglekar, T. Gaffey, and R. Marr, *Final report v/stol tilt rotor study-volume v: A mathematical model for real time flight simulation of the bell model 301 tilt rotor research aircraft,* NASA CR **114614** (1973).

[33] G. D. Padfield, *Helicopter flight dynamics: including a treatment of tiltrotor aircraft* (John Wiley & Sons, 2018).

[34] B. Manimala, G. Padfield, D. Walker, M. Naddei, L. Verde, U. Ciniglio, P. Rollet, and F. Sandri, *Load alleviation in tilt rotor aircraft through active control; modelling and control concepts,* The Aeronautical Journal **108**, 169 (2004).

[35] M. B. Tischler, *Frequency-response identification of XV-15 tilt-rotor aircraft dynamics*, Ph.D. thesis, Stanford University (1987).

[36] J. Hodgkinson, *Aircraft handling qualities* (Oxford, 1999).

[37] J. How, *16.333 Aircraft Stability and Control,* Fall 2004, Massachusetts Institute of Technology: MIT OpenCourseWare, https://ocw.mit.edu/, license: Creative Commons BY-NC-SA.

[38] J. Mulder, W. van Staveren, J. van der Vaart, and E. de Weerdt, *Ae3212 Aerospace Flight Dynamics,* March 2013, Delft University of Technology.

[39] N. A. T. O. A. G. for Aerospace Research and D. F. M. Panel, *Handling Qualities of Unstable Highly Augmented Aircraft*, AGARD advisory report (AGARD, 1991).

[40] J. C. Gibson, *Piloted handling qualities design criteria for high order flight control systems,* AGARD-CP-333, Criteria for Handling Qualities of Military Aircraft (1982).

[41] M. D. Pavel and G. D. Padfield, *Defining consistent ads-33-metrics for agility enhancement and structural loads alleviation,* in *Annual Forum Proceedings-American Helicopter Society*, Vol. 58 (American Helicopter Society, INC, 2002) pp. 900–914.

[42] D. Krishnan, A. Borkar, P. Shevare, and H. Arya, *Hardware in loop simulator for cooperative missions,* in *Second International Conference on Advances in Control and Optimization of Dynamical Systems* (2011).

[43] W. Blajer, J. A. Goszczyński, and M. Krawczyk, *The inverse simulation study of aircraft flight path reconstruction,* Transport **17**, 103 (2002).

[44] D. Thomson and R. Bradley, *Inverse simulation as a tool for flight dynamics research—principles and applications,* Progress in Aerospace Sciences **42**, 174 (2006).

[45] M. D. Pavel and G. D. Padfield, *Progress in the development of complementary handling and loading metrics for ads-33 maneuvers,* in *Annual Forum Proceedings - American Helicopter Society*, Vol. 59 (American Helicopter Society, 2003) pp. 1160–1172.

[46] J. Andres, H. Huber, and J. Renaud, *The tilt-rotor aircraft: A response to the future? from european interrogations to eurofar actions,* (1986).

[47] E. A. Fradenburgh, *Technical notes: A simple autorotative flare index,* Journal of the American Helicopter Society **29**, 73 (1984).

[48] P. F. Scaramuzzino, M. D. Pavel, D. M. Pool, O. Stroosma, G. Quaranta, M. Mulder, *et al.*, *Investigation of the effects of autorotative flare index variation on helicopter flight dynamics in autorotation,* in *45th European Rotorcraft Forum (ERF 2019)* (2019) pp. 1–14.

[49] M. Scully, *Adventures in Low Disk Loading VTOL Design* (National Aeronautics and Space Administration, Ames Research Center, 2018).

[50] A. Sridharan, B. Govindarajan, V. Nagaraj, and I. Chopra, *Design considerations of a lift-offset single main rotor compound helicopter,* in *Proceedings of the AHS Technical Meeting on Aeromechanics Design for Vertical Lift* (Vertical Flight Soc., Fairfax, VA, 2016).

[51] D. Yilmaz, B. Dang Vu, and M. Jones, *Rotorcraft pilot coupling susceptibility accompanying handling qualities prospects in preliminary rotorcraft design,* in *39th European Rotorcraft Forum* (MOSCOU, Russia, 2012).

[52] C. Widdison, J. Magee, and H. Alexander, *Conceptual design study of a 1985 commercial STOL tilt rotor transport*, Tech. Rep. (Boeing Vertol Co., Philadelphia, Pa.(USA), 1974).

[53] W. Johnson, *Ndarc-nasa design and analysis of rotorcraft theoretical basis and architecture,* (2010).

[54] E. A. Fradenburgh, *The first 50 years were fine... but what should we do for an encore?—the 1994 alexander a. nikolsky lecture,* Journal of the American Helicopter Society **40**, 3 (1995).